THE HONG KONG POLYTECHNIC UNIVERSITY
香港理工大學
Pao Yue-kong Library
包玉剛圖書館

Copyright Undertaking

This thesis is protected by copyright, with all rights reserved.

By reading and using the thesis, the reader understands and agrees to the following terms:

1. The reader will abide by the rules and legal ordinances governing copyright regarding the use of the thesis.
2. The reader will use the thesis for the purpose of research or private study only and not for distribution or further reproduction or any other purpose.
3. The reader agrees to indemnify and hold the University harmless from and against any loss, damage, cost, liability or expenses arising from copyright infringement or unauthorized usage.

IMPORTANT

If you have reasons to believe that any materials in this thesis are deemed not suitable to be distributed in this form, or a copyright owner having difficulty with the material being included in our database, please contact lbsys@polyu.edu.hk providing details. The Library will look into your claim and consider taking remedial action upon receipt of the written requests.

Pao Yue-kong Library, The Hong Kong Polytechnic University, Hung Hom, Kowloon, Hong Kong

http://www.lib.polyu.edu.hk

REAL-TIME STRUCTURAL SEISMIC DAMAGE ASSESSMENT INTEGRATING PHYSICS-BASED AND MACHINE LEARNING ALGORITHMS

XIONG QINGSONG

PhD

The Hong Kong Polytechnic University

This programme is jointly offered by The Hong Kong
Polytechnic University and Tongji University

2025

The Hong Kong Polytechnic University

Department of Civil and Environmental Engineering

Tongji University

Department of Civil Engineering

Real-time Structural Seismic Damage Assessment Integrating Physics-based and Machine Learning Algorithms

Xiong Qingsong

A thesis submitted in partial fulfilment of the requirements
for the degree of **Doctor of Philosophy**

June 2025

CERTIFICATE OF ORIGINALITY

I hereby declare that this thesis is my own work and that, to the best of my knowledge and belief, it reproduces no material previously published or written, nor material that has been accepted for the award of any other degree or diploma, except where due acknowledgement has been made in the text.

___________________ (Signed)

XIONG QINGSONG (Name of student)

To

My Family

and

Spirit of Staying True to Academic Aspiration All Along

ABSTRACT

Structural seismic damage assessment (SSDA) has been asserted as one of the major objectives in structural health monitoring (SHM). Traditional empirical methods based on field investigations and analytical methods based on model calculation are difficult to meet the requirement of real-time operation. In recent decades, vibration-based approaches, assisted by machine learning (ML) techniques, have emerged as a captivating strategy for uncovering knowledge of structural damage or integrity. However, the issues of data noise, data loss and data scarcity in field monitoring pose significant obstacles in vibration-based SSDA.

This study aims to tackle the above challenges through exploiting advanced techniques integrating physics-based and ML algorithms. It delves into corresponding tasks including vibration signal denoising, seismic response prediction and structural condition assessment, aiming at enhancing applicability and accuracy of SSDA.

A deep convolutional image-denoiser network is first developed for vibration signal denoising. It incorporates specialized pseudo-clean signal definition and time-frequency domain transformation to denoise signal without clean baseline signals. This method is applied to the field measurement of the 632-meter-tall Shanghai Tower, the tallest skyscraper in China. Linear parametric evaluation and nonlinear analysis are performed to verify its denoising effectiveness. Modal identification results using the denoised data are more accurate than those without denoising.

A parameter-free physics-informed neural network is devised to rapidly predict structural seismic responses. A novel physics-informed mechanism is devised by construing the differential nexus of state variables extended from initial acceleration responses and embedded for constraint training. A numerical mass-spring-damper system and historical monitoring datasets of a real-world building are adopted for validation. The results confirm the effectiveness and superiority of the proposed method in time history prediction of seismic responses.

Considering data scarcity in structural condition assessment, three different approaches, namely semi-supervised label propagation, zero-shot knowledge transfer, and class-conditional data augmentation algorithms are proposed. Thereinto, the semi-supervised method leverages novel damage-sensitive feature extraction and optimized fuzzy clustering algorithm to facilitate pseudo-label propagation. The zero-shot transfer learning method incorporates an innovative domain adaptation technique based on signal representation and reconstruction, enabling enhanced cross-domain knowledge transfer for structural condition assessment. Regarding the class-conditional data augmentation method, class-imbalance reweighted mechanisms are integrated into an auxiliary classifier generative adversarial network to improve data synthesis. These three techniques can deal in tandem with data scarcity issues in vibration measurement, thus enabling adaptive and reliable structural condition assessment in different data scarcity situations.

With primary research focus on real-time SSDA, the developed methods integrating physics-based and ML algorithms in this study can be extended to other data-driven fields toward next-generation SHM with wide-reaching benefits.

PUBLICATIONS

Journal Papers

1. **Xiong, Q.**, Xia, Y., Xiong, H., Yuan, C., Chen, J., & Kong, Q. (2025). Re-ACGAN: Structural damage identification with class-imbalance reweighted ACGAN for data augmentation. *Engineering Structures,* 329, 119814.

2. **Xiong, Q.**, Kong, Q., Xiong, H., Chen, J., Yuan, C., Wang, X., & Xia, Y. (2024). Zero-shot knowledge transfer for seismic damage diagnosis through multi-channel 1D CNN integrated with autoencoder-based domain adaptation. *Mechanical Systems and Signal Processing*, 217, 111535.

3. **Xiong, Q.**, Kong, Q., Xiong, H., Liao, L., & Yuan, C. (2024). Physics-informed deep 1D CNN compiled in extended state space fusion for seismic response modeling. *Computers & Structures*, 291, 107215.

4. **Xiong, Q.**, Kong, Q., Yuan, C., Li, Y., Ji, K., & Xiong, H. (2024). Fusing physics-based and machine learning models for rapid ground-motion-adaptative probabilistic seismic fragility assessment. *Journal of Building Engineering*, 87, 108938.

5. **Xiong, Q.**, Xiong, H., Yuan, C., & Kong, Q. (2024). Three-stage unsupervised learning approach fusing novel pseudo-label diffusion and math-physics translating for real-time structural damage detection. *Engineering Applications of Artificial Intelligence*, 138, 109438.

6. **Xiong, Q.**, Yuan, C., He, B., Xiong, H., & Kong, Q. (2023). GTRF: A general deep learning framework for tuples recognition towards supervised, semi-supervised and unsupervised paradigms. *Engineering Applications of Artificial Intelligence*, 124, 106500.

7. **Xiong, Q.**, Xiong, H., Yuan, C., & Kong, Q. (2023). A novel deep convolutional image-denoiser network for structural vibration signal denoising. *Engineering Applications of Artificial Intelligence*, 117, 105507.

8. **Xiong, Q.**, Xiong, H., Kong, Q., Ni, X., Li, Y., & Yuan, C. (2022). Machine learning-driven seismic failure mode identification of reinforced concrete shear walls based on PCA feature extraction. *Structures*, 44, 1429-1442.

9. Kong, Q., X**iong, Q.**, Xiong, H., He, C., & Yuan, C. (2023). Semi-supervised networks integrated with autoencoder and pseudo-labels propagation for structural condition assessment. *Measurement,* 214, 112779.

10. Xiong, H., **Xiong, Q.**, Zhou, B., Abbas, N., Kong, Q., & Yuan, C. (2023). Field vibration evaluation and dynamics estimation of a super high-rise building under typhoon conditions: data-model dual driven. *Journal of Civil Structural Health Monitoring*, 13(1), 249-235.
11. Ni, X., **Xiong, Q.**, Kong, Q., & Yuan, C. (2022). Deep HystereticNet to predict hysteretic performance of RC columns against cyclic loading. *Engineering Structures,* 273, 115103.
12. **Xiong, Q.**, Chen, L., & Xiong, H. (2024). Modal frequency recognition analysis of Shanghai Tower under typhoon excitation. *Building Structure*. (Online published, in Chinese)
13. **Xiong, Q.**, Xiong, H., Yuan, C., & Kong, Q. (2024). Digital-physical hybrid interactive feedback based theoretical framework for near-real-time seismic damage assessment of structures. *Structural Engineers* (in Chinese), 40(1): 1-10.
14. **Xiong, Q.**, Xiong, H., Kong, Q., Chen, L., Ding, Y., & Yuan, C. (2024). Vibration recognition of high-rise building structures based on deep representation learning on vibrational signals. *Engineering Mechanics* (in Chinese), 41(9): 134-143.
15. **Xiong, Q.**, Xiong, H., Yuan, C., Chen, L., & Kong, Q. (2024). Damage identification of building structures based on multi-channel one-dimensional convolutional neural networks. *Journal of Vibration and Shock* (in Chinese), 43(24): 216-224.

Conference Papers

16. **Xiong, Q.**, Yuan, C., Ji, K., He, C., & Xiong, H. (2023). Vibration Recognition Based on Feature Extraction by Deep Autoencoder. In Proceedings of the *2023 International Conference on Frontiers of Artificial Intelligence and Machine Learning* (FAIML), April 14-16, 2023, Beijing, China.
17. **Xiong, Q.**, YUAN, C., XIONG, H., & KONG, Q. (2023). GTRF: A General Tuples Recognition Framework Towards Deep Learning-Driven Structural Health Monitoring Adapted to Diverse Supervision Paradigms. In Proceedings of the *14th International Workshop on Structural Health Monitoring* (IWSHM), September 12-14, 2023, Stanford University, CA, America.
18. **Xiong, Q.**, Kong, Q., & Xia, Y. (2024). A framework for structural vulnerability assessment with consideration of seismic uncertainty. In Proceedings of the *11th European Workshop on Structural Health Monitoring* (EWSHM), June 10-13, 2024, Potsdam, Germany.

ACKNOWLEDGEMENTS

For every moment in my life, I wish to maximize my full potential and dedicate myself to knowledge, so as to awaken my spirit through hard work and lead an extraordinary life. Completing this dual-award PhD journey has been one of the most challenging yet rewarding endeavors of my life, and I owe immense gratitude to the people who supported me along the way. Due to the space limitation, I would like to highlight a few.

First and foremost, I extend my deepest gratitude to my supervisor, Prof. Yong Xia, whose expertise, patience, and unwavering encouragement guided me through every stage of this research. His insightful critiques, willingness to engage in spirited discussions, and faith in my potential are essential in shaping this work. I would also like to express my appreciation to him for his enduring patience and understanding throughout this journey, granting me the freedom to explore diverse paths in my research. His meticulous attitude towards research, exceptional academic acumen, and charismatic character will continue to serve as a lifelong benefit in my future academic pursuits. I am equally grateful to my supervisors at Tongji University, Prof. Haibei Xiong and Prof. Qingzhao Kong, who gave me continuous support and encouragement all along.

I would also like to express my sincere thanks to Associate Prof. Cheng Yuan from Guangzhou University and Prof. Zheng Lu from Tongji University, for providing me with numerous constructive suggestions and hands-on guidance. I would also like to extend my gratitude to those researchers who have encouraged and enlightened my research journey in these years, including but not limited to Prof. Xilin Lu from Tongji University, Prof. Bill F. Spencer from University of Illinois Urbana-Champaign, Prof. Eleni Chatzi from ETU Zurich, and Prof. Brain Sheil from University of Cambridge.

I thank all my colleagues in Prof. Xia's group for fostering a stimulating and collaborative environment, Drs. Xiaoyou Wang, Yushi Shan, Yixian Li, Fei Wang, Lingfang Li, Rongpan Hu, Xiaoming Lei, Wei Tian, Yuxuan Zhang, Lu Zhang, and Tian Lu, Yunxin Hu, Lanxin Luo, Binggui Huang, Chenyue Wang, Peng Ni, Haoliang Zhao et al. Special thanks to Dr. Xiaoyou Wang and Dr. Yushi Shan for their camaraderie, technical suggestions, and moral support during moments of doubt, as well as Lanxin Luo, Binggui Huang, Qimeng Guo, Zhaojie Chen, Pengchang Wei, et al. for accompanying me during my staying at PolyU. Research groups of Prof. Xiong and Prof. Kong at Tongji University are also specially acknowledged who accompanied me during the first three years of my PhD journey.

Sincere gratitude is also expressed to the panel members of my viva, Prof. Michael D. Todd, Prof. Ka-Veng Yuen, and Prof. Kaiming Bi, who have dedicated valuable time to reviewing this thesis and gave invaluable feedback. Their insights have been instrumental in shaping the final form of this research.

On a personal note, my heartfelt thanks go to my family for their unwavering companionship, care, and support. They have offered me in-depth love while always respecting my choices and offering unconditional encouragement. I owe thanks to my beloved partner, Dr. Fan, whose emotional strength and empowering belief in me have been a constant source of motivation. Their companionship has profoundly shaped my perspectives and imbued my life with a far-reaching sense of belonging and responsibility.

Finally, I extend gratitude to friends and mentors outside academia who reminded me to embrace work-life balance and life orientation. All who walked this path with me are sincerely acknowledged, who have been always lighting my way towards the future.

TABLE OF CONTENTS

CHAPTER 3 DEEP CONVOLUTIONAL IMAGE-DENOISER NETWORK FOR VIBRATION SIGNALS

LIST OF FIGURES

LIST OF TABLES

ABBREVIATIONS

ANN	Artificial neural network
BiLSTM	Bidirectional LSTM
BN	Batch-normalization
CE	Cross entropy
CI	Correlation index
CNN	Convolutional neural network
CORR	Cross correlation coefficient
CWT	Continuous wavelet transform
DA	Domain adaptation
DAE	Deep autoencoder
DCIMN	Deep convolutional image-denoiser network
DCR	Dynamic class reweighting
DFT	Discrete Fourier transform
DGM	Deep generative model
DL	Deep learning
DOF	Degree-of-freedom
DP	Damage pattern
DS	Damage scenario
DSF	Damage sensitive feature
DWT	Discrete wavelet transform
EMD	Empirical mode decomposition
FCM	Fuzzy c-means
FDM	Finite differentiate method
FEM	Finite element model
FFT	Fast Fourier transform
FN	False negative
GAN	Generative adversarial network
GM	Ground motion
GNN	Graph neural network
HS	Healthy status

IDA	Incremental dynamic analysis
IMF	Intrinsic mode function
IoT	Internet of things
IS	Intact structure
KNN	K-nearest neighbors
LD	Light damage
LSTM	Long short-term memory
MAE	Mean absolute error
MD	Moderate damage
ML	Machine learning
MLE	Maximum likelihood estimation
MLP	Multilayer perceptron
MSDS	Mass-spring-damper system
MSE	Mean squared error
OCSVM	One-class support vector machine
ORSR	Original-to-reconstructed signal ratio
PBEE	Performance-based earthquake engineering
PEER	Pacific Earthquake Engineering Research Center
PGA	Peak ground acceleration
PINN	Physics-informed neural network
Re-ACGAN	Reweighted auxiliary classifier GAN
RMSE	Root mean square error
RNN	Recurrent neural network
SD	Severe damage
SDOF	Single-degree-of-freedom
SHM	Structural health monitoring
SNR	Signal-to-noise ratio
SSDA	Structural seismic damage assessment
SSL	Semi-supervised learning
SSM	State space model
STFT	Short-time Fourier transform
SVD	Singular value decomposition

TL	Transfer learning
t-SNE	T-distributed stochastic neighbor embedding
UL	Unsupervised learning
VAE	Variational autoencoder
VMD	Variational mode decomposition
WPD	Wavelet packet decomposition
WT	Wavelet transform
1D	One-dimensional
2D	Two-dimensional
3D	Three-dimensional

CHAPTER 1 INTRODUCTION

1.1 Background

Extreme earthquake events cause widespread loss of life, property damage, and long-term economic consequences. In the past decades, great endeavor has been devoted to improving the seismic performance of structures via performance-based seismic design and earthquake resistance enhancement, aiming at minimizing the risk of casualties and collateral financial loss. Structural health monitoring (SHM) has been rapidly developed by measuring structural loads and responses for structural diagnosis and prognosis under ambient conditions and hazards such as unexpected earthquake events (Das et al., 2016; Dworakowski et al., 2016).

Timely and accurate structural seismic damage assessment (SSDA) is crucial for urban disaster prevention and mitigation. It provides a substantial fundamental for scientific pre-earthquake planning and rapid post-earthquake reaction (Xu et al., 2022a). With arising concepts such as Resilient City (Hao et al., 2023a), Smart City (Kociuba et al., 2023), and Digital Twins (Juarez et al., 2021), next-generation SHM has put forward higher requirements for SSDA, shifting its target paradigm from static, manual, and post-event to dynamic, automatic, and real-time operation. In addition, a timely damage assessment is urgently required after earthquake disasters to guide the rescue and renovation work (Bhatta & Dang, 2024; Goulet et al., 2015; Tsuchimoto et al., 2024). Therefore, real-time SSDA is not only a research hotspot in the field of earthquake engineering but also meets the current demands for enhancing structural seismic resilience and facilitating next-generation SHM.

1.2 Overview of SSDA approaches

1.2.1 Conventional SSDA methods

Basically, the conventional SSDA methods are mainly divided into empirical methods based on field damage investigations and analytical methods based on model calculation (Lang et al., 2012), as summarized in Table 1-1.

Earthquake damage investigations mainly rely on on-site expert investigation and assessment, which can obtain relatively reliable assessment results, but on-site visits are of extensive workload and time-consuming. In addition, approaches based on digital images (such as satellite images (Macchiarulo et al., 2024; Stramondo et al., 2006; Yu et al., 2024a), drone photography (Giardina et al., 2024; Yu et al., 2024b), is another major way to investigate earthquake damage. By comparing and analyzing high-altitude data before and after the earthquake, a preliminary damage assessment of a large disaster area can be achieved. However, the lag in image acquisition and adverse effects of the climate and environmental conditions deteriorate their SSDA accuracy a lot (Dell'Acqua & Gamba, 2012).

Table 1-1. Advantages and disadvantages of conventional SSDA methods

	Methods	Approaches	Advantages	Disadvantages
Investigation-based empirical methods	Expert investigation	On-site inspection	Accurate and reliable	Manpower intensive and low efficiency
	Digital imaging	Satellite remote sensing, drone photography	Rapid and large scale	Time lags, climate disruptions
Model-based analytical methods	Fragility analysis	Estimate damage levels under different ground motions	Probabilistic description	Sensitivity to structural types and seismic uncertainty
	Static analysis	Capacity-demand spectrum analysis	Simplified calculation	Low accuracy
	Dynamic Analysis	Simplified model calculation	Accurate and dynamic	Difficulty in simplified model development and model fidelity loss

Analytical methods based on model calculation mainly include seismic fragility assessment methods, static analysis methods, and dynamic analysis methods. Thereinto, seismic fragility assessment is to calculate the probability of different damage states of a specific structure type under the premise of specified damage thresholds. The obtained fragility curves describe the corresponding relationship between ground motion intensity and structural damage state from a macro perspective (Cao et al., 2023; Feng et al., 2023; Yazdanpanah et al., 2023). Although this method has been widely used during the past decades, it is difficult to fully consider the structural or seismic uncertainty and is sensitive to certain structural types. Especially, for those areas lacking historical data of actual earthquake events, the applicability of the traditional seismic fragility analysis is extensively compromised, leading to unreliable assessment results.

Static analysis methods are mostly based on response spectrum analysis on a structural capacity-demand model. Taking actual earthquake damage as a reference, static analysis methods delve into structural damage mechanisms through constructing a corresponding relationship between the bearing capacity and seismic demand associated with different damage states. One representative static analysis method is the basic seismic damage prediction based on capacity-demand analysis proposed by the Federal Emergency Management Agency (FEMA) (Prestandard and Commentary for the Seismic Rehabilitation of Buildings, 2000). Nonetheless, it generally uses a single-degree-of-freedom (SDOF) model to simulate the building structures without consideration of influence due to high-order vibration modes, thus leading to a reduction in estimated accuracy. In addition, it is also difficult to represent the duration and pulse characteristics of earthquake motions when constructing the structural capacity spectrum based on the pushover analysis (Cheng et al., 2017).

To make up for the limitations of static analysis methods in considering seismic and structural uncertainties, dynamic analysis methods, or time history analysis methods, have received extensive attention and progress in recent decades. Considering the huge time cost of traditional time history analysis calculations based on refined finite element models (FEMs), the dynamic analysis for SSDA at this stage is to establish a simplified structural model and calculate real-time structural responses, such as incremental dynamic analysis (IDA). On this basis, structural responses are estimated and predicted to obtain relevant damage-indicative parameters (such as modal properties, inter-story drift) for SSDA (Lu & Guan, 2021; Tsarpalis et al., 2021; Xiong et al., 2020). This kind of approach embraces a clear physical concept of mechanics, and time history analysis can fully characterize the seismic ground motions. However, the calibration of simplified models (especially the establishment of elastic-plastic constitutive models) is quite difficult and complicated in practice. In addition, even if real-time calculations can be achieved under cloud server architecture by constructing simplified structural models, the dimensionality reduction from a large nonlinear system to a simplified model will inevitably cause fidelity loss and model distortion. Consequently, the calculated structural responses based on the simplified model are often limited to preliminary threshold evaluations, such as inter-story drift ratios (Lu et al., 2014). At present, reliable rapid SSDA using conventional approaches remains challenging.

1.2.2 Machine learning-driven SSDA methods

To improve accuracy and realize real-time operation of SSDA, researchers have sought to explore advanced technologies and methods for structural damage identification, including machine learning (ML), data mining, computer vision, etc. ML technologies can realize automatic detection and quantification of structural damage by well-trained models (Bhatta & Dang, 2023; Li et al., 2024a; Mangalathu et al., 2019; Xiong et al., 2022). Data mining technologies can extract potential damage patterns and detect anomalies from SHM data (Lu et al., 2024; Wang et al., 2023a; Wang et al., 2023b). Computer vision technologies leverage image classification (Ji et al., 2023), semantic segmentation (Tavasoli et al., 2023), object detection (Kong et al., 2023), among others, to extract high-dimensional abstract features of images, allowing for damage mapping relationships based on the differences in the spatial and temporal distributions of images. However, structural damage identification based on images is often limited to local visible damage on the surface of structures (cracks, spalling, corrosion, etc.). At the structural-level, damage assessment should integrate the results of components with designated weights (Feng et al., 2024).

With the continuous development of sensing and transmission technology, vibration-based SSDA has gained great attention and progress. By analyzing dynamic behavior of structures under earthquakes, vibration analysis can capture change in the structural vibrations and identify its damage condition including presence, location, and severity. In the past decades, vibration-based approaches are widely used in SHM for bridges (Doebling et al., 1996), buildings (Kaya et al., 2023), dams (Zar et al., 2023), wind turbines (Li et al., 2018) and other structures.

Vibration-based approaches equipped with ML techniques have achieved substantial research advances and successful applications (Desjardins & Lau, 2022; Lu et al., 2021; Xu et al., 2020, 2021a; Kamariotis et al., 2023; Zhang et al., 2025), offering new strategies for realizing real-time SSDA. Taking structural damage identification as an example, although numerous relevant ML algorithms have been proposed in recent years, the majority of related works involves training and validation of ML models using sufficient samples from pre-set damage scenarios in laboratory experiments (Avci et al., 2021; Li et al., 2023a; Lin et al., 2017a). Hence, even though a plethora of data-driven algorithms have shown satisfactory results in identifying experimentally induced damage, they are hardly applied to real-world structures under as-is service conditions due to the lack of monitoring data under damage scenarios. One major reason is that the dataset has many examples of undamaged or normal operating conditions but much fewer examples of critical damage states. Persistent data imbalance is ubiquitous in engineering practice (Gao et al., 2021; Miele et al., 2023), which becomes a primary bottleneck and limits the application of ML-driven algorithms.

In addition to the above data scarcity issue, data for vibration-based SSDA faces another two practical obstacles in engineering practice, that is, data noise and data loss issues. Specifically, data noise issue refers to the inevitable noise contaminant in the field measurement, which deteriorates accuracy of data-driven analysis, such as modal-based structural integrity evaluation (Wei et al., 2023). Data loss issue refers to the potential loss of monitoring data due to unexpected sensor failures (Fan et al., 2019). These data issues of vibration measurement pose significant obstacles in real-time SSDA.

1.3 Research scopes of the thesis

1.3.1 Scientific problems

In the basic paradigm proposed by Farrar and Worden (2012) that is widely accepted for modern SHM, four procedures are defined as: 1) Operational evaluation; 2) Data Acquisition; 3) Feature selection; 4) Statistical modelling for feature discrimination. Thereinto, data cleaning is inherent in steps 2 to 4 of this paradigm. With continuous advancement of sensing and ML techniques, data has now been widely accepted as a main factor of SHM especially in the context of this paradigm. This study aims to delve into three key data issues in vibration-based SSDA including data noise, data loss and data scarcity.

Correspondingly, vibration signal denoising and seismic response prediction are first performed to address the data noise and data loss issues, respectively. For data scarcity issue that widely exists in structural damage diagnosis, this study focuses on damage severity classification. It should be clarified that the scopes of structural damage diagnosis basically comprise hierarchical levels of increasing complexity including: 1) damage presence (i.e., damaged/undamaged); 2) damage localization; 3) damage quantification (i.e., severity); 4) damage prognosis (e.g., remaining life prediction, etc.) (Rytter, 1993; Doebling et al., 1996). This study addresses the data scarcity issue in damage presence detection and damage severity classification, for conciseness, which are denoted as structural condition assessment in this thesis.

In practical implementation of the above three task implementation, there are several aspects worthy of attention and development:

(1) In the realm of noise reduction of vibration measurement, purely clean signals without noise components do not exist, which hinders supervised ML techniques for signal denoising. Therefore, special techniques need to be considered to develop an automatic denoising method for vibration signals.

(2) In the realm of seismic response prediction, conventional regression-based ML algorithms might exhibit poor prediction accuracy and model explainability, special attention incorporating physics-informed knowledge (i.e., structural dynamics or theorical equations) need to be introduced in the establishment of surrogate models. In particular, the parameter accessibility of devised physics-informed constraints is essential to network applicability.

(3) In the realm of structural condition assessment, data scarcity issue is the main and common challenge in different ML-based approaches, including weak-supervised methos, transfer learning methods and data augmentation (DAug) methods. Special techniques should be embedded into algorithm development to enhance their prediction accuracy and model adaptability.

1.3.2 Integrating physics-based and ML algorithms

A basic strategy to address data issues in this study is the integration of traditional physics-based models with cutting-edge ML algorithms. This hybrid approach leverages the strengths of both methodologies. Physics-based models established with engineering principles provide a foundational understanding of structural behavior. These models offer interpretability and theoretical validation but may struggle with complex and nonlinear structural responses or uncertain parameters. ML algorithms excel at identifying patterns and anomalies in complex datasets that traditional approaches might miss. These algorithms can adapt to evolving structural conditions and improve over time with additional data, though they may lack the physical meaning and interpretability.

The ’real-time’ operation of the developed methods is owing to the integration of physics-based and ML algorithms. The developed methods in this study retain the basic feature of ML, that is, after the model training is completed, the prediction can be completed quickly in the testing phase, thus allowing for a real-time inference for relevant risk-informed decisions.

Notably, deep learning (DL) is a subcategory of ML, as shown in Figure 1-1(a). In particular, the concept of “physics-based” term in this study includes field measurement and numerical simulation, which provide monitoring and simulation data, respectively, as shown in Figure 1-1(b). The physics-based and ML algorithms are integrated into the developed methods in this study.

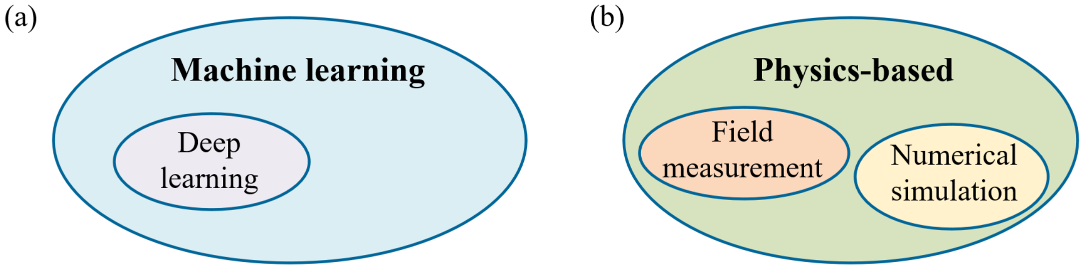

Figure 1-1. Venn diagrams of term interpretation (a) ML; (b) Physics-based

1.4 Research objectives and thesis organization

1.4.1 Research objectives

This study aims to develop advanced techniques for vibration-based real-time SSDA by integrating physics-based and ML algorithms. With emphasized interests focused on the three key data issues, namely data noise, data loss and data scarcity, the research objectives of this study are:

(1) To develop an automatic signal denoising method for vibration measurement,

which attains fully automatic data cleaning without reliance on clean labeled data, thus enhancing structural integrity evaluation via vibration-based modal identification.

(2) To develop a parameter-free PINN for seismic response prediction, which attains rapid data synthesis without reliance on stiffness or mass matrices, thus allowing for better interpretability and accuracy of the surrogate models.

(3) To develop advanced semi-supervised label propagation, cross-domain knowledge transfer and class-conditional DAug algorithms to address data scarcity issues, thus enabling superior accuracy and applicability for structural condition assessment in different data scarcity scenarios.

1.4.2 Thesis organization

This thesis is organized into eight chapters, as depicted in Figure 1-2.

Chapter 1 introduces the background and overview of SSDA approaches in general. Three data issues of vibration-based SSDA are demonstrated, namely data noise, data loss and data scarcity. Research scopes and research objectives of this thesis are correspondingly claimed.

Chapter 2 conducts a systematic literature review on approaches dealing with the data issues in vibration-based SSDA. References from conventional methods to state-of-the-art techniques for corresponding tasks are presented, where limitations and challenges of existing studies are discussed.

Chapter 3 to Chapter 7 introduce the newly developed methods in this study. Chapter 3, Chapter 4 and Chapter 5 to 7 address a different critical challenge in the SSDA framework, including data noise, data loss, and data scarcity. These challenges are specific and distinct in nature, requiring the development of specialized methods to solve them. Consequently, the validation process is tailored to align with the unique objectives and expected outcomes of each method. It should be first clarified that the methods are not sequentially dependent, meaning the output of one chapter is not directly fed as input into the next. Instead, these methods operate in parallel, each focusing on a specific aspect of the broader SSDA framework. Therefore, the five methods presented in these chapters utilize distinct objective structures and data sources for solid validation. Together, these components form a comprehensive framework that integrates data preprocessing (denoising), rapid predictive modeling (seismic response prediction), and robust diagnostic methods (structural condition assessment), with an inherent consistence with Farrar and Worden (2012) SHM paradigm.

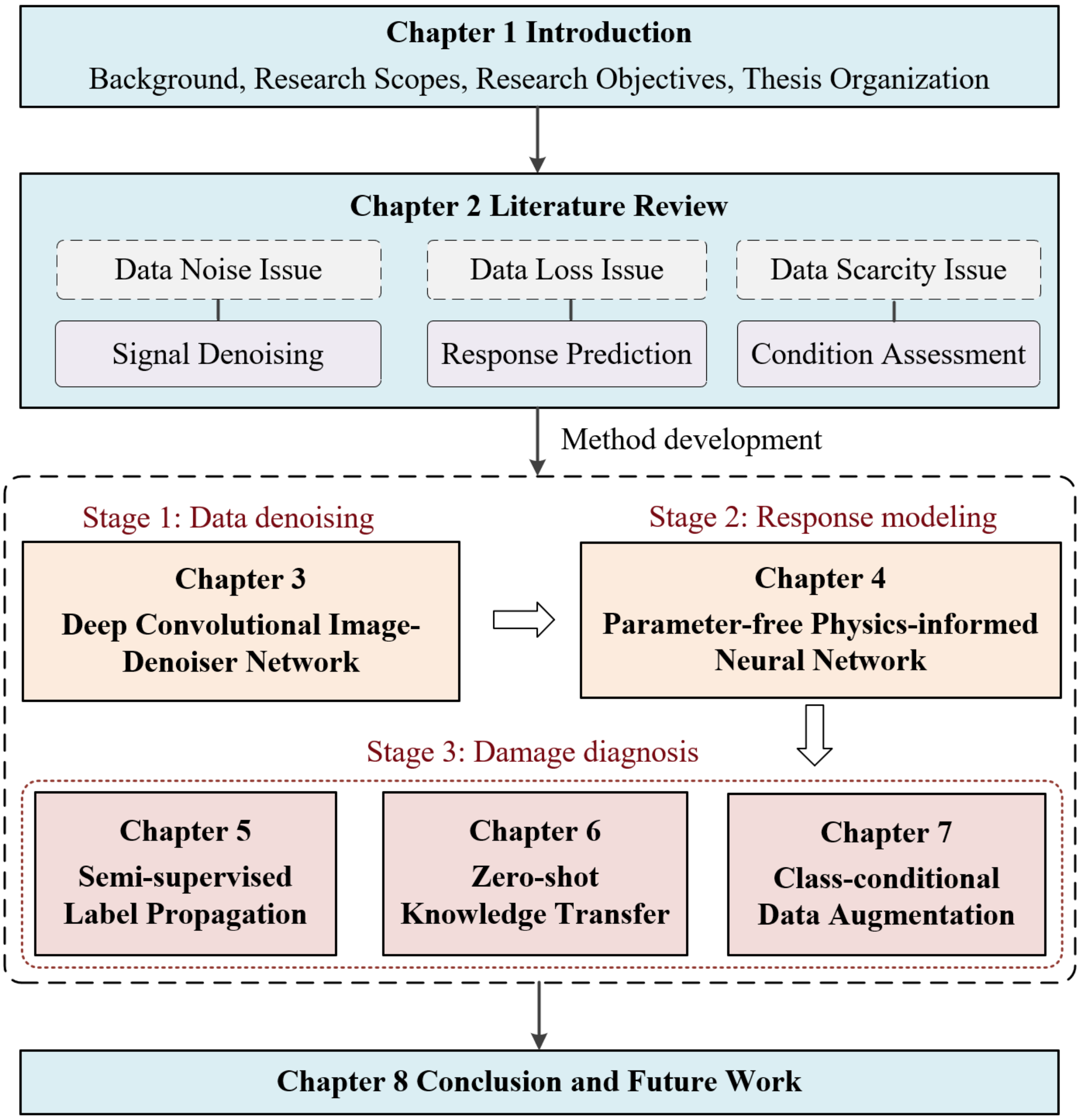

Figure 1-2. Organization of thesis

Specifically, in Chapter 3, a deep convolutional image-denoiser network is proposed to denoise vibrational signals. It delves into two major technical problems of label calibration of purely-clean signals and high-dimensional feature extraction of vibrational data, thus realizing automatic data cleaning without any prior knowledge of vibration measurement.

In Chapter 4, a parameter-free PINN is devised for rapid seismic response prediction. A novel physics-informed mechanism is proposed derived from the state space representation of the dynamic systems, which is embedded into the surrogate regression models for constraint training. The merit of this method is that it does not rely on structural dynamic parameters (such as mass or stiffness matrices), as usually required in most existing related works.

To deal with the obstacles of data scarcity in vibration-based structural condition assessment, three different approaches, namely weak-supervised label propagation, cross-domain knowledge transfer and class-conditional DAug are respectively explored in Chapter 5, 6 and 7.

- Chapter 5 develops a semi-supervised label propagation method for structural condition assessment. It leverages self-supervised representative learning, optimized fuzzy clustering and supervised classification techniques to realize the semi-supervised workflow.
- Chapter 6 proposes a zero-shot knowledge transfer approach with an innovative domain adaptation (DA) technique. A deep autoencoder is trained for representative learning using the source-domain data and then utilized to reconstruct the target-domain data into a similar feature space, allowing for an improved cross-domain knowledge transfer. The proposed method is validated to transfer the structural condition knowledge from FEMs to real structures.
- Chapter 7 introduces an innovative class-imbalance reweighted auxiliary classifier generative adversarial network to augment vibration data. It

incorporates two class-conditional reweighting mechanisms to adeptly address the class imbalance issue during the data synthesis. The proposed data augmentation method is validated to be capable of improving the prediction accuracies of the classifiers trained for structural condition assessment.

Finally, Chapter 8 concludes the thesis and discusses the future work.

CHAPTER 2 LITERATURE REVIEW

This chapter reviews the literature on three tasks in vibration-based SSDA, namely vibration signal denoising, seismic response prediction and structural condition assessment, which correspondingly focus on data noise, data loss and data scarcity issues, respectively.

2.1 Vibration signal denoising

The monitoring vibration signals are inevitably interfered by noise components, which will affect the accuracy of modal identification results. The noise existed in the field measurement data cast significant obstacles on the preliminary SSDA. Therefore, denoising the measured vibration data, that is, filtering or reducing the noise from the original signal before analysis, is a promising strategy to accurately extract structural dynamic properties, thus benefiting the preliminary SSDA.

2.1.1 Conventional methods

Among the traditional vibration signal denoising methods, filtering process is a classic approach that can be performed in time and frequency domain. analysis based on time-frequency transformation (He et al., 2013; Miao et al., 2020a; Ravizza et al., 2021). Thereinto, frequency-domain analysis involves transforming signals from time domain to frequency domain, where the noise components are identified and filtered out. However, this process generally assumes that the signal is stationary, which is often not true for actual vibration signals. Commonly used filters include low-pass, high-pass, band-pass, and notch filters, which are designed to pass signals within a specific frequency range while attenuating other frequency components. For example, a low-pass filter can remove high-frequency noise, but it is difficult to effectively remove noise in frequency band that is close to the signal component. In addition, Kalman filtering technology (Dean, 1986) has been widely applied in vibration signal denoising

(Chen et al., 2017; Erazo et al., 2019; Wernitz et al., 2022). As a recursive algorithm, it produces an estimate of the state of the system as an average of the system's predicted state and of the new measurement using a weighted average. Nonetheless, its denoising effectiveness relies on accurate linear system models, Gaussian noise assumptions, and precise noise covariance parameters, which may fail in highly nonlinear systems or non-Gaussian, complex noise environments.

Different from Fourier transform, wavelet transform (WT) can analyze local changes in both the time domain and frequency domain, thus providing multi-scale analysis of signals. Therefore, WT is suitable for non-stationary signals (Liu & Gao, 2020; Wang et al., 2010). Commonly used WT methods include discrete WT (DWT) (Pasti et al., 1999) and continuous WT (CWT) (Lewis & Burrus, 1998). The WT-based denoising process mainly includes decomposing the signal into wavelet coefficients, thresholding the coefficients to remove noise, and then reconstructing the signal. For instance, Miao et al. (2020b) introduced a signal denoising approach that combines an enhanced median filter with wavelet packet technology. An improved self-adaptive wavelet packet denoising method was employed to eliminate residual white noise. Experimental results indicated that this approach could effectively remove complex mixed noises while preserve important fault detail features of rotating machinery. Even though WT can consider time-frequency domain features simultaneously, its denoising effect is quite sensitive to the selection of wavelet basis functions. Yet, reasonable selection of related parameters in practice often requires sufficient experience and might be objective, thus degrading the automation of denoising process (Chegini et al., 2019).

In addition, researchers have also developed a variety of improved signal denoising methods. For example, empirical mode decomposition (EMD) (Huang et al., 1998) is an adaptive method that can decompose the signal into intrinsic mode functions (IMFs) representing different oscillation modes. By selectively reconstructing the signal, EMD only retains the IMFs representing the actual signal components, which can effectively reduce noise (Zhou et al., 2022). Singular value decomposition (SVD) (Zhao & Jia, 2017) is another classic denoising method as a linear algebra technique. The basic idea is to construct the observed signal into a matrix and use SVD to decompose it to obtain singular values and singular vectors. Since the fact that noise often corresponds to small singular values, the signal component can be separated by retaining the first several largest singular values and their corresponding singular vectors, thereby achieving the purpose of denoising (Yang & Peter, 2003). Variational mode decomposition (VMD) has also proven its capability in vibration signal denoising (Chen et al., 2020; Fang et al., 2023; Zhou et al., 2023). These methods have their respective advantages and disadvantages. In practical applications, no method is universally applicable to all scenarios.

2.1.2 ML-based methods

For tedious vibration measurement of large-scale structures, traditional probability and filtering-based methods are not competent for automatic signal denoising due to the lack of prior knowledge for frequency-band distribution of signal or noise components. The recent rapid development of ML technology has provided a new solution for structural vibration signal denoising. Compared with traditional denoising methods, signal denoising based on ML is expected to avoid complex manual parameter settings and get rid of the dependence on prior information of structures and noise distribution. ML-driven signal denoising technologies, such as autoencoders (Vincent et al., 2010), artificial neural networks (ANN) (Fichou & Morlock, 2018), recurrent neural networks (RNN) (Chen et al., 2024), and convolutional neural networks (CNN) (Gawande et al., 2024), have been widely developed and applied in images (Li et al., 2024) and audio (Kheddar et al., 2024). In essence, by mining the mapping relationship between the original noisy signal as input and the clean signal as output, a denoising

ML model is pre-trained and constructed, thus can be used to remove the noise of new signal as the testing input.

Currently, there are relatively few studies on ML-driven denoising on vibrational signals compared to images or audio. The main obstacle is that it is impossible to obtain purely clean vibration signals in field measurement, which hinders constructing corresponding neural networks without training labels.

Therefore, researchers have sought to utilize a concept of ‘pseudo-clean’ signal to tackle this issue, as depicted in Figure 2-1. Specifically, artificial noise is first injected into the original vibration measurement. Compared to the mixed signals, the initial data can be regarded as comparatively clean, i.e., the ideal signal. In this manner, the original signals can be defined as the ideal denoising output while specifying the mixed ones as the noisy input.

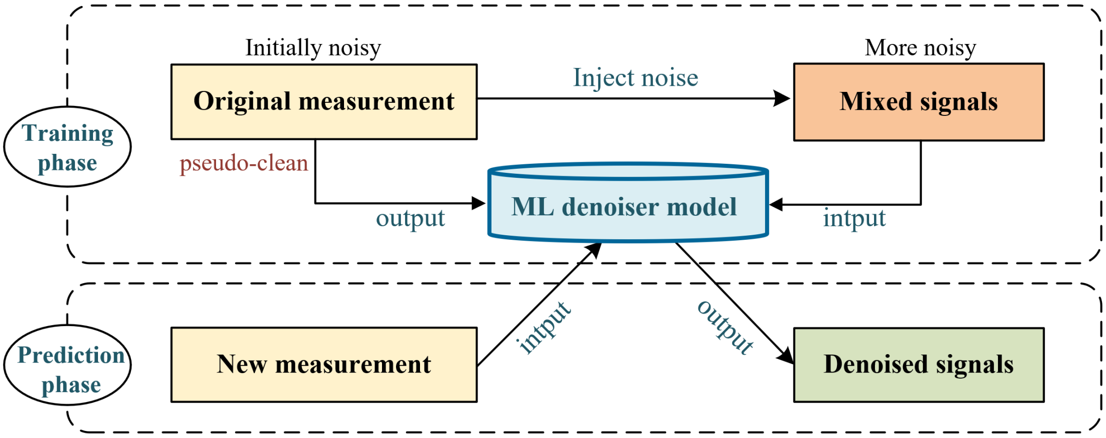

Figure 2-1. Schematic workflow of pseudo-clean strategy in ML-based signal denoising

Remarkably, Fan et al. (2020) proposed a vibration signal denoising method based on residual neural network (ResNet) (He et al., 2016b). In this study, white noise and pink noise were artificially added to the measured acceleration signal. The obtained mixed signal was utilized as the model input while the original signal was trained as the input. In this way, ResNet was well trained in a classic supervised learning paradigm. The effectiveness of the proposed method was verified using monitoring acceleration data from the 600-meter Canton Tower. In addition, the denoising processing was also confirmed capable of improving the accuracy of structural modal identification. However, the model input in this study used the original time-domain data, which exhibited a limitation in extracting high-dimensional features of vibration signals. Particularly, the measured data was first processed with a low-pass filter with corresponding cutoff frequencies set manually. Liang et al. (2023) presented a three-stage ensemble denoising approach that integrates multiple signal ensembles and ML predictions. Features were first extracted using fast Fourier transform (FFT) and WT techniques. A bi-directional long short-term memory (LSTM) network was then employed to denoise the noisy signal, which was combined with the FFT results. A CNN was utilized to create a condensed feature representation of the signal, therewith fully-connected layers generating the final denoised output. The proposed method was validated to be effective in footstep-induced signal analysis. Wang et al. (2022a) devised a denoising network based on an encoder-decoder architecture associated with a joint learning CNN for coupling task implementation of structural diagnosis and signal denoising. Experimental results on bearing systems confirmed this architecture allowing for deep cooperation and mutual learning between the detection task and the denoising task. The research group also performed a similar work on vibration signal denoising using the convolutional autoencoder network (Han et al., 2022). However, pure signals were assumed to be available in these studies which extensively degrade their applicability in engineering practice. Du et al. (2024) utilized a convolutional autoencoder to learn noise modules via encoding and decoding the noise components. A multilevel residual module was designed to address the gradient disappearance problem. In this method, noise learning replaces the traditional clean signal learning. The effectiveness of this method was verified by analog signals and vibration signals of bearing systems with different faults.

As aforementioned, convolutional autoencoder is one of the most popular network architectures used for denoising vibration signals (Shi et al., 2020). The encoder-decoder denoising network architecture is designed to remove noise from input data by encoding the noisy signal into a compressed representation and then decoding it back into a denoised output. The encoder consists of convolutional layers that extract features and downsample the input, while the decoder uses transposed convolutions to reconstruct the original signals from the latent representation. In addition, some state-of-the-art ML algorithms, such as threshold neural network (Zhang, 2001), U-net (Ronneberger et al., 2015) are also investigated for noise reduction, as summarized in Table 2-1.

Table 2-1. Summary of ML-based vibration signal denoising

Authors	**ML architecture**	**Denoising data domain**	**Vibration source**
Fan et al. (2020)	ResNet	Original time history	Canton Tower*
Liang et al. (2023)	LSTM	FFT results	footstep-induced
Wang et al. (2022a)	Convolutional autoencoder	Original time history	Bearing system
Han et al. (2022)	Convolutional autoencoder	Original time history	Bearing system
Du et al. (2024)	Convolutional autoencoder	Original time history	Bearing system
Shi et al. (2020)	Convolutional autoencoder	CWT spectrum	Bearing system
Li et al., (2017)	Threshold neural network (Zhang, 2001)	WT coefficients	Vehicle platform
Xie et al. (2024	U-net (Ronneberger et al., 2015)	Original time history	Elevator
Chen et al. (2023a)	Transformer (Vaswani, 2017)	Original time history	Motor shaft

*Vibration denoising targeted for building structures.

Generally, these denoising models are trained on pairs of noisy and clean signals and optimized by minimizing the difference between the reconstructed and original signals. When ideal clean signals are unavailable, the concept of pseudo-clean signals (as depicted in Figure 2-1) are utilized to define the input-output pairs. However, a common limitation exists in these studies, that is, only particular noise types that have been injected (e.g., white noise and pink noise) were considered. In practical monitoring, the measured vibration signals might contain diverse noise contaminants. Compared to machinery systems, studies on ML-based vibration signal denoising for infrastructures are extensively lacking. It remains challenging to realize fully automatic vibration signal denoising regardless of noise types, especially for those structures without any prior knowledge of noise or signal distribution.

2.2 Seismic response prediction

In performance-based earthquake engineering (PBEE), to evaluate the damage degree of structures under earthquakes at different performance levels, it is necessary not only to calculate the elastic structural response under low-intensity seismic ground motions, but also to comprehensively consider the capacity-demand relationship of the structure under extreme loads through conducting nonlinear dynamic analysis under high-intensity earthquakes, such as IDA or nonlinear time history analysis.

However, nonlinear calculations are often time-consuming and computationally expensive, with obvious time lags, making it difficult to meet the real-time requirements of SSDA. In addition, in vibration-based SSDA, structural seismic response is the basis of relevant data-driven analysis. In actual engineering, the monitoring of vibration responses of structures during sudden earthquakes is prone to problems such as sensor disconnection or data loss, which greatly hinders subsequent vibration-based assessment. Therefore, it is urgent to develop efficient and reliable surrogate models to achieve rapid modeling and prediction of seismic response of structures.

2.2.1 Classic ML regression-based approaches

Recently, with the rapid development of ML technology, building a data-driven surrogate regression model has provided new ideas for structural seismic response prediction. Through ML models, a mapping relationship between seismic excitations (such as ground motions, GMs) and structural dynamic response is constructed to achieve rapid prediction of structural seismic response. According to different types of prediction output, regression-based approaches can be roughly divided into seismic response parameter prediction and seismic response time history prediction, as summarized in Table 2-2.

Table 2-2. Several typical seismic response prediction methods based on ML

	Reference	ML algorithm	Input	Output
Peak prediction	Zhang et al. (2022a)	ANN	GMs	Story drift
	Wen et al. (2022)	CNN	GMs Building inventory	Story drift Peak acceleration
	Oh et al. (2020)	MLP	Intensity measure	Story drift Peak displacement
	Kim et al. (2019)	CNN	GMs	Peak response
	Li et al. (2022a)	ANN+LSTM	Variables of GMs and structures	Shear force Bending moment
Time history prediction	Xu et al. (2022b)	LSTM	GMs	Acceleration
	Zhang et al. (2019)	LSTM*	GMs	Displacement
	Torky and Ohno (2021)	CNN-LSTM	GMs	Displacement
	Perez-Ramirez et al. (2019)	NARX-RNN	Floor acceleration response	Floor acceleration
	Yu et al. (2020)	LSTM+ANN*	Force and system vectors	Acceleration/velocity
	Huang and Chen (2021)	CNN+LSTM	GMs	Drift response
	Li et al. (2022b)	RNN	GMs	Displacement
	Chen et al. (2023a)	Transformer, Informer	GMs	Displacement
	Zhou et al. (2024)	CNN*	GMs, structural matrices	Acceleration/Velocity /Displacement
	Hu et al. (2024)	LSTM*	GMs	Displacement
	Zhang et al. (2024a)	Autoencoder CNN	GMs	Acceleration
	Hao et al. (2025)	CNN+LSTM	GMs, structural parameters	Acceleration

Mark of * denotes integration design with physics-guided mechanism.

Thereinto, the prediction of seismic response parameters is mainly used to predict specific parameters indicative of structural seismic response, such as maximum inter-story drift ratio, maximum displacement, etc. For example, Zhang et al. (2022a) proposed an ANN-based method to predict the seismic response of frame structures. In this model, GM acceleration was used as input, inter-story displacement vector was used as model output. A performance evaluation metric was proposed using drift peak amplitude and maximum amplitude as parameters, which could effectively balance prediction accuracy and training efficiency. Wen et al. (2022) successfully realized the rapid seismic response prediction of reinforced concrete frames with limited building information based on CNN. The network took GMs and five basic building parameters (design intensity, number of floors, floor height, column spacing and total span) as input, maximum inter-story drift ratio and floor peak acceleration as output. The analysis results showed that the proposed method could comprehensively consider the GM dynamics and structural characteristics to a certain extent. Oh et al. (2020) used multilayer perceptron (MLP) to establish the mapping relationship between GMs and structural responses of multi-degree-of-freedom structures. Four parametric features (i.e., average and dominant periods, significant duration, and peak acceleration) were extracted from the GMs as model input and maximum inter-story drift ratio was used as output. The effectiveness of the method was confirmed by multiple sets of artificial GMs datasets.

Different from the prediction of seismic response parameters that provide low-dimensional parametric indicators, time history prediction assigns the time history of the structure response under earthquake action as the prediction output target. For example, Xu et al. (2022b) used LSTM networks to predict the nonlinear seismic response displacement of multi-story frame structures. (Zhang et al., 2019) proposed a data-driven structural seismic response time history prediction method based on LSTM networks. In addition, this study introduced an unsupervised learning (UL) algorithm to cluster earthquake inputs to make full use of the existing training dataset. Torky and Ohno (2021) proposed a hybrid convolutional LSTM network for predicting multi-component seismic response and constructed a mapping relationship between the acceleration time series of the building base and the superstructure. These studies have suggested the feasibility of ML regression algorithms in rapid seismic response prediction.

2.2.2 Physics-informed neural networks

Although ML has been successfully applied in many scenarios for rapid prediction of structural seismic response, its "black box" characteristics lead to poor model interpretability, poor robustness and generalization during the training of surrogate models (Areosa & Torgo, 2019). To overcome these limitations, physics-informed neural network (PINN) has been developed by adding physical information constraints into training process, that is, by introducing physical equations or prior knowledge to constrain model training (Xu et al., 2023). Through ensuring that the prediction results meet specific physical paradigms, the interpretability and robustness of the model are expected to be improved.

PINN may embed physical constraint equations in neural networks in a specific way (such as initial conditions, boundary conditions, loss functions, and optimization constraints). It aims to integrate data-based ML models with physics-based models, combining physical laws and data-driven methods to improve the physical consistency and generalization ability of the model. It is generally believed that the formal concept of PINN was proposed by Raissi et al. (2017) towards the task of solving nonlinear partial differential equations. PINN not only fit data, but also satisfy physical constraints, thus allowing for generating more reliable predictions, and reducing the dependence on large amounts of labeled data. This technique largely compensates for the limitations of traditional “black box” neural networks, especially when dealing with problems involving complex physical phenomena. It has been widely used in fluid mechanics (Cai et al., 2021), energy (Huang & Wang, 2022), chemical (Wu et al., 2023), and other fields. The development and application of PINN in civil engineering and SHM have been summarized by (Cross et al., 2022; Vadyala et al., 2022; Wu et al., 2024).

Nevertheless, studies of PINN for structural seismic response prediction are relatively few, but it has gradually attracted more attention. For example, Zhang et al. (2020) developed a physics-guided CNN for data-driven structural seismic response modeling. In this study, physics-informed mechanism was designed based on the classical structural motion equation:

$$\mathbf{M}\ddot{x}(t) + \boldsymbol{h}(t) = -\mathbf{M}\Gamma\ddot{x}_g(t) \tag{2.1}$$

where $\mathbf{M}$ is the mass matrix, $\ddot{x}, \ddot{x}_g$ are the accelerations of the structure and GMs, respectively, $\boldsymbol{h}$ is the generalized restoring force vector, and $\boldsymbol{\Gamma}$ is the inertial force distribution vector. Assuming that all the above parameters are assumed to be known, this study obtained the loss function definition that satisfies the physical constraints through specific equations. Yet, this assumption is obviously inconsistent with the actual structural situation. Therefore, this study only verified it through an SDOF system with all parameters known. When facing the actual structure, due to the unknown relevant parameters, the loss function of the proposed network directly became the root mean square error in the traditional "black box" mode. Thus, it could not realize real physical information constraint. Similarly, Zhou et al. (2024) proposed a physical information-guided seismic response time history prediction network based on the structural motion equation by performing a specific mathematical formula transformation. In this method, the mass matrix, stiffness matrix and other parameters of the structure were extracted through the refined FEM of the structure. In other words, this method was only applicable to numerical models. Similarly, the verifications in this study were limited to cases using FEM and no verification was performed on the actual structure.

In ML-driven seismic response prediction, a common challenge is that traditional surrogate models often target a single structure or specific measurement points. This limitation leads to redundancy and inefficient resource allocation when multiple networks are required to model various structures. To tackle this issue, it is necessary to incorporate structural uncertainties related to input variables, particularly those linked to GMs. For instance, Li et al. (2024c) developed a structural temporal fusion network aimed at predicting responses of various homogeneous structures with a single model. The method combined seismic waves with structural variables, like the number of stories, to generate diverse time history responses. This method was validated on two numerical experiments, including an ideal SDOF structure and a regular multistory reinforced concrete frame. Essentially, this kind of knowledge fusion can be regarded as certain physics-guided integration. Even advancing progress has been achieved in several circumstances, the structural populations are mostly limited to ideally regular parametrized models, such as SDOF and regular multistory frames. It remains challenging to predict diverse homogeneous structures with a single network, not to mention heterogeneous structures.

In addition to straightforward embedding structural uncertainties, graph neural networks (GNNs) (Scarselli et al., 2008) have been emerging as a feasible solution to fuse structural uncertainties into seismic response predictive models. GNNs are a powerful tool particularly suitable for analyzing and learning from graph-structured data. The flexibility of the GNN architecture enables it to handle graphs with different topologies through representation-learning and message-passing of nodes, edges, and entire, allowing for feasible seismic response modeling across structural population (Wu et al., 2020). Fei et al. (2024) leveraged GNN to develop a surrogate model for elastic drift estimation of shear-wall structures subjected to GMs. Geometric and topological information of buildings and design conditions were fully integrated using their proposed model-to-GNN technique named Graph-GEN (Fei et al., 2023a). Kuo et al. (2024) proposed a fusion model based on GNN and LSTM network that could accurately predict nonlinear structural responses of multiple steel moment-resisting frames. In this study, the prototype of structural information was transformed into graph-structured data, in the form of multidimensional tensors that preserved the geometric properties and physical details of the buildings. Song et al. (2022) devised a GNN-based surrogate model to predict the elastic static response of numerical frame structures. A self-supervised learning paradigm driven by structural mechanics was employed to release the model from the demand in training data.

These research cases have demonstrated the powerful capability and feasible potential of GNNs in accelerating seismic response modeling for structural populations. Nonetheless, the idea is still at its initial stage, where objectives are limited to homogeneous structures with regular parameters. To this regard, further endeavor needs to be devoted to gaining a deeper insight into physics-informed and GNN-based approaches for seismic response prediction.

2.3 Structural condition assessment

As a key indicator for evaluating the post-earthquake safety and integrity, damage levels of a structure reflect the overall damage severity to the structure after suffering an earthquake. Compared with the local damage of a single component, damage levels of the structure can better characterize the decline in the overall seismic performance of the structure, which helps to quickly assess the condition of the affected structure and provide foundation for risk-informed decision making. The quantification of damage levels is closely related to subsequent functional assessment, repair plan formulation, and economic loss assessment. The traditional empirical methods based on earthquake damage investigation, or the analysis methods based on model evaluation have been discussed in Section 1.2.1. This section mainly reviews the literature on ML approaches for vibration-based structural damage identification.

The identification of structural damage levels driven by ML algorithms is essentially a classification or clustering problem, that is, to construct a mapping relationship between structural vibration signals and damage categories. For example, when the damage classification criteria are given, the degree of structural damage can usually be divided into intact, slight damage, moderate damage, severe damage, and destruction. In actual operation, according to the specific data availability and analytical depth requirements in different scenarios, the identification of structural damage includes binary damage detection (healthy or damaged state) and multi-class damage classification.

In traditional damage identification algorithms, different ML models are often trained using a large amount of labeled data in a supervised learning paradigm, that is, to establish a mapping relationship between structural vibration signals and corresponding damage levels (i.e., labels) (Das et al., 2016; Toh & Park, 2020; Wang et al., 2025). These supervised learning algorithms require sufficient labeled data of structures in different damage conditions so that the model can be fully trained and make accurate predictions. However, in actual engineering, data on structures in damaged states are often extremely scarce compared to that in normal service states. For example, compared to intact or slightly damaged structures, instances of severe damage may be rare. This imbalanced distribution of training data labels (also known as a “long-tail” distribution (Fei et al., 2023b) can easily lead to large deviations in the model when predicting small-sample categories (He & Garcia, 2009).

In the realm of ML-based damage identification, pervasive conflict exists in algorithm applicability versus data availability, as depicted in Figure 2-2. Generally, the supervised learning algorithms manifesting satisfactory precisions (in a side-by-side comparison) possess poor applicability in engineering practice. The scarcity and imbalance of training data labels pose a huge challenge to data-driven structural condition assessment or damage identification assisted by ML technology.

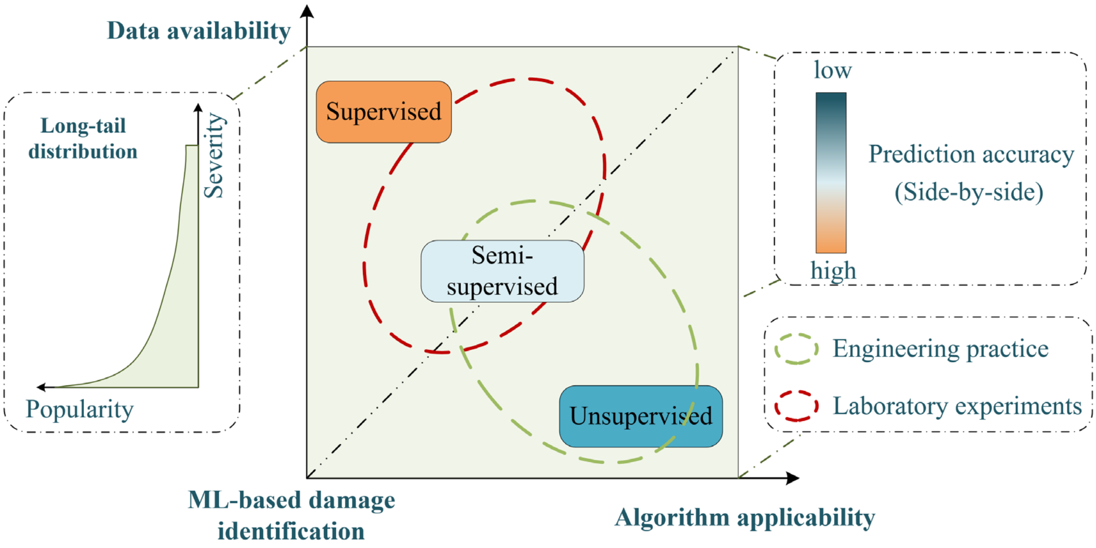

Figure 2-2. Algorithm applicability versus data availability in ML-based damage identification

To cope with the above difficulties, researchers began to explore more advanced ML algorithms for structural damage identification using limited labeled data. According to the principle of solving the problem of data scarcity in different data availability scenarios, these methods mainly include weak-supervised learning algorithms, transfer learning (TL) algorithms, and DAug algorithms (Bull et al., 2020), as summarized in Table 2-3.

Table 2-3. Main strategies to solve data scarcity with diverse data availability scenarios

Data availability	Imbalanced data	No labeled data	Limited labeled data
Strategy	Weak-supervised	Knowledge transfer	DAug
ML algorithms	Semi-supervised Unsupervised	Transfer learning	Generative ML

Specifically, weak-supervised learning algorithms aim to uncover clustering patterns between datasets in a semi-supervised (relying on partial labeled data) or unsupervised (completely independent of any labeled data) training manner. The TL algorithms mainly introduce a large amount of labeled data that is easy to obtain in the source domain to train the model and then use it to diagnose target structural damage with missing labeled data. More other TL paradigms will be elaborated subsequently. It is essentially a cross-domain knowledge transfer process from the source domain to the target domain. As the name suggests, the DAug algorithms expand the existing limited data and increase the number of samples in the training data set, thereby achieving the purpose of improving the prediction accuracies.

The above three categories are reviewed as follows.

2.3.1 Weak-supervised learning approaches

Unlike supervised learning, relying on a large amount of labeled data for training, weak-supervised learning utilizes partial labeled samples (such as semi-supervised learning, SSL) or gets fully rid of labels (i.e., UL). In vibration-based structural damage identification, the monitoring data of the structure under normal service conditions (healthy state) is generally easy to obtain and huge in quantity, both SSL and UL can be applied.

Specifically, UL does not require any labeled data. Instead, it automatically identifies abnormal patterns or clustering features from the original unlabeled data by mining the intrinsic structure and patterns of the data itself, thereby detecting abnormal structural damage states or damage levels. Typical UL algorithms include clustering (Saxena et al., 2017), dimensionality reduction (Nanga et al., 2021), and outlier detection (Wang et al., 2021), etc. Among them, the core of clustering algorithms is to divide the data into different clusters based on the similarity between clustering samples and then optimize the clustering pattern based on clustering quality assessment. Numerous clustering algorithms have been developed based on different similarity measurement benchmarks, such as the distance-based K-Means algorithm (Krishna & Murty, 1999), the density-based DBSCAN algorithm (Sander et al., 1998), the connectivity-based hierarchical clustering algorithm (Nielsen & Nielsen, 2016), and the graph-based spectral clustering algorithm (Von Luxburg, 2007).

Cha and Wang (2018) improved the original density peak-based clustering algorithm into an UL method for structural damage detection and location by adding training and testing processes. Based on the CWT, the sensitive features of structural damage were defined, cluster analysis was carried out on this feature space, and the Gaussian kernel function was introduced to calculate the local density of sample points, thereby improving the model performance. The effectiveness of this method was verified using a scaled steel frame structure. Ghiasi et al. (2024) developed a data-driven anomaly detection method to evaluate and identify geometric defects of tracks. In this study, the acceleration response collected when the train was running in the intact track area was used as the input of a one-class support vector machine (OCSVM), and the abnormal feature parameters were defined as the relative change from the intact state. The effectiveness of this method was verified using field measured data of a high-speed train in France. Wan et al. (2025) introduced an UL approach for detecting structural anomalies using a deep convolutional variational autoencoder (DCVAE) for feature extraction, combined with support vector data description (SVDD) for anomaly detection. Zhu et al. (2025) introduced an innovative approach that combines an attention-guided conditional latent diffusion probabilistic model with SVDD to detect anomalies in structural data under changing environmental conditions. The proposed method enhanced detection accuracy by modeling the conditional probability distribution of monitoring data, incorporating low-dimensional latent representations, and utilizing an attention mechanism to capture features from multi-source data.

Entezami et al. (2023) proposed an outlier detection method by combining the DBSCAN algorithm (Sander et al., 1998) and the spectral clustering algorithm (Von Luxburg, 2007), which was verified using the long-term modal frequencies data of two actual bridges. In addition, the research team also modeled the time series of structural vibration signals based on an autoregressive model. On this basis, two damage indicators were defined using the parameters and residuals of the autoregressive model.

Then, based on the distribution characteristics of the damage indicators in the healthy state, the limiting thresholds of the two damage indicators were determined, thereby realizing unsupervised monitoring of structural damage (Entezami & Shariatmadar, 2017). Recently, the team also proposed a non-parametric clustering method for structural damage detection with limited vibration data (Entezami et al., 2024). In this study, the limited vibration data was first divided into different clusters to capture the underlying patterns and characteristics of the data. Then, a density-based damage indicator was developed to carry out damage alarms based on set thresholds. Similarly, the effectiveness of this method was validated using short-term modal frequency monitoring data of an actual bridge structure.

Noteworthily, one of the keys to developing UL algorithms for damage identification lies in the definition and acquisition of damage sensitive features (DSFs) (Solorio-Fernández et al., 2020). Then on this basis, the structural damage state can be judged according to threshold setting or clustering analysis.

SSL has a certain degree of dependence on labeled data between that of supervised learning and UL. It generally involves label propagation or data clustering through partially labeled data. SSL makes full use of the limited labeled data and unlabeled samples to assist in training the classifier model. Compared with UL algorithms, it can effectively improve the accuracy and generalization performance of the predictive model. Classic SSL algorithms include label propagation methods, autoencoder-based methods, generative learning methods, etc. Thereinto, label propagation uses the label information of labeled samples to predict the category labels of unlabeled samples through graph structure propagation. At present, it is relatively rarely used for structural damage identification (Hao et al., 2023b; She & Wang, 2022; Wen & Changzhi, 2022). The generative learning methods will be elaborated subsequently in the context of DAug in Section 2.3.3. In addition, techniques such as autoregressive models (Kauss et al., 2024), graph neural networks (Huang & Burton, 2022), genetic algorithm (Silva et al., 2016), Bayesian theory (Rogers et al., 2019) are also investigated for structural damage identification in an SSL schema, which are not included in this section for conciseness.

Deep autoencoders (DAEs) based approaches have gained wide attention in the field of structural damage identification in recent years due to their powerful performance in extracting DSFs. Silva et al. (2021) utilized DAE to extract DSFs from raw vibration data for structural damage detection. In this study, a high-dimensional modal parameter matrix was defined as the input of the DAE and compressed into a lower-dimensional feature space. The output feature space of the DAE was eventually used as the input feature of linear classifiers. Validations were performed on the field monitoring data of an actual bridge. Wang and Cha (2020) proposed a weak-supervised learning method based on OCSVM and DAE. To achieve structural damage detection under limited label data, this method first used acceleration data in a healthy state to train the DAE as a feature extractor and then input the extracted damage features into the OCSVM as a damage classifier. The proposed method was successfully verified using a numerical model of a 12-story building structure and a laboratory structure of a steel bridge. Following this strategy, Pollastro et al. (2023) proposed an SSL damage detection method utilizing a variational autoencoder to substitute the DAE combined with OCSVM. Similarly, Rastin et al. (2021) trained a convolutional DAE with health status data for data compression and then used the difference in compressed data between the signal to be tested and the healthy signal to define DSFs. Structural damage detection was achieved by comparing the extracted DSFs with the set threshold.

The general workflow of the weak-supervised learning approaches towards damage identification is shown in Table 2-3. In the UL paradigm, DSFs are first obtained from sample data, and then damage detection is conducted based on threshold setting or realizing damage quantification using clustering analysis. In the SSL paradigm, damage labels are extended from limited available labeled samples to those unlabeled samples using some label propagation strategies. Particularly, the obtained DSFs assigned with corresponding pseudo-labels are utilized to train a damage classifier in a supervised way. The trained classifier can be functionalized as the predictive model of damage levels or scenarios.

Noteworthily, for both damage identification using SSL and UL approaches, the accuracy of the predictive models depends primarily on the effectiveness of the extracted DSFs, that is, damage sensitivity; on the other hand, the credibility of the pseudo-labels assigned to unlabeled samples also directly affects the training performance of the final damage classifier. Thus, more in-depth attention is needed for the credibility of the pseudo-labels assigned to unlabeled samples in the further work of the related scope.

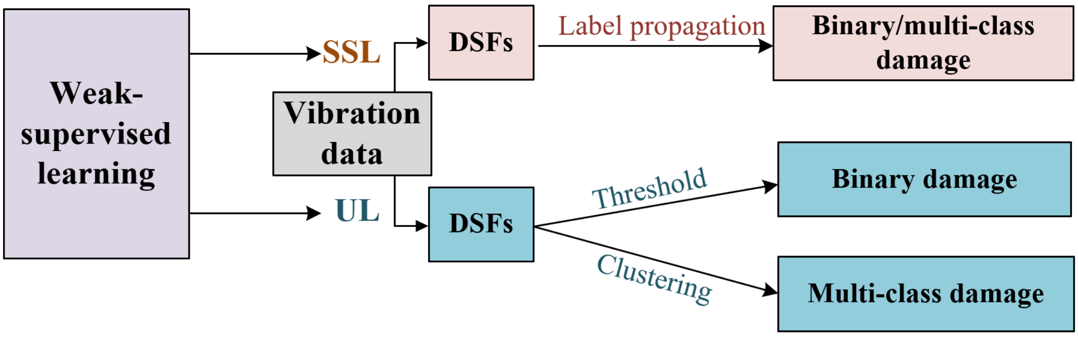

Figure 2-3. Classic workflow of weak-supervised damage identification

2.3.2 TL-based approaches

Unlike traditional supervised learning algorithms, TL does not require training a completely new model from scratch. Instead, it effectively leverages knowledge from labeled data in the source domain to enhance performance in the target domain. According to different knowledge transfer strategies, TL algorithms are primarily categorized into parameter-based (or model-based), instance-based, feature-based, and relational-based methods (Zhuang et al., 2020). In the field of structural damage assessment, parameter-based TL algorithms are predominant. Therefore, the term TL in the remainder of this thesis will specifically refer to parameter-based TL unless otherwise specified.

In practice samples of damage state are far less than those of undamaged/healthy condition, researchers have sought to use numerical simulations, such as FEM, to acquire response data for structures under various damage conditions. Therefore, source domain data with rich labels can be utilized to compensate for the scarcity of labeled data in the target structure, making TL another promising avenue for structural damage assessment (Lin et al., 2021).

Typically, in TL methods, a model is first pre-trained using source domain data and then fine-tuned with limited target domain data to achieve effective damage diagnosis in the target domain (Zhang et al., 2024b). To achieve satisfactory knowledge transfer from the source domain to the target domain, it is essential that the joint probability distribution between structural response data and damage labels in different domains remain identical or highly similar (Pan & Yang, 2010). However, due to various influencing factors such as computational assumptions, material properties, loads and boundary conditions, the results of numerical simulations inevitably differ from those of real structures. The different data distribution characteristics between the surrogate model (source domain) and the prototype structure (target domain) can significantly diminish the effectiveness of knowledge transfer, leading to poor cross-domain prediction performance (Li et al., 2023b).

The cross-domain heterogeneity between the source and target domains poses significant challenges for structural damage assessment using TL algorithms. The data distributions within different domains often exhibit distinct probability distributions, feature spaces, and semantic relationships, necessitating specific measures to reduce these disparities between domains. As an important subfield of TL, DA (Farahani et al., 2021) has garnered increasing attention in recent years due to its effectiveness in addressing the challenges associated with cross-domain knowledge transfer.

Classic DA methods include joint domain adaptation (JDA) and transfer component analysis (TCA). In the JDA approach, a classifier trained on source domain data is used to predict pseudo-labels for target domain samples. This is followed by minimizing the difference in joint distribution or marginal distribution, whilst maximum mean discrepancy is usually measured to optimize predictions for target domain samples (Gardner et al., 2021; Giglioni et al., 2024). Similarly, in the TCA method, iterative optimization based on a loss function is achieved by learning a nonlinear transformation from the feature space to a Hilbert space (Gardner et al., 2020). Although these methods do not rely on labels from the target domain, they still require a substantial amount of target domain sample data for pseudo-label prediction and optimization training.

In recent years, DA methods based on Generative Adversarial Networks (GANs) (Goodfellow et al., 2020) have gained increasing attention, as they utilize generative adversarial learning to align the feature distributions of different domains (Brophy et al., 2023; Chen et al., 2023b; Qin et al., 2021; Martakis et al., 2023). Xu and Noh (2021) proposed a multi-domain adversarial learning framework for cross-domain structural damage identification. This framework employs a generative adversarial DA approach to extract domain-invariant feature representations from data collected from different buildings. The feature extraction network and the damage prediction network are trained in an adversarial schema, ensuring that the extracted feature distribution effectively characterizes structural damage states and maintains robustness against variations in structural characteristics. The effectiveness of this method has been successfully validated using numerical simulations and field measurement data from multiple building structures. Similarly, Wang and Xia (2022b) introduced a re-weighted generative adversarial DA method for cross-domain structural damage identification. Considering that the label spaces between the source and target domains may not be consistent, a weight parameter was introduced to enhance the importance of the shared label space during DA process. The proposed method simultaneously trains a feature generator and two classifiers (a domain discriminator and a damage classifier) using generative adversarial techniques, allowing it to learn domain-invariant damage-sensitive features for damage identification in target structures. The effectiveness of this method was validated using numerical and experimental data from a simply supported beam and a cantilever beam. Liu and Fang (2024) utilized the target and source domain data to jointly pre-train a DAE for feature extraction, after which a supervised fine-tuning was performed on the trained model. This method was confirmed to be capable of achieving cross-domain damage identification between a plane frame and three-dimensional frame structure. Zeng et al. (2025) integrated two DA techniques, cycle-consistent GAN and domain-adversarial neural network to translate measurement of different miter gates into a unified domain for their damage detection. Although these studies have achieved satisfactory results in cross-domain damage identification under various scenarios, they share a common limitation: the need for a sufficient amount of target domain sample data when training the feature extraction and damage identification networks adversarially. Even though these target domain samples are unlabeled, the applicability of adversarial learning-based DA methods is significantly reduced in situations where target sample data is scarce, such as in online damage detection without any prior knowledge.

Zero-shot TL, unlike conventional TL, refers to the ability to seamlessly transfer knowledge from the source domain to the target domain for task learning and generalization without any training samples for the target task (Rohrbach et al., 2011). With ability to make predictions on tasks that have never explicitly been trained on, zero-shot TL is particularly useful in scenarios where labeled data is scarce or unavailable for certain tasks. Due to the stringent requirements for data availability and knowledge transfer paradigms, current research on zero-shot knowledge transfer for structural damage diagnosis is extremely limited.

Recently, Soleimani-Babakamali et al. (2023) proposed a zero-shot TL algorithm framework for structural damage detection. In this study, under the condition of only providing health status data for the target structure, a DA module transfers binary knowledge of healthy or damaged states from the source domain to the target domain, enabling damage detection in the target structure. Experimental results indicate that this method successfully achieves cross-domain damage detection among three heterogeneous target structures. However, this approach has two limitations. First, it requires enough labeled data for the health status of the target structure for training, which prevents it from being applicable to strict zero-shot knowledge transfer (without labels or data). Second, the proposed method is limited to binary damage detection and cannot quantify different levels of structural damage. Notably, it remains as a challenge to achieve the zero-shot knowledge transfer for structural damage diagnosis.

2.3.3 DAug approaches

In addition to weak-supervised learning and TL methods, DAug is another important approach to address the issue of data scarcity in structural damage detection. As a commonly used data preprocessing technique in the field of ML, DAug aims to generate new effective samples from existing training data, either artificially or algorithmically, thereby expanding the scale and diversity of the training set. This, in turn, enhances the model's generalization capability and reduces the risk of overfitting. For one-dimensional (1D) time series data (such as vibration data), conventional DAug methods include adding noise, interpolation, stretching, sliding window sampling (Iglesias et al., 2023), etc. However, the affine transformations can only generate samples that are highly correlated with the original data and cannot synthesize diverse data.

Benefiting from the rapid development of DL, deep generative models (DGMs) have emerged as a promising research area in the field of DAug in recent years. They provide a framework for generating synthetic data that aligns with the characteristics of real data. Among these models, one of the representative generative models suitable for augmenting 1D time series data is generative adversarial network (GAN) (Goodfellow et al., 2020).

As a powerful tool originally designed for generating two-dimensional images, GANs have made significant research advancements in the field of structural damage detection based on computer vision (Dunphy et al., 2022; Gao et al., 2019; Gao et al., 2021). Recently, researchers have gradually introduced GANs into the domain of vibration-based structural damage identification. For instance, Luleci et al. (2023) successfully used a deep convolutional GAN to augment labeled acceleration data. In this network architecture, Wasserstein distance was introduced as the loss function, and gradient penalty was embedded to improve network training. On a steel frame experimental model, the proposed method augmented the sample data with 60 training samples for both healthy and damaged states, and the results indicated that the generated data effectively enhanced the prediction accuracy of the CNN damage detection model. Similarly, Wan et al. (2021) employed a deep convolutional GAN integrated with structural information to augment monitoring data for bridge structures. This model generated new data by learning and integrating the coupling relationships among various bridge monitoring factors, and spectral normalization was introduced to optimize the weight training process. The proposed method was successfully applied to a binary damage detection task for a specific bridge structure. These studies demonstrate the feasibility of using GANs to augment structural vibration signals. However, most of these studies are limited to binary damage detection, exhibiting significant limitations in algorithm applicability when addressing multi-class damage severity quantification tasks.

In addition to the GAN architecture, other DGMs have also shown potential in time series modeling. For instance, deep autoregressive models are well-suited for time series processing as they generate data sequentially, aligning with the physical logic of real-time series generation (Wang et al., 2023c). Another alternative strategy is the Variational Autoencoder (VAE) (Kingma & Welling, 2019). As a deep generative model for UL, VAE first compresses high-dimensional data into a lower-dimensional latent space and then reconstructs the output. Notably, unlike the deterministic latent variables in the DAE, the latent variables in VAE are probabilistic; that is, given an input, the latent variables follow a certain probability distribution (e.g., Gaussian distribution). DAE aims to learn an efficient encoded representation of the input data by minimizing reconstruction errors, enabling accurate reconstruction of the input data. In contrast, VAE is optimized by minimizing the difference between the input data and the reconstructed data, as well as the divergence between the latent variable distribution and the standard Gaussian distribution (variational inference). This allows VAE to learn the latent probability distribution of the input data, enabling it to generate new samples similar to the training data, thus demonstrating superior applicability in data generation and augmentation. For example, Li and Betti (2023) proposed a DAug method based on conditional VAE to generate samples of structural acceleration response power cepstrum coefficients under various damage states. In this method, the statistical distribution of power cepstrum coefficients is utilized as a feature for signal representation, effectively performing the DAug process in the indirect data space. Although this method has been validated through numerical and experimental cases, similar limitations persist, as the damage classification is performed in a binary mode.

In the field of vibration-based structural damage detection, augmenting vibration signal data not only requires the generation of diverse samples that closely resemble real conditions but also necessitates the ability to associate different structural damage states. In other words, data generation needs to occur within a class-conditional framework. Compared to image data generation, there is currently limited research on achieving class-conditional DAug for time series data using DGMs (Wen et al., 2020).

Moreover, in practical engineering scenarios, there are significant disparities in the label distribution of sample data across various damage states. Data for healthy structural conditions is often abundant, while data for damaged states tends to be scarce. This persistent imbalance in data can lead to DGMs being biased towards the majority class (e.g., healthy states), resulting in ineffective learning of the characteristics of minority classes (e.g., moderate or severe damage) (Oksuz et al., 2020). However, in the realm of SSDA, related studies on class-conditional vibration DAug are comparatively limited at present, more in-depth research can be investigated with more advanced ML networks in the future.

2.4 Summary and challenges

Approaches integrating physics-based and ML techniques to address the three key data issues in vibration-based SSDA have been reviewed. Although considerable progress has been achieved in related task implementation to deal with data noise, data loss and data scarcity issues, there are several challenges to be further addressed:

(1) Without sufficient input-output pairs of training samples due to the inaccessibility of purely clean signals of as-is structures, conventional ML regression-based denoising networks can be hardly applied to vibration signals. Compared to machinery systems, studies on ML-based vibration signal denoising for civil structures are extensively lacking. ML-based approaches toward fully-automatic vibration signal denoising need to be explored further.

(2) Regression-based ML techniques manifest poor interpretability as ‘black-box’ models in developing surrogate models for seismic response prediction. PINNs provide a promising strategy via embedding physics-informed mechanisms. However, most existing physics-informed strategies rely on structural dynamic parameters (such as mass, stiffness matrices) and can be hardly applied to real-world structures. Specialized parameter-free PINN with superior applicability is worthy of developing for structural

seismic response prediction.

(3) As a widely-existed issue in vibration-based SSDA, data scarcity impedes practical applications of conventional ML techniques in structural condition assessment. More advanced ML algorithms, such as weak-supervised learning methods (SSL, UL), TL methods and generative learning for DAug, have been widely studied in recent decades. However, some challenges exist and need to be further addressed:

- Specifically, in weak-supervised methods, accuracy of extracted DSFs and credibility of assigned pseudo-labels have a direct impact in prediction performance. Special attention needs to be paid to these two aspects for improved label propagation.
- In TL approaches, domain bias between the source domain and the target domain poses great obstacles in reliable cross-domain knowledge transfer. Most DA approaches rely on extensive target-domain data, which degrades applicability to circumstance without sufficient target data. Few-shot and zero-shot TL approaches toward SSDA are comparatively lacking at present.
- Regarding the DAug approaches for enhanced structural condition assessment, persistent imbalance in training samples shall result in biased learning towards the majority undamaged class whereas ineffective learning of the minority damaged classes. Class-conditional DAug method with joint consideration of class-imbalance issues is worthwhile further study.

This study will address the above difficulties and carry out research in the following chapters.

CHAPTER 3 DEEP CONVOLUTIONAL IMAGE-DENOISER NETWORK FOR VIBRATION SIGNALS

Typically, to train a DL model for vibration denoising, pairs of noisy and clean samples of vibrational signals are needed for input-output training. However, in practical scenarios, clean spectra (the training output) are often unavailable, posing a significant obstacle to the denoising task. In this chapter, a novel signal denoising approach based on deep convolutional image-denoiser network (DCIMN) is proposed. In this method, specified strategies with novelties including noise injection in label definition, dimension expansion in feature extraction, and optimizer embedding in encoder-decoder are utilized to enhance the denoising performance. This method does not require an exactly noise-free training dataset or any prior knowledge of input signals.

3.1 The proposed DCIMN

Vibration signal data are 1D time-series data. The signal spectrum can be plotted into a spectrogram, which is a 2D representation containing high-dimensional signal information. Besides, CNN consists of multiple convolutional blocks and is ideal for processing 2D images. It can automatically extract high-order features of input data via convolutional kernels. CNN is efficient in extracting features in speech recognition and reducing noise in images (Ghose et al., 2020; Singh & Shankar, 2021).

Therefore, this chapter extends the superiority of both spectrogram and CNN to perform the denoising task of 1D vibration signals. A novel signal denoising network named DCIMN is proposed. In this method, the 1D vibration signal is first converted into a 2D spectrogram using STFT to expand the feature extraction dimension. Then, pseudo-clean label definition is performed through the addition of artificial noise to generate pairs of input-output training data. Subsequently, an image denoising network is constructed based on a deep convolutional encoder-decoder architecture. By inputting the spectrogram of the signal to be tested into the trained model, a denoised spectrogram can be generated. The denoised 1D time-domain signal is then reconstructed using inverse STFT (ISTFT). The main process of the method is shown in Figure 3-1. Detailed methodologies are elaborated as follows.

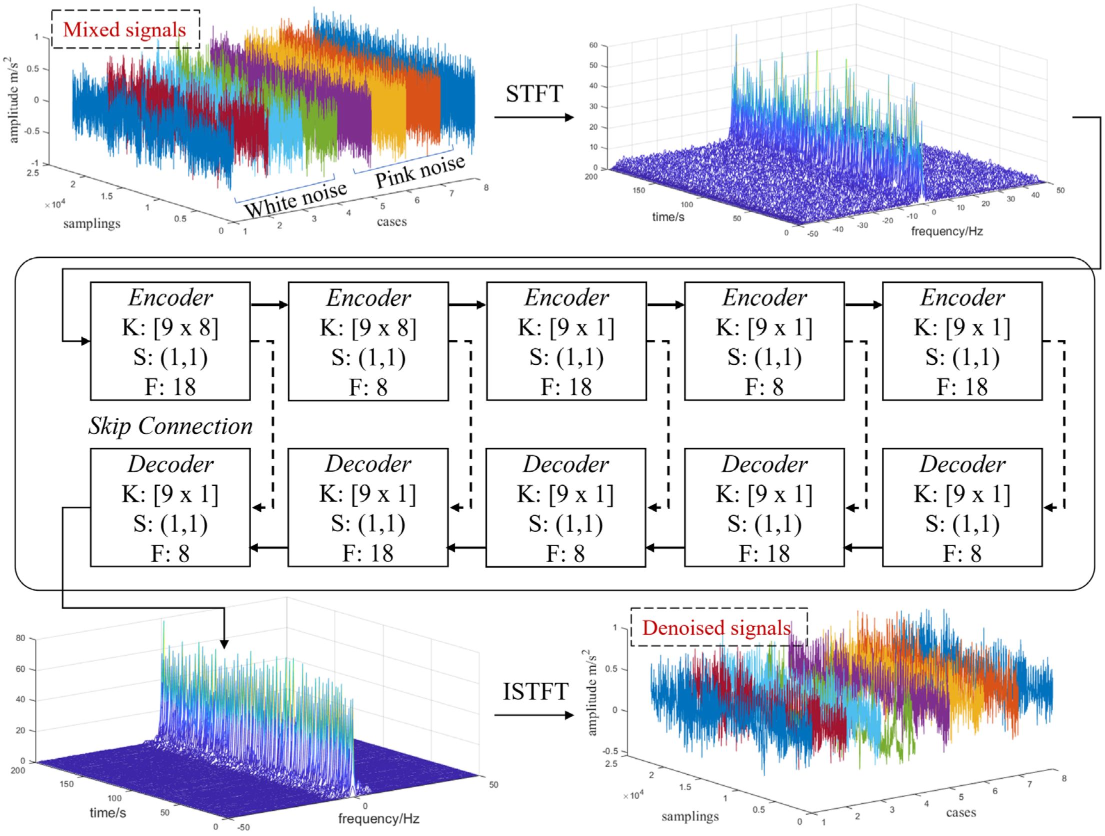

Figure 3-1. Workflow of signal denoising using the proposed DCIMN

3.1.1 STFT processing and pseudo-clean label definition

To obtain the spectrogram of vibration signals through STFT, discrete Fourier Transform (DFT) is performed within a sliding window. By moving the window function, the spectral information of the signal at different time points can be obtained, allowing the signal characteristics to be observed simultaneously in both the time and frequency domains. The fundamental parameters to determine a window function include mainly window type, window length and hop size, which need to be set manually according to the knowledge of processing signals, such as sampling frequency.

Without loss of generality, a periodic Hamming window with a length of 256 and a hop size of 64 in adopted in this chapter. The squared magnitude of the STFT represents the power spectral density of the function. The magnitude vector is extracted from the 256-point STFT vector, and after eliminating half of the symmetry, the first 129 points are retained. Subsequently, consecutive spectra are concatenated to form the input through window sliding. As a result, the original 1D vibration signal is transformed into a 2D representation with dimensions of ($129 \times N_f$), where N_f refers to the frame numbers determined by the sliding process along the whole-length signals.

Considering that it is impossible to obtain a completely pure signal in the measured signal, this chapter adopts the pseudo-clean concept as elaborated in Figure 2-1. That is, by artificially adding noise to the original measured signal, the measured signal can be regarded as "relatively pure" compared to the obtained mixed signal. During the training process, the mixed signals are used as the model input, and the original measured signals are used as the output. In this way, a mapping relationship between the clean signal spectrum and the spectrum containing the additional noise components can be established. Furthermore, when the model training is completed, given the real vibration signal of the structure, the trained model can reconstruct and predict the spectrum that eliminates the corresponding noise components. In this way, the construction of a labeled training set can be achieved without any prior knowledge.

Field observations could be contaminated by various types of noise. It is impractical for a denoising method to be only susceptible to eliminating specific kinds of noise in SHM. Without loss of generality, two typical kins of noise, i.e., white noise and pink noise are considered in this study. Among them, the embedding method of white noise is as follows:

First, the vibration signal without noise is trained as a target. In contrast, the synthetic noisy signal allocated for white and pink noise separately, with different noise levels varying from 20% to 80% are trained as predictors. Specifically, white noise is injected as follows:

$$\tilde{X} = X + \Omega \times L_n \tag{3.1}$$

where X is the original measured signal; $\tilde{X}$ is the mixed signal after embedding noise; Ω is a zero-mean normally distributed random vector with the same standard deviation as the original signal, and L_n is the noise level. This study considers four different noise levels of 20%, 40%, 60% and 80%.

Unlike white noise where the energy intensity is evenly distributed throughout the frequency band, the power spectral density of pink noise is inversely proportional to the frequency. The method of embedding pink noise to generate a mixed signal is similar to that of white noise, using formula (3.1). The difference is that the noise vector becomes a time series of pink noise with a zero mean and a standard deviation equal to the standard deviation of the original signal.

3.1.2 Convolutional encoder-decoder network

Unlike the basic concept of the traditional encoder-decoder architecture, which first encodes input data into a low-dimensional representation space and then reconstructs it to the original dimension, the denoising network described in this section maps the input spectrum to a higher-dimensional feature space in the encoding layer for redundant representation. Subsequently, in the decoding layer, the features are projected back to their original dimensions, producing the clean signal spectrum as output. This method of reconstructing signals through redundant feature representation has been successfully applied in audio signal processing (Park & Lee, 2016). Based on the convolutional encoder-decoder architecture (Vincent et al., 2010), this section builds the DCIMN with the architecture shown in Figure 3-2. The basic idea is to extract redundant representations of a noisy spectrum at the encoder and map it back to a clean spectrum at the decoder. The entire processing can be regarded as mapping the spectrum to a higher dimension and projecting the features back to a lower dimension.

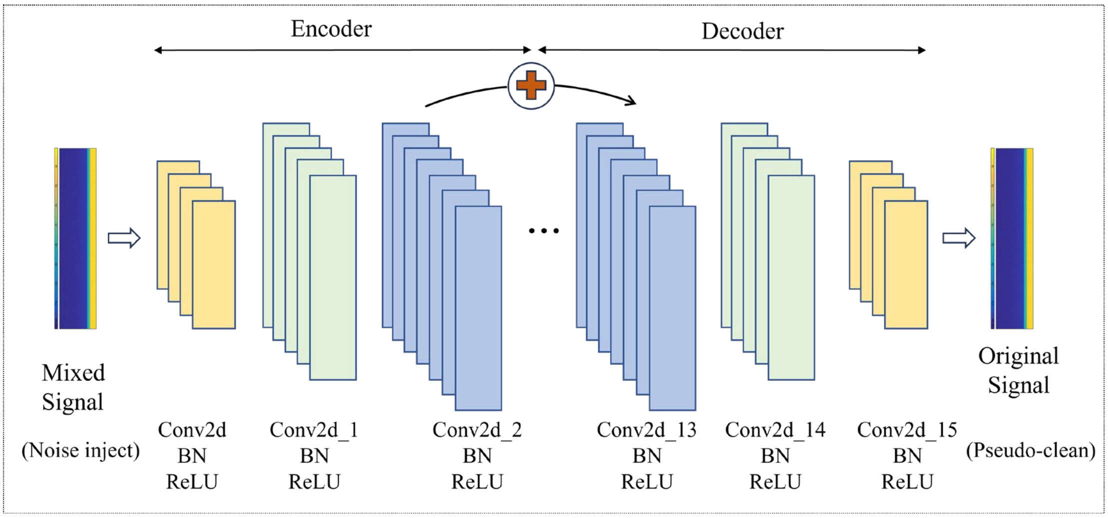

Figure 3-2. Architecture of the proposed DCIMN

The proposed denoising network consists of repetitions of a convolution, batch-normalization (BN), max-pooling, and a ReLU activation layers. The network consists 16 of such blocks with a total of 33000 parameters. The Adam optimizer with 0.0003 is used to optimize the training output. The spatial dropout is set as 0.2 for the entire training process. Similar to Resets (He et al., 2016a), skip connections are deployed between convolutional blocks, allowing information to be passed across different layers. This helps accelerate model convergence and reduces the risk of gradient vanishing.

Given a segment of noisy spectrogram $\{x\}$ and clean spectrogram $\{y\}$, the aim is to learn a mapping f which generates a segment of denoised spectrogram that approximates the clean one. The denoising function can be expressed as follows:

$$\underset{\Theta}{\arg\min} \frac{1}{N} \sum_{k=1}^{N} \left\| y_k - f_\Theta(x_k) \right\|_2^2 \tag{3.2}$$

where N is batch number; Θ is the training parameters of the denoising network. The subscript k refers to the k-th element of $\{x\}$ and $\{y\}$.

3.1.3 Evaluation indicators for denoising effectiveness

3.1.3.1 Linear parameter indicators for signals with prior knowledge

For those signals with known prior information, it is an effective and straightforward method to evaluate the denoising effect through actual parameters, namely the signal-to-noise ratio (SNR) and the root mean square error (RMSE), which can directly describe the statistical characteristics and noise-level information of signals. Specifically, the SNR of a system or component is defined as the ratio of signal level to the noise level and is expressed in decibels. It is calculated by dividing the signal power by the noise power as follows:

$$SNR = 10\log_{10}\left(\frac{\sum_{i=1}^{n} x_i^2}{\sum_{i=1}^{n} (\tilde{x}_i - x_i)^2}\right) \tag{3.3}$$

where x means clean signal series; and $\tilde{x}$ means the noisy signal series. Generally, the more SNR is, the better the denoising effect will be.

3.1.3.2 Nonlinear systematic indicators for signals without prior knowledge

(1) Correlation dimension

Signal frequency bands usually overlap with noise due to the broad frequency spectrum and pseudo-random characteristics in chaotic time series such as vibrational signals. It is difficult to directly recognize the noise or signal component from raw series. Consequently, the linear parameter evaluating indicator method or conventional signal processing techniques based on the probability and statistics model are no longer suitable for denoising vibrational signals without prior conditions (Lim & Puthusserypady, 2007). Thus, a nonlinear time series analysis method will be adopted in this chapter. It is mainly based on phase space reconstruction where m-dimensional phase space coordinates are formed by time-delay embedding of 1D observations. In practice, a 1D time series $x(t_i)$ with a delay time τ is used as coordinates to represent vector S_i in the reconstruction space of dimension M, which is set to 4 in this study:

$$S_i = [x(t_i), x(t_i + \tau), \ldots, x(t_i + (M-1)\tau] \tag{3.4}$$

Then the vibration signal is transformed into the reconstructed phase space, from which the essence of the underlying dynamics can be extracted (Ambika & Harikrishnan, 2020).

In chaos theory, the correlation dimension is a measure of the dimensionality of the space occupied by a group of random points, usually called a fractal dimension. Grassberger and Procaccia (1983) introduced this technique to distinguish chaotic behavior (deterministic) and truly random motions. For N sampling points in m-dimensional phase space, the correlation integration is defined as follows (Abraham et al., 1986):

$$C_N(r,m)=\frac{1}{N^2}\sum_{\substack{i,j=1\\ i\neq j}}^{N} H(r-\left|X_i-X_j\right|) \tag{3.5}$$

in which $C_N(r, m)$ refers to correlation integration; H represents the Heaviside step function; and r means the Euclidean distance between two-phase points. Then the correlation dimension for m-dimensional space (denoted by D^m) could be calculated by the following equation (Abraham et al., 1986):

$$D^m \equiv \lim_{r\to 0}\frac{\log C_N(r,m)}{\log r} \tag{3.6}$$

In vibrational time series, chaotic signals are deemed to be dominated by low-dimensional dynamic systems, while noise is usually produced by high-dimensional ones. Given that ideal white noise has an infinite dimensionality, the correlation dimension of a signal is expected to increase when it is contaminated by noise. This increase reflects the added complexity introduced by the noise in the signal's structure. Thus, the convergence speed of the correlation dimension curve (i.e., the gradient of the curve) can be used as a test indicator of the signal denoising effect. The faster the curve converges, i.e., the steeper the slope, the more significant the noise components.

(2) Poincaré mapping

It is worth noting that it is difficult to describe high-dimensional space using the phase space reconstruction method. The Poincaré mapping method can be used to convert the trajectory of the dynamic system to its intersection with a particular cross-section (i.e., Poincaré cross-section). The result proves that the continuous trajectory of the phase space behaves as a mapping between some discrete points on the Poincaré section, from which some motion characteristics can be obtained (Kumar & Varshney, 2021).

For example, given a phase space trajectory composed of a set of vectors Λ_i:

$$\Lambda = [\Lambda_1^T, \Lambda_2^T, \Lambda_3^T, \cdots, \Lambda_p^T] \tag{3.7}$$

A covariance matrix $\Gamma = \Lambda^T \Lambda$ is constructed. A set of fully orthogonal bases in the reconstructed phase space is obtained through a full-rank linear transformation. Then, the eigenvectors corresponding to the two largest eigenvalues are selected as the principal axes, and the trajectory is projected onto the plane formed by these two principal axes, resulting in the Poincaré section. If the point set displayed on the Poincaré section is neither finite nor a closed loop, the motion is determined to be chaotic; if it forms a closed curve, the motion is determined to be periodic or quasi-periodic (Chen, 2017). Based on this, the chaotic characteristics of a system can be determined by analyzing the Poincaré mapping of its phase space trajectory.

The dynamic response of a structure can be approximated by the superposition of a small number of its eigenmodes. When subject to noise contamination, the system may exhibit altered dynamics that can obscure the underlying chaotic behavior. While the deterministic nature of chaos is characterized by specific attractors with finite fractal dimensions, noise introduces stochastic elements that disrupt these patterns. As a result, the observed variability in the system's output may resemble chaotic behavior, but it does not imply that noise transforms the system into a truly chaotic state. In the absence of noise, the mapped points will form specific, regular structures that reflect the characteristics of chaotic attractors. While under the influence of noise, the mapped points may display greater dispersion, lacking a clear structure. Therefore, by reconstructing the velocity and displacement components from structural acceleration signals and obtaining the system's phase space trajectory for Poincaré section mapping, the chaotic characteristics of the vibration signal can be evaluated through the distribution of discrete points on the section. This, in turn, allows assessment of the noise intensity.

In empirical analysis, the wider the distribution of discrete points in the Poincaré section of the structural vibration phase space, the weaker the periodic characteristics of the motion, the stronger the chaotic characteristics, and the greater the noise intensity. The velocity and displacement components can be obtained by performing one and two integrations of the acceleration signal, respectively. This study adopts a frequency-domain integration method (Zhu et al., 2020) to eliminate the “drift phenomenon” (i.e., trend terms) during the integration of time-domain acceleration signals. It first applies the Fourier transform to convert the acceleration signal into the frequency domain, then integrate each frequency component by multiplying to obtain the velocity and displacement spectra, and finally use the inverse Fourier transform to convert these back to the time domain.

Furthermore, to confirm denoising capability and superiority of the proposed DCIMN, a classic WT denoising method (Hu et al., 2021) is introduced for comparison study. Specifically, the WT denoiser is designed using an empirical Bayesian approach with Cauchy prior and posterior median threshold rules. The denoising principle is omitted in this chapter, with its basic workflow and a denoising case shown in Figure 3-3.

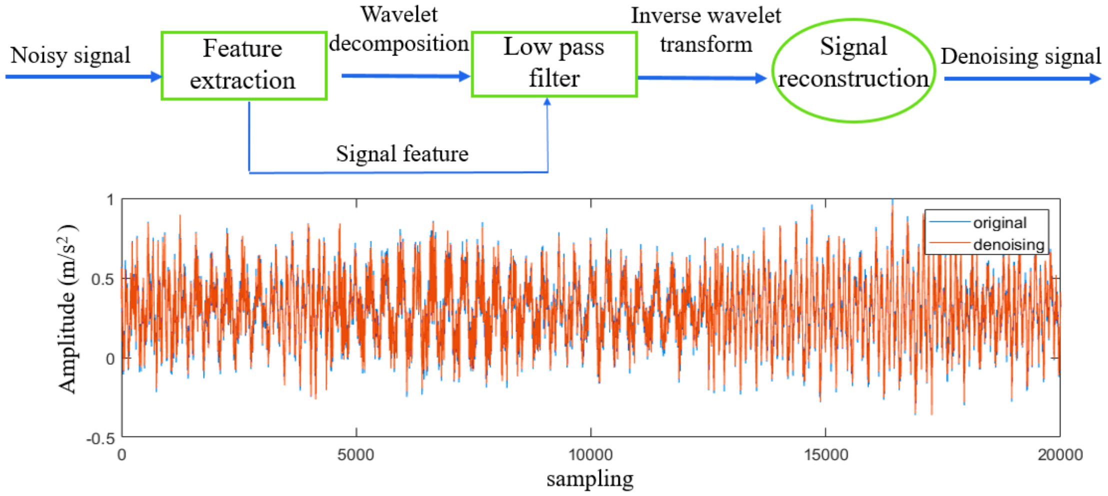

Figure 3-3. Time-domain signal denoising by WT

3.2 Experimental validations

3.2.1 Shanghai Tower and its SHM system

The Shanghai Tower is a 632-meter tall, 128-story skyscraper in Shanghai. It is currently the third tallest building in the world and the tallest building in China. The Shanghai Tower has deployed a long-term SHM system for collecting data from more than 400 sensors of 11 types (Zhang et al., 2016). These sensors are deployed to monitor and collect mainly three types of parameters: load (gust, temperature, and earthquake), structural response (settlement, inclination, strain, and acceleration), and environmental factors (ambient temperature and wind). For instance, a total of 71 accelerometers are arranged on key floors to collect acceleration response at a sampling frequency of 100 Hz, as shown in Figure 3-4. The basic parameters of the accelerometers are presented in Table 3-1.

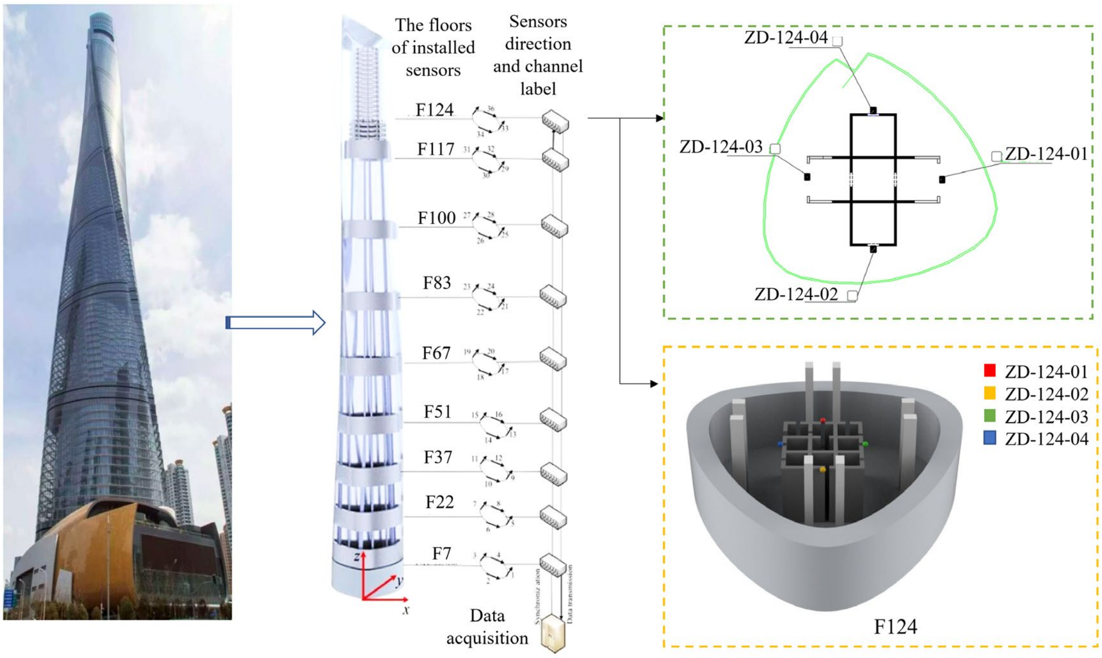

(a)Aerial view (b) Vertical layout of accelerometers (c) Plan layout of accelerometers

Figure 3-4. Shanghai Tower and layout of accelerometers

The monitoring data collected by sensors is inevitably contaminated, which casts many obstacles for further data-driven analysis. The baseline motivation of this study is to explore out an effective and intelligent way to address this urgent, to lay groundwork for further vibration-based investigation in SHM scope.

Table 3-1 Parameters of installed acceleration sensors

Type	Measuring Range/g	Sensitivity / (V·g $^{-1}$)	Resolution / g	Sampling frequency / Hz	Total number
LC0132T	0.1	50	4×10^{-7}	100	71

Therefore, to investigate the effectiveness of the proposed DCIMN, experimental validation is carried out using accelerometer signals of Shanghai Tower, which includes a training dataset for raw signals and nonlinear systematic analysis for denoising ones. In this chapter, the acceleration signals collected by the accelerometers installed on the 124th floor (i.e., ZD124-01) under the excitation of three typhoon conditions, namely Typhoon Ampil, Rumbia, and IN-FA are introduced. Without loss of generality, 20000 data points of acceleration signals are chosen randomly in each case with their RMS values shown in Table 3-2.

Table 3-2 Historic monitoring data acquisition of Shanghai Tower

Cases	Typhoon	Date	RMS value (m/s^2)
1	Ampil	2018.7.19	0.3602
2	Rumbia	2018.8.16	0.2967
3	IN-FA	2021.7.26	0.2637

3.2.2 Linear parameter verification for denoising performance

White noise and pink noise with noise levels ranging from 20% to 80% are added to the measured acceleration signal according to the process described in Section 3.1.1, and mixed signal (noisy signal) and original signal (pseudo-clean signal) datasets are constructed as model input-output pairs. Among them, 80% are randomly divided as training and validation sets, and the remaining 20% are used as test sets.

The DCIMN model is built based on the open-source ML framework TensorFlow. The proposed DCIMN is trained in a supervised learning paradigm, and the maximum number of iterations (Epoch) is set to 500. The program is operated on a PC with dual-core Intel(R) Xeon(R) Silver 4116 CPU @ 2.10GHz and dual-core NVIDIA GeForce RTX 2080Ti. At the same time, to improve the network computing efficiency, the unified computing architecture device CUDA (Compute Unified Device Architecture) (Manavski & Valle, 2008) is used for parallel computing in the environment configuration, and the computing performance is improved by calling the processing power of the graphics processor GPU.

After the model training is completed, the trained DCIMN model and WT method are used to perform denoising on the test set data. The linear evaluation parameters SNR and RMSE are calculated for the denoising results (the original measured data is regarded as the benchmark data here). Table 3-3 gives the average values of the two linear evaluation indicators of the denoising results, where the bold marks correspond to the optimal group. At the same time, for a more intuitive comparison, the parameter results are given in the form of bar graphs in Figure 3-5 and Figure 3-6.

Table 3-3 Parameter evaluation of denoising effectiveness by WT and DCIMN

Noise type	Noise level	SNR			RMSE		
		Noisy	WT	DCIMN	Noisy	WT	DCIMN
White noise	20%	2.7321	5.4071	**6.6358**	0.2196	0.1600	**0.1386**
	40%	2.5846	5.6086	**5.8571**	0.2220	0.1571	**0.1521**
	60%	2.5328	5.6109	**6.5553**	0.2236	0.1569	**0.1404**
	80%	2.5206	5.5515	**6.3777**	0.2236	0.1583	**0.1432**
Pink noise	20%	2.5122	**2.9768**	1.2013	0.2243	**0.2124**	0.2611
	40%	2.3640	2.8723	**3.4757**	0.2281	0.2150	**0.2014**
	60%	2.6118	3.0618	**3.8862**	0.2217	0.2101	**0.1948**
	80%	2.5210	2.8885	**3.4207**	0.2256	0.2163	**0.2063**

Overall, the SNR of the signal after denoising is significantly improved and the RMSE is significantly reduced compared with the mixed signal with added noise. At the same time, compared with the classic WT denoising method, the proposed DCMIN can achieve better denoising effects in most situations. For example, for white noise at the levels of 20%, 40%, 60%, and 80%, the SNR value of DCIMN is increased by 1.46, 1.08, 1.31, and 1.27 times that the WT method, and the RMSE is reduced by 1.36, 1.08, 1.25, and 1.23 times that the WT method.

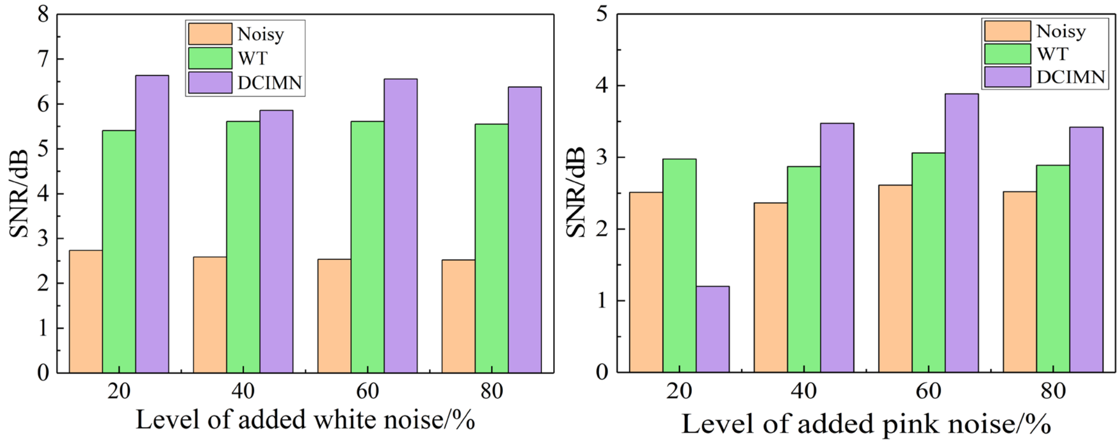

Figure 3-5. SNR evaluation of denoising performance by WT and DCIMN

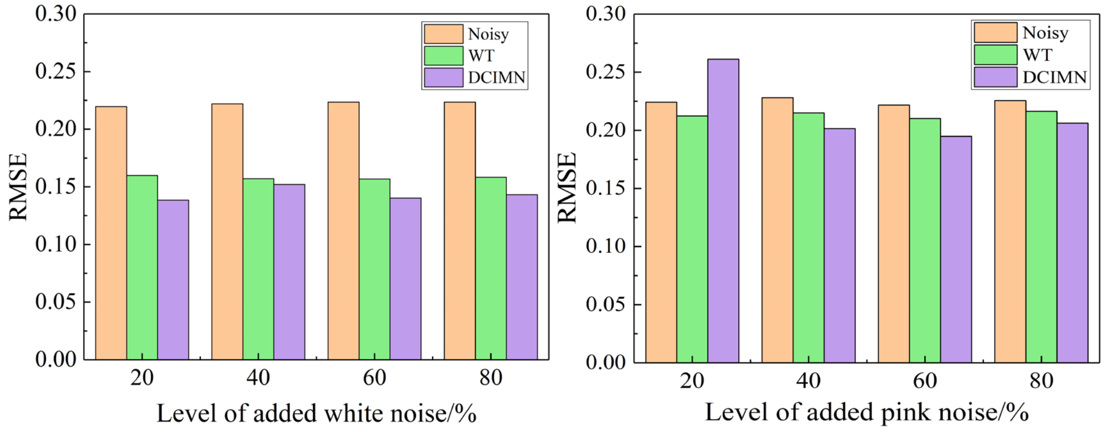

Figure 3-6. RMSE evaluation of denoising performance by WT and DCIMN

In general, although the proposed DCIMN denoising network shows obvious advantages in most cases compared with the classic WT method, for signals mixed with 20% pink noise, the denoising results of SNR and RMSE are abnormal, that is, the SNR of the processed signal decreases and the RMSE increases. Combining the denoising principle and model training process of the proposed denoising method, the preliminary analysis shows that the denoising effect of a specific signal depends to a certain extent on its similarity with the training set. Therefore, for vibration signals with very different frequency band distributions, the added lower level (i.e., 20%) of pink noise is difficult to identify and distinguish. This limitation is also a common problem faced by most ML models, but with the subsequent expansion of training data sets, this limitation can be effectively compensated in order to obtain a more robust signal denoising network.

3.2.3 Nonlinear analysis for denoising performance

As mentioned above, the evaluation method based on the quantification of the error of the denoising results is only applicable to the situation where there is a reference benchmark (i.e., a pure signal label), and for the denoising of the real vibration signal, it is often impossible to effectively obtain the corresponding reference benchmark. Therefore, this section further analyzes the denoising results based on the two nonlinear evaluation methods described in Section 3.1.3.2, namely, the correlation dimension curve and the Poincaré mapping. Different from the linear evaluation in which the average values of the parameters are obtained, this section randomly selects a certain acceleration signal under the excitation of three typhoon environments for qualitative analysis.

The correlation dimension curves with embedded space dimensionality, namely 5, 10, 15 and 20 are obtained based on vibration signals denoised by WT and DCIMN under three typhoon cases, as shown in Figure 3-7. A slight improvement emerged in terms of the convergence speed of the Correlation Dimension curve of signal denoised by WT in all three typhoon conditions. Notably, after being processed by DCIMN, the slope of the signal correlation dimension curve is remarkably reduced. For instance, in the case of typhoon IN-FA with an embedded space dimensionality of 20, the slope of curve denoised by DCIM is approximately 5.4 (4.28 / 0.79), while that by WT is approximately 11.1 (7.77 / 0.70). According to the criteria demonstrated in Section 3.1.3.2, the results suggest the superiority of the proposed method in eliminating noise components in vibration measurement compared to the classic WT method.

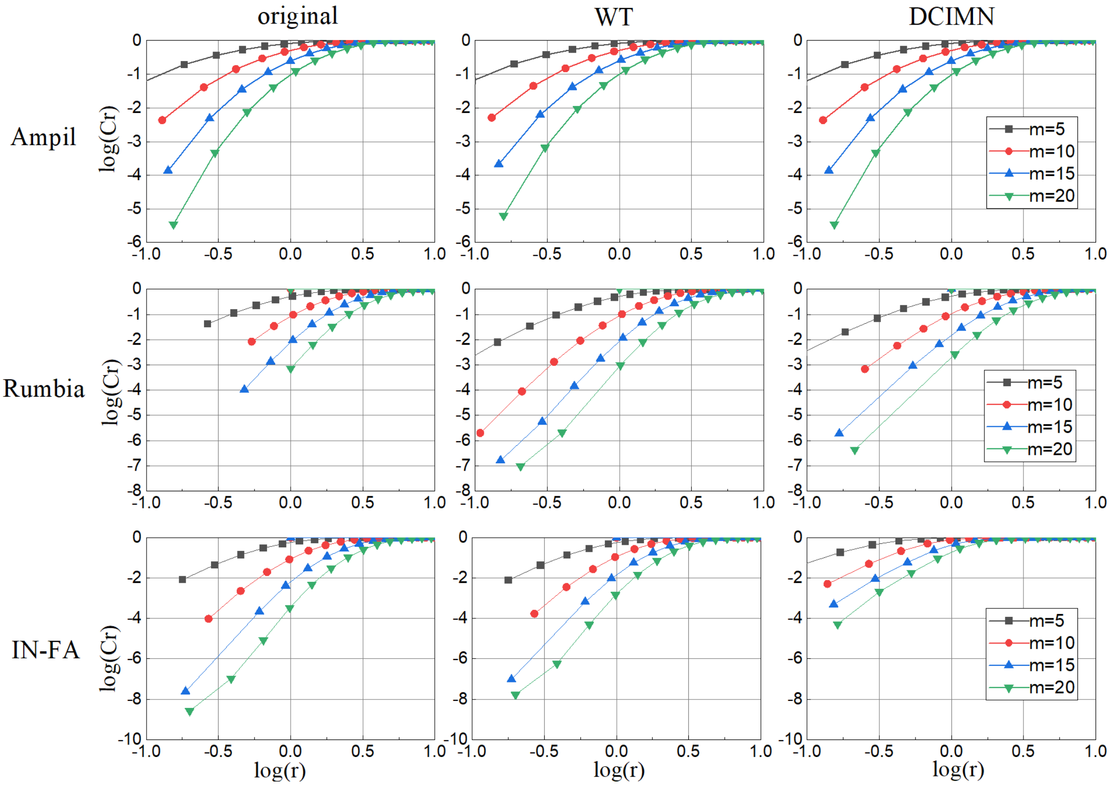

Figure 3-7. Correlation Dimension curve of vibration signals during three typhoons

To set a standard comparison to illustrate the correlation between noisy levels and Poincaré trajectory distribution, a clean periodic signal produced by Rössler Equation (Rössler, 1976) is introduced for intuitive display. It defines a continuous-time dynamic system that exhibits chaotic dynamics associated with the fractal properties of the attractor, as shown in Figure 3-8(a). Only few discrete points in its Poincaré map of clean signal are produced by Rössler Equation as shown in Figure 3-8(b), while dense dots appeared in those of the noisy vibrational signal as shown in Figure 3-8(d).

In general, after denoising by DCIMN and WT methods, the discrete points on the Poincaré map of the signal are significantly reduced, indicating that both methods can remove noise to a certain extent. The calculated discrete points in Poincaré map of signals denoised by DCIMN are less than that by WT, which suggests the denoising superiority of the proposed method.

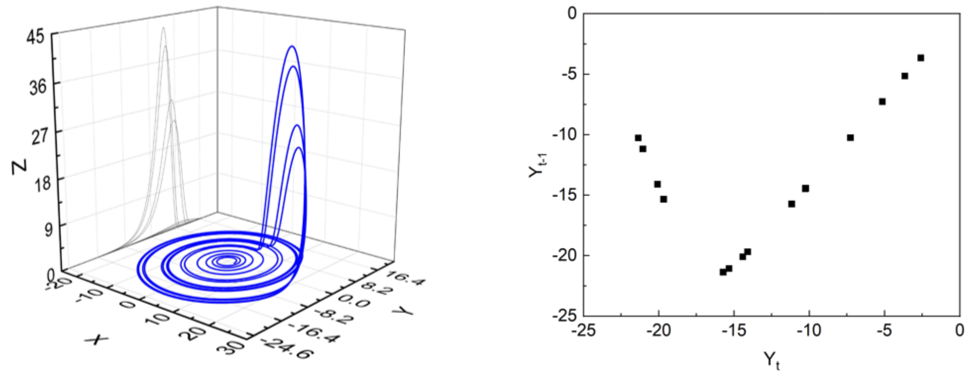

(a) Rossler attractor: a=0.2,b=0.2,c=5.7 (b) Poincaré map of Rossler system

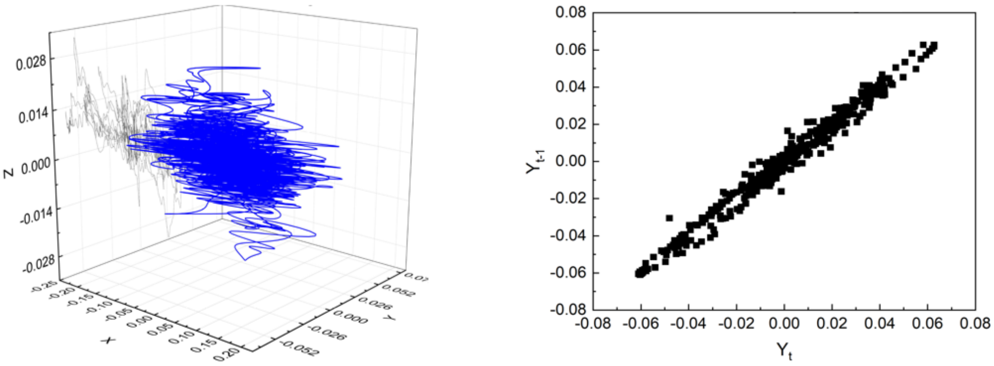

(c) Fractal attractor of original signal (d) Poincaré map of original signal

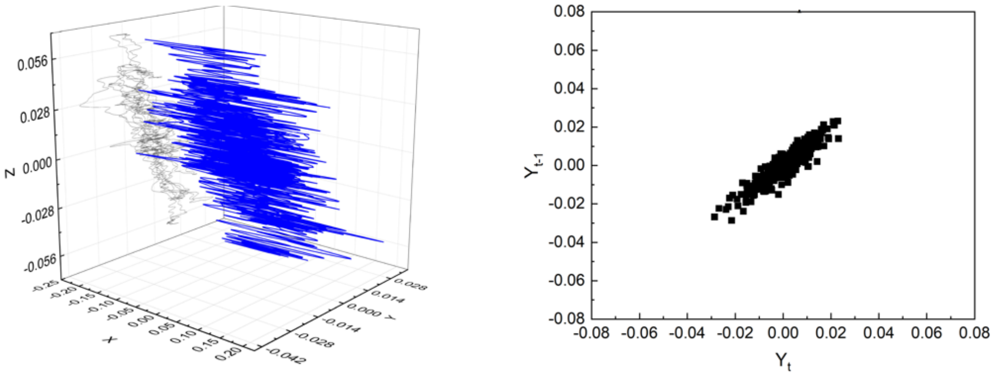

(e) Fractal attractor of WT-denoised signal (f) Poincaré map of WT-denoised signal

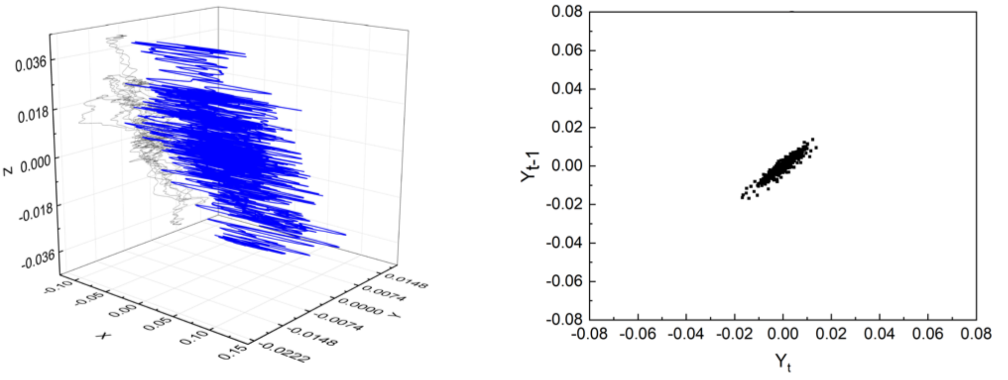

(g) Fractal attractor of DCIMN-denoised signal (h) Poincaré map of DCIMN-denoised signal

Figure 3-8. Fractal attractor and Poincaré maps of vibrational signals

3.3 Enhanced modal frequency identification

The previous section verified the effectiveness of the proposed denoising method from a statistical and theoretical perspective based on linear and nonlinear evaluation methods. On this basis, this section further verifies and analyzes the proposed method for modal identification, which is carried out based on the measured vibration signal after denoising.

In this section, the covariance-driven stochastic subspace method (SSI-COV) combined with the stability map (Magalhães et al., 2009) is adopted to estimate the modal frequencies of the Shanghai Tower respectively driven by original signals and denoised results. Assuming the excitation of structure as a white noise, the SSI-COV method performs the modal identification using a discrete stochastic space model.

$$\begin{aligned} r_{k+1} &= A \cdot r_k + w_k \\ z_k &= C \cdot r_k + v_k \end{aligned} \tag{3.8}$$

where r_k is the state vector at time instant k and z_k is observation vector; A is the systematic matrix and C is the observation matrix; w_k represents discrete stochastic noise vector owing to ambient interference and modeling inaccuracies, and v_k is observation noise generated during on-site measurement.

Other than commencing with block Hankle matrices built from the input and output sequences as that in stochastic subspace identification (SSI) method (Thai et al., 2007), the SSI-COV method performs the identification based on the covariance matrices of the structural response, which could be calculated as follows:

$$R_i = \frac{1}{N-1} \sum_{k=0}^{N-i-1} z_{k+i} \bullet z_k{}^T \tag{3.9}$$

where N is the dimension of z_k and superscript T means transpose.

The key to the identification process is to determine the system mode order. To accurately obtain the structural modal features, stabilization diagram technique is adopted to eliminate the interference of false modes on the recognition results in SSI-

COV method. Its basic idea is to use the characteristic that the eigenvalues of the system are pairwise conjugate and to compare the frequency calculation results of the adjacent orders in a 2D graph of frequency-orders. In this way, the distance between two modes can be calculated as follows:

$$d_{i,j} = \left| \frac{f_i - f_j}{f_j} \right| + (1 - MAC_{i,j}) \tag{3.10}$$

where f_i is the i-th estimated frequency and $MAC_{i,j}$ is the modal assurance criterion between the i-th and j-th modes (Pastor et al., 2012). If the difference between the two is short (within the set tolerance range, practically), they are probably representing the same mode, which will be processed in the same cluster as a stable point, otherwise an unstable point.

Without loss of generality, five periods of time during the typhoon conditions are chosen randomly to estimate the modal frequency of the Shanghai Tower, which are denoted as Case 1 to Case 5. Each segment is a 10-minute time series collected by accelerometers with a down sampling frequency of 10 Hz. A stabilization diagram of modal identification in a random sample signal is presented in Figure 3-9.

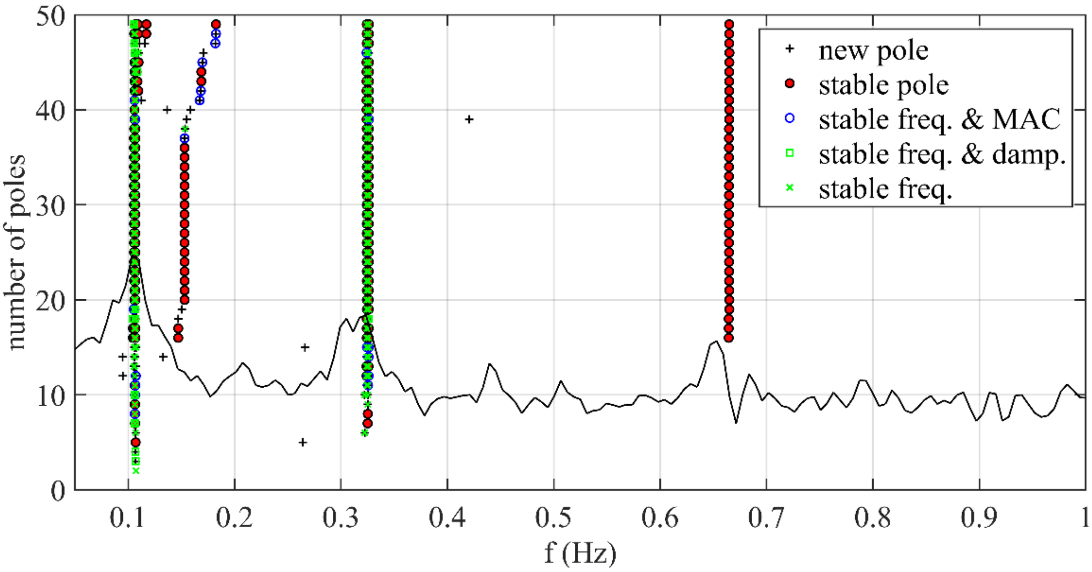

Figure 3-9. Stabilization diagram of modal identification

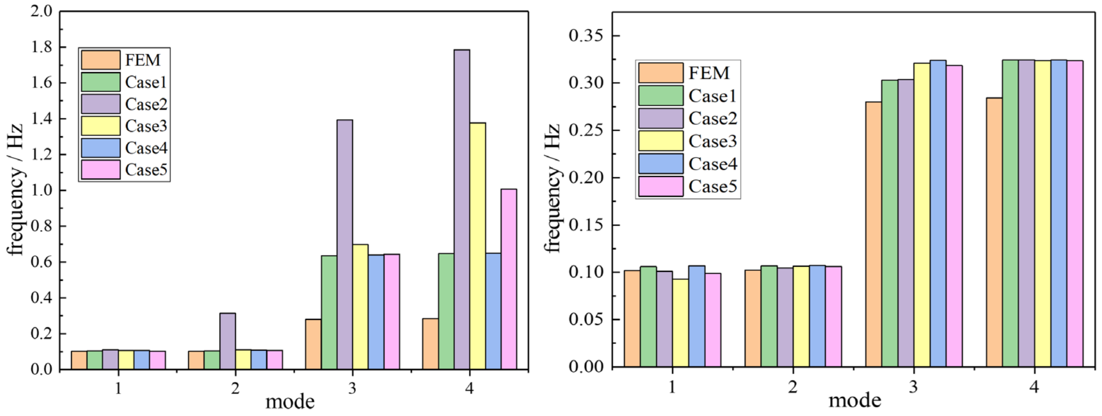

(a) Modal frequencies estimated by original signals (b) Modal frequencies estimated by denoised signals

Figure 3-10. Modal frequencies estimated by the original and denoised signals

To eliminate the interference of weak robustness in extracting the torsional modes, only the first two-order translation modal frequencies are calculated to investigate the effectiveness of the proposed denoising method. The FEM calculation results by Lu et al. (2011) are introduced to play as reference benchmark, denoted as FEM. They are compared with the identification results based on the vibration measurement, as shown in Figure 3-10, where modes 1 and 2 represent the first-order translation in X (North-South) and Y (West-East) direction, respectively, and modes 3 and 4 represent the second-order in X and Y direction, respectively.

The identification results based on raw vibration data show a dispersion in high-order modes. For the first-order sway mode in two orthogonal directions, the identification results of most cases fluctuate in a reasonable range compared to the FEM results. However, for the second mode, the results deviate severely from the FEM, especially for Case 3. By contrast, the identification results using the denoised signals agree with the FEM results consistent with all the five cases, verifying the effectiveness of the proposed denoising method and enhancing accuracy of modal identification.

3.4 Summary

3.4.1 Limitations and discussions

In the proposed denoising method, the reliance on white and pink noise assumes that the noise characteristics in real-world applications will closely align with these profiles. However, many environments introduce complex noise types that may not fit these categories, potentially leading to suboptimal denoising performance. Variations in spectral content and temporal behavior can significantly impact the model's ability to generalize. While the proposed method shows promise, addressing these limitations will be crucial for enhancing the model's effectiveness and applicability in diverse real-world scenarios. Future research should focus on expanding the noise training dataset to include a wider range of noise types, such as incorporating synthetic noise profiles that mimic the characteristics of nonstationary noise. Implementing adaptive denoising techniques in future iterations of the model will also enhance the ability to handle varying noise conditions.

3.4.2 Concluding remarks

This chapter proposes an innovative signal denoising method for structural vibrational signals. Field measurement of the 632-meter-tall Shanghai Tower is adopted for validation. Linear parametric analysis using SNR and RMSE is conducted for denoising performance evaluation. Compared with the WT denoising method, the proposed DCIMN improves the SNR of the acceleration signals by 1.46 times and decreases the RMSE by 1.36 times. Besides, nonlinear analysis of vibration signals without reference benchmark is carried out. The correlation dimension curves and Poincaré maps of vibration signals are constructed and analyzed, which confirm the effectiveness and advantage of the proposed method. The measured raw data and denoised data are further used for modal identification via SSI-COV technique. The results validate the capability of the proposed denoising method in enhancing the accuracy of modal identification. It should be noted that the proposed DCIMN does not rely prior information of vibration signals or any factitious intervention, thus enabling enhanced vibration-based structural integrity evaluation.

CHAPTER 4 PARAMETER-FREE PHYSICS-INFORMED NEURAL NETWORKS FOR RAPID SEISMIC RESPONSE PREDICTION

PINNs provide a promising strategy to overcome the “black box” limitation of conventional ML regression algorithms in developing surrogate models for rapid structural seismic response prediction. However, in most existing PINNs designed for this task, their physics embedding mechanisms rely on certain prior knowledge such as mass matrices, stiffness coefficients and damping ratios, which hinders applicability on real-world structures. Thus, this chapter proposes a novel parameter-free PINN for rapid seismic response prediction. The term ‘parameter-free’ refers to the proposed method doesn’t rely on structural mass matrices, stiffness coefficients and damping ratios. In this method, the parameter-free physics-embedding mechanism is propounded by construing differential nexus of state variables, which are derived from state-space representation using acceleration signals. 1D CNN is adopted as the prototype regression model due to its powerful capability in multivariate time series processing and forecasting (Ozcan et al., 2021; Pantiskas et al., 2020; Shao & Kim, 2022).

With integration design of state space model and 1D CNN, the proposed network (denoted as SSM-CNN) attains rapid seismic response prediction without reliance on stiffness or mass matrices, thus allowing for better interpretability and adaptability of the surrogate models.

4.1 SSM-CNN

Figure 4-1 depicts the designated architecture of SSM-CNN and the adopted physics-informed mechanism for performance enhancement. The proposed SSM-CNN consists of three major components, namely prototype deep 1D CNN, extended SSM and physics-informed mechanism, which are elaborated as follows.

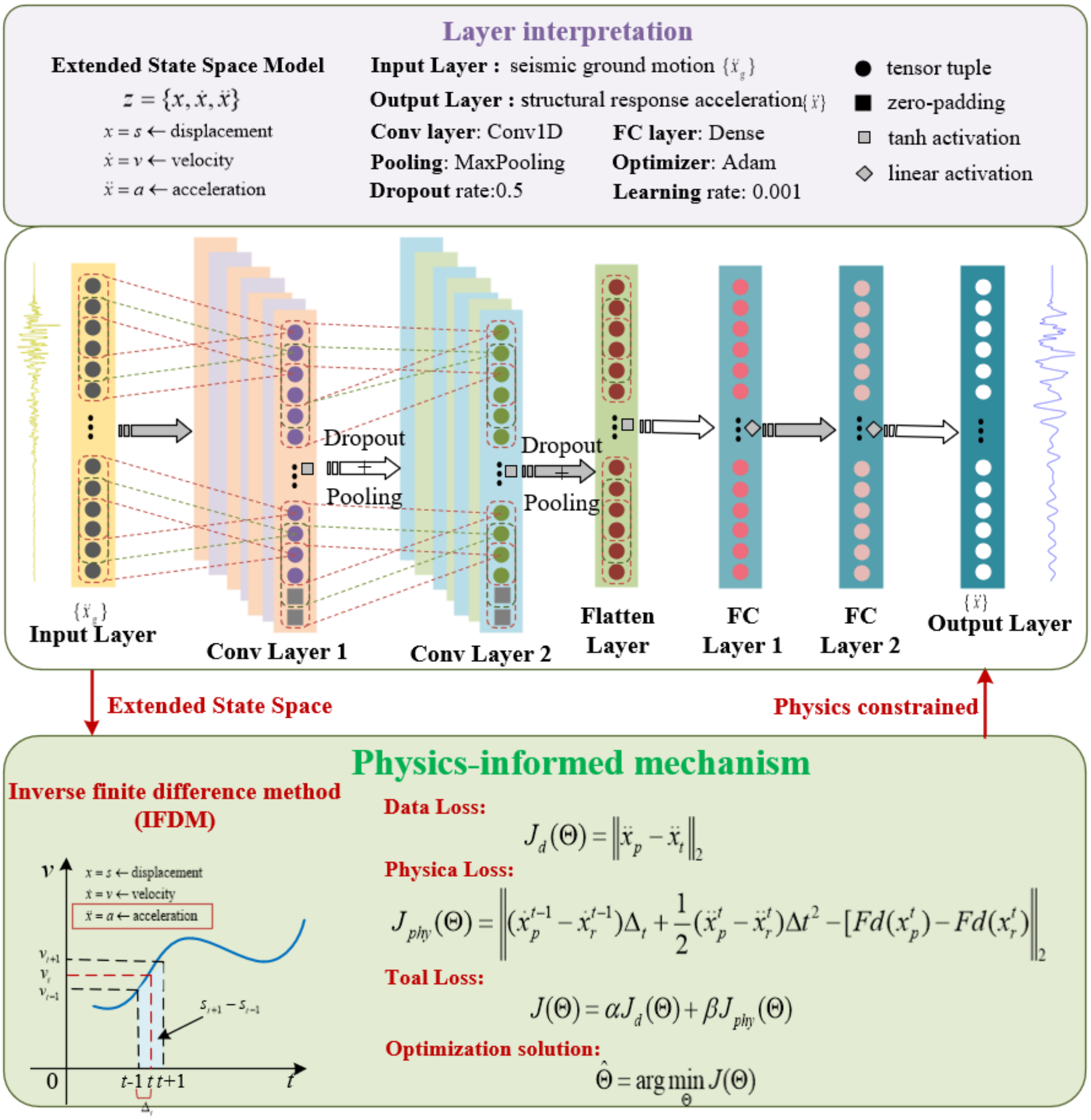

Figure 4-1. The proposed SSM-CNN for seismic response prediction

4.1.1 Prototype-model: Deep 1D CNN

In the broader family of deep learning, CNNs are a type of advanced feed-forward neural networks which have proven capable and powerful for various computer vision and machine operations (Ghose et al., 2020; Yuan et al., 2021; Zhao et al., 2022). 2D CNNs are normally designated to operate exclusively on 2D data such as images and videos. In fact, there are another two types of CNNs, namely 1D CNNs and 3D CNNs. Specifically, the 1D CNNs have recently demonstrated a superior performance and become the state-of-the-art technique for processing naturally 1D signals such as vibrational time series. Notably, due to the lower computational complexities compared to 2D CNNs, the compact 1D CNNs are promising and well-suited for real-time operations including rapid seismic prediction. Therefore, a sophisticated 1D CNN is allocated and designed as the prototype model of proposed SSM-CNN in this present study. The configuration of a 1D CNN is determined by several major hyperparameters, including number of hidden layers, filter or kernel size, subsampling factor, and the designation of pooling and activation functions. The upper part of Figure 4-1 presents the designated architecture and layer interpretation of the proto-model, involved mechanism (i.e., basic features and blocks) of which are elaborated subsequently.

To facilitate the convergence and prevent overfitting, dropout, pooling and flatten layers are employed into the 1D CNN architecture. Specifically, the dropout layers randomly re-define the values of certain neurons to zero with a given frequency rate at each training step, which is set to be 0.2 in the SSM-CNN to deter overfitting. The pooling layers are allocated for reducing the dimensions of the feature neurons, which is beneficial for the computational cost control. And after the convolution operation by the last Conv1D layers, the output representation feature maps are first reshaped into 1D-array (i.e., so-called flattened) by the flatten layers before being fed into the downstream fully-connect layers. The flatten tensor will have an equal length of the element number without affecting the batch size. Since the target output of the SSM-CNN is seismic response acceleration, the nonlinear activation functions are not suited any more. Therefore, the activation function in dense layers (stacked behind duplicated Conv1D layers) is defined as linear function.

Hereto, the basic architecture of deep 1D CNN as the prototype model of SSM-CNN has been elaborated. On this basis, the subsequent novel physics-informed constraint strategy based on state space representation propounded in this study is applied for performance enhancement.

4.1.2 Extended SSM

In controlling engineering, SSM is a typical mathematical model featured as a state-space representation of a physical system comprising a set of inputs and outputs along with some set of state variables, which are conjunct with first-order differential equations or difference equations (Rojas & Wachel, 2022). Given a set of state variables depending on the values of input in an SSM, the values of output variables will evolve with the state and input variables. Through this way, the full motion knowledge of a dynamic system can be represented in a convenient and compact form. Specifically, the most general state-space representation of a linear time-invariant system can be expressed in the following formulation:

$$\begin{aligned}\dot{x}(t) &= Ax(t) + Bu(t) \\ y(t) &= Cx(t) + Du(t)\end{aligned} \tag{4.1}$$

where x is the state vector; y is the output vector; u is input vector; and A, B, C, D refer to corresponding coefficient matrices, which are all allowed to be time-invariant.

Conventionally, the state vector of a dynamic system comprises of the displacement and velocity components. However, confronting the usual situation where the dynamic parameters (i.e., k, c) are generally unavailable and the field measurement of monitoring system are confined to structural acceleration responses, it remains a challenge to develop the formulized SSM of a kinematic system with specified parameters designated. Nonetheless, instead of making endeavor to obtaining the estimated values of parameter matrices, the finite difference method (FDM) provides an alternative way to calculate the approximate vector of velocity and displacement derived from the acceleration measure. In FDM, the differential equations are processed through approximating derivatives with finite differences, where both the spatial-domain variables and time-domain intervals are discretized. To this regard, a classical Taylor series expansion is first created:

$$f(x_0 + h) = f(x_0) + \frac{f'(x_0)}{1!}h + \frac{f^{(2)}(x_0)}{2!}h^2 + \cdots + \frac{f^{(n)}(x_0)}{n!}h^n + R_n(x) \tag{4.2}$$

Thus, it is natural to come up with the following approximations:

$$f'(a)=\lim_{h\to 0}\frac{f(a+h)-f(a)}{h} \tag{4.3}$$

$$f^{(2)}(a)=\lim_{h\to 0}\frac{f(a+h)-f(a)-f'(a)h}{h^2/2} \tag{4.4}$$

Furthermore, when considering the motion equations of the dynamic system, the approximate estimation of velocity and displacement variables can be obtained as follows:

$$\dot{x}(t)\cong \dot{x}(t-\Delta_t)+\ddot{x}(t)\Delta_t \tag{4.5}$$

$$x(t)\cong x(t-\Delta_t)+\dot{x}(t)\Delta_t+\frac{1}{2}\ddot{x}(t)\Delta_t{}^2 \tag{4.6}$$

Assuming the initial state variables as zero, the approximate estimation of velocity and displacement state vector $Z=\{x,\dot{x},\ddot{x}\}$ can be obtained from purely acceleration measurement $Z_{fm}=\{\ddot{x}\}$. Particularly, it should be clarified that even though the round-off error in the inverse FDM might degrade the accuracy, the effective knowledge comprised in the extended state vectors can be beneficial to compile the neural networks after introducing special physicals laws.

4.1.3 Parameter-free physics-informed mechanism

Conventionally, neural networks adopt optimization strategies such as stochastic gradient descent for minimizing the regression error to quantifiably evaluate the prediction performance. As the fundamental basis of parameters optimization and model tuning, the loss definition is actually implemented by using a loss function, such as mean squared error (MSE) and mean absolute error (MAE). All those loss functions are explicit in mathematics, but nonetheless, none of them have any insight into the underlying physical laws of the involved data. Hence, a parameter-free physics-informed mechanism is designed and employed in the proposed SSM-CNN to enhance the prediction performance.

In the proposed SSM-CNN, the integrated loss definition is determined by both data fidelity loss and physical loss. Thereinto, the data loss describes the inherent loss in model fidelity by adopting the MSE loss function:

$$J_d(\Theta) = \left\| \ddot{x}_p - \ddot{x}_r \right\|_2 \tag{4.7}$$

where ||x||$_2$ denotes the L$_2$ norm (i.e., Euclidean distance), $\ddot{x}_p$ is the predicted acceleration series, and $\ddot{x}_r$ is the real acceleration.

Regarding physical loss, the motion equation law derived from the extended state space representation is embedded, which is defined as:

$$J_{phy}(\Theta) = \left\| (\dot{x}_p^{t-1} - \dot{x}_r^{t-1})\Delta_t + \frac{1}{2}(\ddot{x}_p^t - \ddot{x}_r^t)\Delta t^2 - [F_d(x_p^t) - F_d(x_r^t) \right\|_2 \tag{4.8}$$

where variables $\ddot{x}$, $\dot{x}$ and x represent the acceleration, velocity and displacement series, respectively. The superscript *t* or (*t*-1) represents the discrete time interval, subscript *p* and *r* represent prediction values and real values, respectively. $F_d(\cdot)$ denotes the first order difference operation.

Hence, the total loss is defined as:

$$J(\Theta) = \alpha J_d(\Theta) + \beta J_{phy}(\Theta) \tag{4.9}$$

where α and β are the weights of corresponding loss functions, which are set to be in a range of 0 to 1 depending on the source type of given dataset, and are adjusted manually in this study. A more in-depth investigation of optimizing the loss weights can be performed in the future work, which is beyond the essential scope of present study. Note that a combination of $\alpha = 0.25, \beta = 0.75$ exhibits a satisfactory performance in this study according to some parallel experiments. And the essence is to solve the optimization problem:

$$\hat{\Theta} = \arg\min_{\Theta} J(\Theta) \tag{4.10}$$

In this way, the mapping relationship between the ground motion (input) and the seismic response acceleration of structures (output) can be built through the proposed SSM-CNN. The trained model can be used to rapidly reconstruct the structural dynamic responses under the excitation of seismic events. Notably, the assumption of zero initial conditions is primarily adopted for mathematical tractability. The current formulation does not explicitly account for arbitrary initial states, which may introduce systematic errors or drift in the predicted response, particularly for strongly nonlinear systems. Future work should focus on extending the formulation to explicitly incorporate initial condition dependencies, thereby mitigating potential sources of error and drift in the loss function. In addition, while the proposed method does not impose the full form of the traditional equations of motion, it encapsulates the essential physical structure by constraining the model to respect the differential relationships intrinsic to the underlying dynamics. Although without directly imposing physical laws in their parameterized form, it provides a physics-inspired regularization. Particularly, considering the trade-off between the parameter-free superiority, it is deemed reasonable and acceptable to claim this method as a physics-informed technique.

Both numerical and experimental validations are performed to verify the effectiveness in the subsequent sections. Particularly, a conventional CNN without physics-informed mechanism designated with identical network configuration will be compared with the proposed method. The programming in this study is executed on a parallel computing platform namely CUDA (Manavski & Valle, 2008) on a standard PC with 12-core AMD Ryzen 9 3900X CPU and a NIIDIA GeForce RTX 3070 GPU. Remarkably, with compact network design and accelerated simulation platform, the model training procedure is less than 200 s, and the model prediction is within 0.01 s.

4.2 Numerical validations

4.2.1 Mass-spring-damper system (MSDS)

An MSDS is typically utilized to demonstrate and illustrate modeling and simulation application of kinematic physics. It can be described as the following equation:

$$F(t) - c\dot{x}(t) - kx(t) = m\ddot{x}(t) \tag{4.11}$$

where $F(t)$ denotes an external force applied to the system; c is the damping constant; k is the stiffness of the spring; m is an object mass. $x(t)$ is the displacement of the object, $\dot{x}$ is the velocity; and $\ddot{x}$ is the acceleration.

Based on fundamental equations, higher order differential equations can be reformulated into an SSM form. Specifically, given denotation set $x = x_1$, $\dot{x} = x_2$, a standard formulation of SSM can described as:

$$\begin{bmatrix} \dot{x}_1 \\ \dot{x}_2 \end{bmatrix} = \begin{bmatrix} 0 & 1 \\ -\frac{k}{m} & -\frac{c}{m} \end{bmatrix} \begin{bmatrix} x_1 \\ x_2 \end{bmatrix} + \begin{bmatrix} 0 \\ \frac{1}{m} \end{bmatrix} F \tag{4.12}$$

In this section, an MSDS with m=20 kg, c=2 Ns/m and k=5 N/m is designed, as shown in Figure 4-2. A total number of 39 far-field earthquake ground motion records recommended in the ATC-63 Project (Kircher & Heintz, 2008), randomly selected from the Pacific Earthquake Engineering Research Center (PEER) Ground Motion Database (Goulet et al., 2021) are used as the input force of the MSDS.

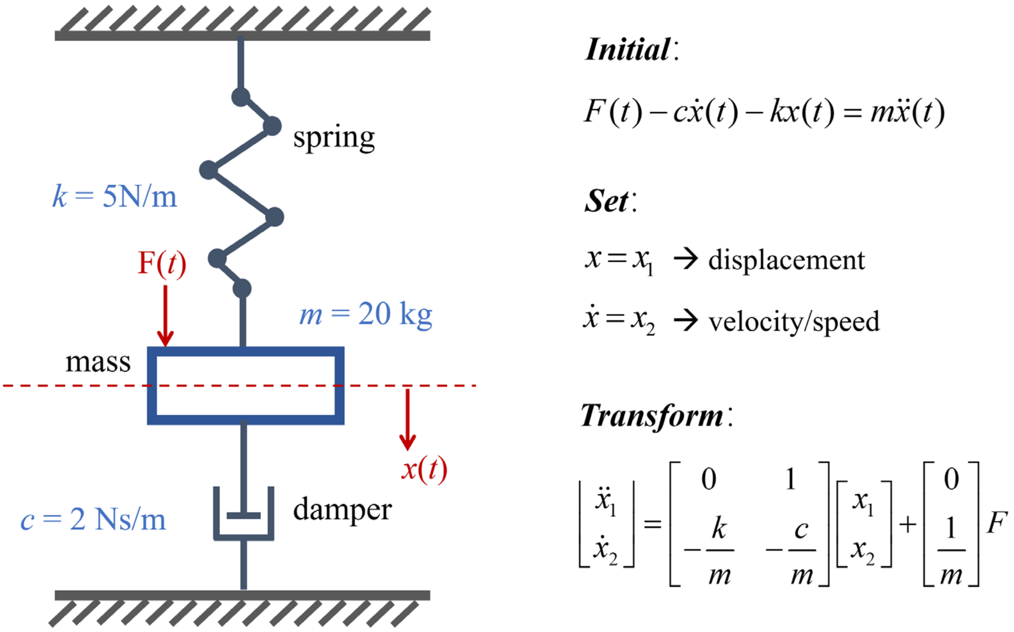

Figure 4-2. An MSDS and its state space representation

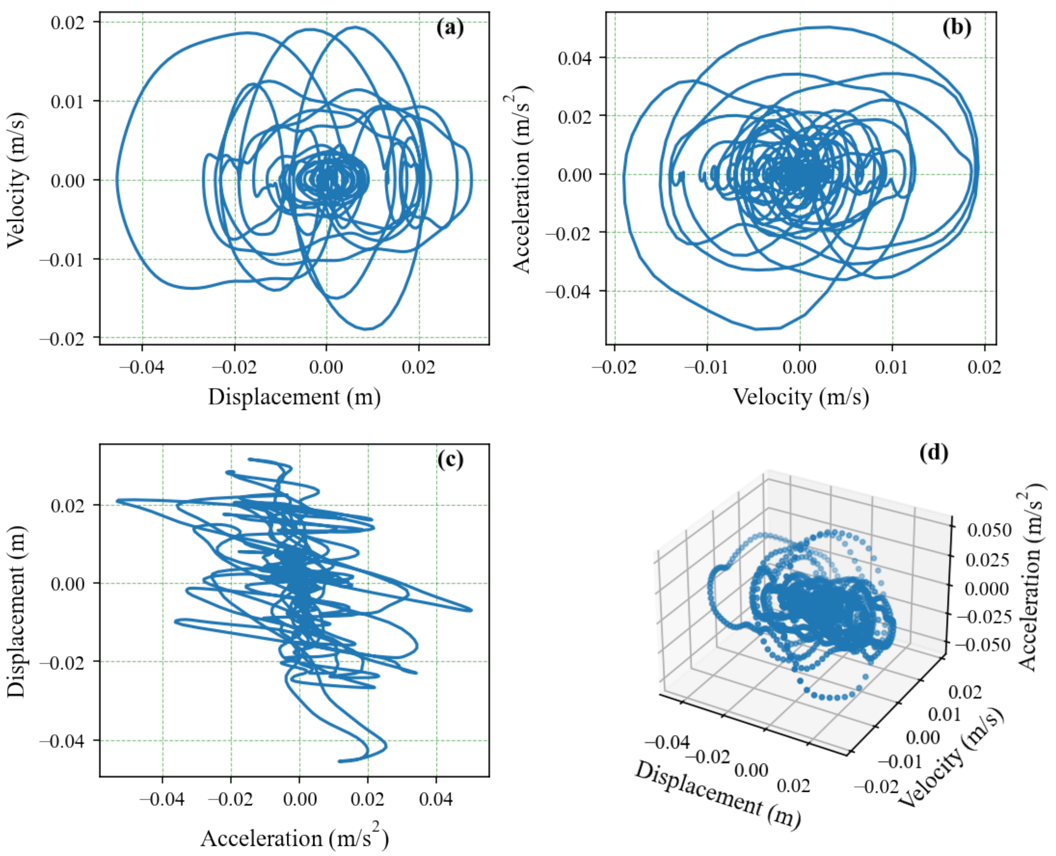

Figure 4-3. State trajectory of the simulation of MSDS

To acquire adequate training dataset, multi-level white noise with an SNR ranging from 50 to 120 are added into the earthquake record for DAug. With all parameters and the time increment set to be 0.1 second, the SSM of MSDS can be readily established and simulated by an open-source library in Python, namely *scipy.signal.lsim*. Figure 4-3 presents the simulation state trajectory of established MSDS under the excitation of certain real earthquake records. The simulated responses of the MSDS exhibit comparatively chaotic dynamics, which suggest that the simulated data are deemed acceptable for numerical validation.

4.2.2 Model training and testing

After processing the augmentation and segmentation operations, a total number of 1872 pairs of seismic force (ground motion) and response acceleration are obtained, which are randomly separated into training set (75%) and testing set (25%). Each segment has 600 sampling points with a time duration of 60 s. The Conv1D and Dense layers in the CNN and SSM-CNN are designed to be compatible with the input and output shape. Table 4-1 summarizes the layout of the model architecture, where the basic principle is to assure the length of tuples at adjacent layers change gently and smoothly. It should be demonstrated that the architecture design of the CNN in the present study can be also adjusted according to the specific task implementation. The Adam optimization algorithm (D. P. Kingma & J. Ba, 2014) with a learning rate of 0.001 is employed to enhance the computational efficiency of model training. Both the irritation epochs of CNN and SSM-CNN are set to be 200.

Table 4-1. Layout of the proposed SSM-CNN

Layer (type)	**Output Shape**	**Parameter**
input_1 (InputLayer)	(None, 600, 1)	0
conv1d (Conv1D)	(None, 593, 32)	288
dropout (Dropout)	(None, 593, 2)	0
max_pooling1d (Max_pooling1D)	(None, 296, 32)	0
conv1d_1 (Conv1D)	(None, 281, 64)	32832
dropout_1 (Dropout)	(None, 281, 64)	0
max_pooling1d_1 (Max_pooling1D)	(None, 140, 64)	0
conv1d_2 (Conv1D)	(None, 109, 128)	262272
dropout_2 (Dropout)	(None, 109, 128)	0
max_pooling1d_2 (Max_pooling1D)	(None, 54, 128)	0
flatten (Flatten)	(None, 6912)	0
dense (Dense)	(None, 128)	884864
dense_1 (Dense)	(None, 256)	33024
dense_2 (Dense)	(None, 512)	131584
dense_3 (Dense)	(None, 600)	307800

Total parameters: 1652,664

Trainable parameters: 1652,664

The trained models are utilized to perform seismic response prediction. Figure 4-4 presents comparison of prediction performance of the two models of three random cases, namely Case 1, Case 2 and Case 3. Both CNN and SSM-CNN produce satisfactory results of time-history response, which coincide well with the ground truth. The local detail of the prediction curves shows that the proposed SSM-CNN with physics knowledge exhibits slightly better performance than the normal CNN. Specifically, a more precise extreme values (the amplitudes at the wave trough and crests) are obtained by the SSM-CNN in Case 1 and Case 2. While regarding Case 3, even with a comparatively well-match prediction performance from the overall viewpoint of Case 3, the reconstruction response by normal CNN exhibited a worse consistency in the local area of wave trough and crests.

To further quantifiably evaluate the prediction performance, the correlation index (CI) is used for correlation analysis between the ground truth and prediction series. It calculates the least-squares regression for two sets of measurements and can be expressed as follows:

$$CI = \frac{\sum (x_i - \bar{x})(y_i - \bar{y})}{\sqrt{(x_i - \bar{x})^2 (y_i - \bar{y})^2}} \tag{4.13}$$

where x_i and y_i denote the two variable sets, and $\bar{x}$, $\bar{y}$ denote the mean of variable. The CI indicator can effectively represent the global similarity between the two sets. With a value of CI calculated closer to 1, a better prediction result is suggested.

Thus, the CI coefficients of all the 468 test samples are calculated and shown in Figure 4-4(a). The quartiles of the CI arrays are used to quantify the global prediction precision of the two models. Particularly, the first quartile (25% empirical point), second quartile (50% empirical point) and third quartile (75% empirical point) of each CI array are denoted as Ci_{q1}, Ci_{q2}, and Ci_{q3}, respectively. As marked in Figure 4-4(a), the CI quartiles of training set and testing set of CNN are (0.79, 0.95,0.97) and (0.75, 0.93, 0.97), respectively. The CI quartiles of training and testing set of the proposed SSM-CNN are (0.89, 0.97, 0.99) and (0.86, 0.96, 0.99), respectively. With extensively satisfactory and slightly higher value of CI quartiles of prediction set, the proposed SSM-CNN exhibits a superior seismic response prediction capability compared to conventional CNN without physics embedding.

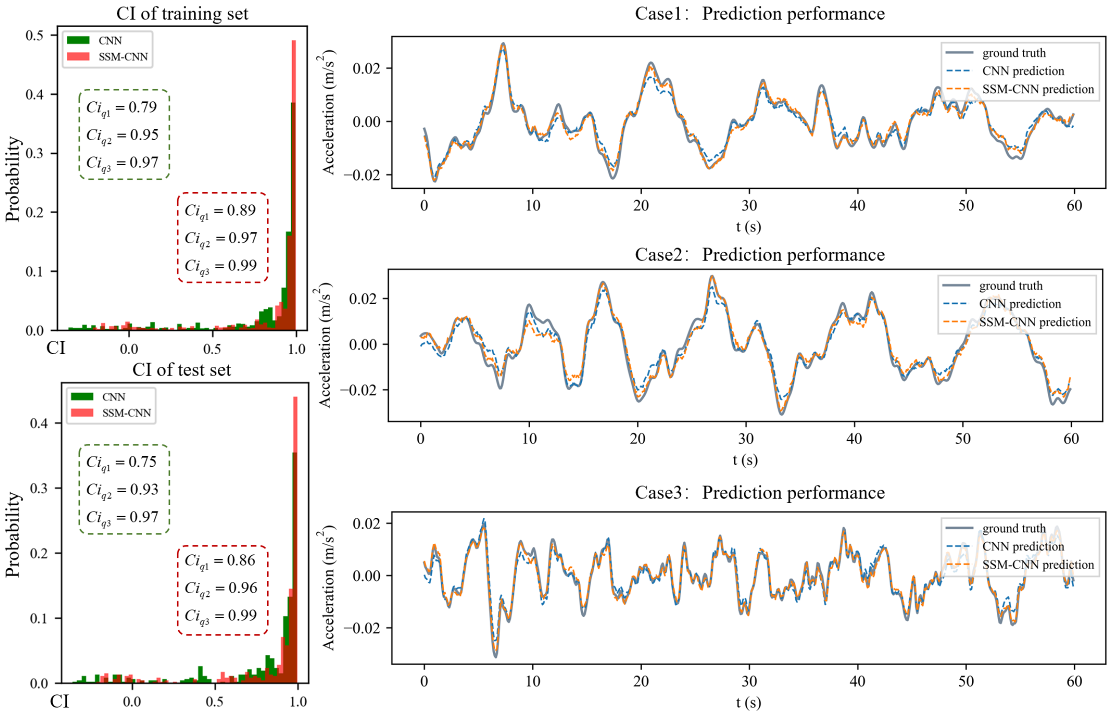

(a) Correlation analysis

(b) Cases comparison of prediction performance

Figure 4-4. Comparison of prediction performance: (a) correlation analysis; (b) cases of prediction history

4.2.3 Model sensitivity analysis

Even though both the CNN and SSM-CNN models turned out to be able to produce a relevantly precise response in most cases, there are still a few cases whose CI values are less than 0.5 and even negative values, suggesting unexpected results with poor prediction performance. To dig out the underlying reasons and potential addressment to this phenomenon, the sensitivity analysis between the scales of input seismic force and prediction accuracy (CI coefficients) are performed in this section. Specifically, the variance of the ground motion is utilized to represent the scales of input seismic force, which is calculated by the following formula:

$$\sigma^2 = \frac{\sum_{i=1}^{n}(x_i-\overline{x})^2}{N} \tag{4.14}$$

where $\overline{x}$ is the mean value of ground motion sequence; and N is the sequence length.

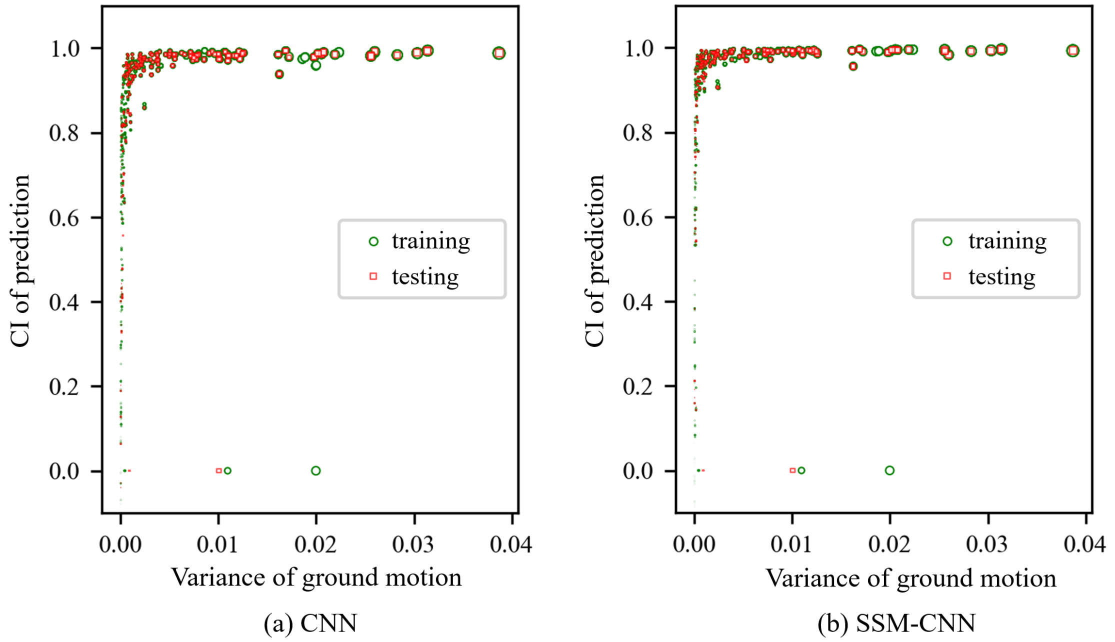

(a) CNN (b) SSM-CNN

Figure 4-5. Sensitivity analysis between motion scales and prediction accuracy

Figure 4-5 depicts the correlation relationship between variances of ground motion and CI indices of reproduction performance of the two models. Both the CNN and SSM-CNN exhibit extensively high accuracy except for those cases with extremely small scales of input seismic forces. This potential low CI of prediction performance does not represent that the surrogate models are invalid for seismic response prediction. In cases with minor ground motions, the ambient factors and measured noise could be a terrible influence on the prediction. The structural responses are generally within an expected amplitude when structural responses are of little interest, thus seldom degrading to the prediction performance.

4.3 Experimental validations

4.3.1 Data acquisition

The proposed surrogate models for seismic response prediction are validated by field-measured data in this section. Historical records of a five-story library building (CSUSB) in San Bernardina, California is acquired from the Center for Engineering Strong Motion Data (CESMD) (Haddadi et al., 2008). The rectangular-configuration library building is an RC shear wall structure designed in 1968 with a total of 10 accelerometers deployed on different levels, as shown in Figure 4-6.

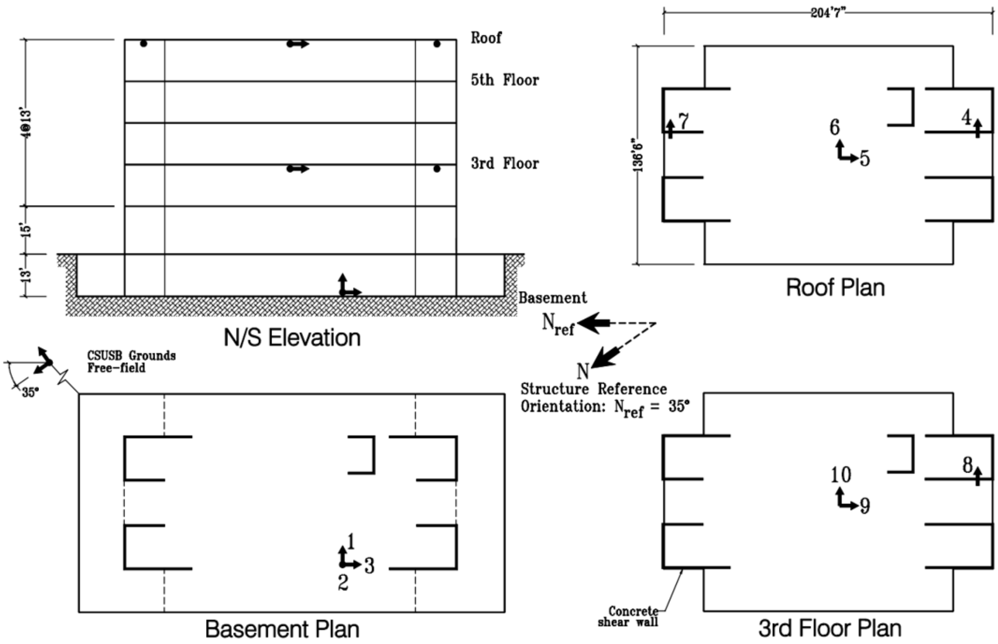

Figure 4-6. Sensor layout of five-story CSUSB library in San Bernardino, CA (CGS station No. 23285) (https://www.cesmd.org/)

The installed sensors recorded multi-directional on-site data of ground motions and structural responses under historical earthquake events from 2008 to 2020. A total of 13 available recorded datasets with a sampling frequency of 200 Hz on CESMD are introduced and utilized to perform the experimental validation, with their basic information summarized in Table 4-2. The peak ground accelerations (PGAs) of the records are in a range of 0.005 to 0.033 g, and the peak response accelerations (PRAs) are in a range of 0.012 to 0.045 g.

Figure 4-7 presents the time-domain history and dispersed spectrum characteristics of ground motions. The primary frequencies and amplitudes differ a lot, which suggests that the selected field records are reasonable and capable of verifying the capability of the proposed surrogate models for seismic response prediction. Among the field-recorded datasets with diverse magnitudes and epicentral distances, 11 out of 13 datasets are randomly selected for the model training and testing, whereas the remaining

2 denoted datasets are allocated for model generalization analysis.

Table 4-2. Basic information of ground motions and structural response records

No.	**Earthquake name**	**Ground PGA (g)**	**Structural PRA (g)**	**Magnitude**	**Epicentral distance (km)**	**Event date (UTC)**
1	Lomalinda	0.008	0.017	4.0 ML	16.2	2008-06-23
2	Yucaipa	0.009	0.017	4.1 ML	34.6	2008-10-02
3	Barstow*	0.004	0.018	5.1 Mw	108.7	2008-12-06
4	Inglewood*	0.005	0.027	4.7 Mw	98.1	2009-05-18
5	Redlands	0.007	0.012	4.1 ML	23.7	1010-02-13
6	Ocotillo	0.003	0.018	5.7 ML	209.9	2010-06-15
7	Fontana	0.012	0.044	4.4 ML	11.7	2014-01-15
8	BigBearLake	0.020	0.045	4.6 ML	29.5	2014-07-05
9	Fontana	0.013	0.030	4.2 ML	15.0	2015-07-25
10	BigBearCity	0.012	0.027	3.9 Mw	44.5	2016-02-16
11	LaVerne	0.007	0.024	4.4 Mw	41.9	2018-08-29
12	SanBernardino	0.007	0.014	3.4 ML	8.0	2019-04-11
13	SearlesValley	0.005	0.024	5.5 Mw	159.2	2020-06-04

Units of magnitudes: Moment Magnitude (Mw); Local Magnitude (ML); Felt Area Magnitudes (MI).

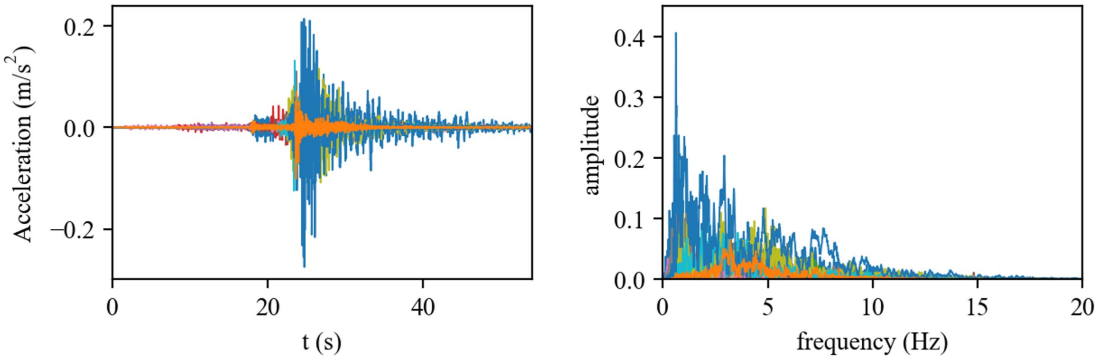

(a) Time history of ground motion (b) Fourier amplitude spectrum of ground motion

Figure 4-7. Time-domain history and Fourier amplitude spectrums of ground motions

4.3.2 Model training and testing

Without loss of generality, the measured data of channel 1 on the basement are selected as the input seismic force (i.e., ground motion), and the measured data of channel 6 on the roof are selected as the output structural seismic response in this section. To make full use of the limited field records, the raw data are resampled for data augmentation. Thus, a total number of 110 pairs of ground motions and response acceleration are obtained. They are separated randomly into training set (80%) and test set (20%). Each segment has 1080 sampling points with a time duration of 54 s.

The Conv1D and Dense layers in the CNN and SSM-CNN are designed to be compatible with the input and output shape. Both the irritation epochs of CNN and SSM-CNN are set to be 500. Figure 4-8 depicts the loss functions of model training history of CNN and SSM-CNN, with a final-epoch loss of 5.83×10^{-5} and 6.34×10^{-5}, respectively.

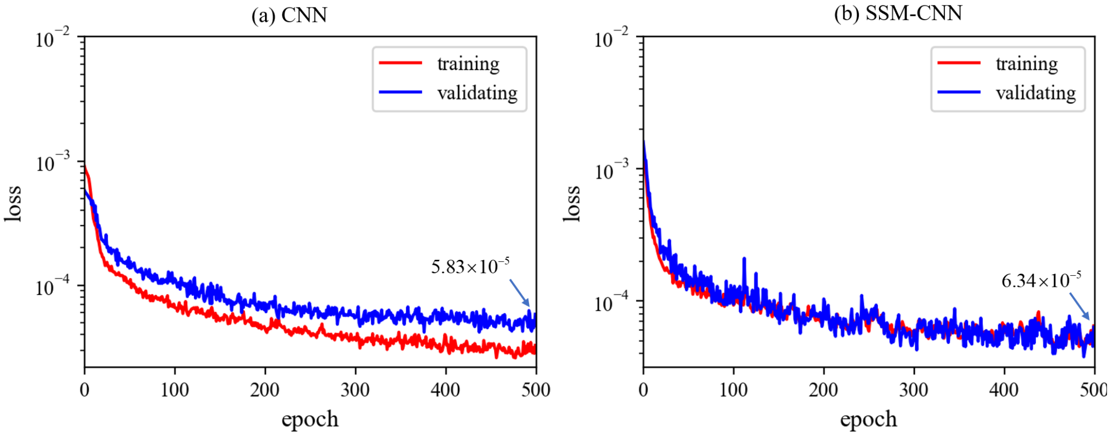

Figure 4-8. The loss functions of model convergence history: (a) CNN; (b) SSM-CNN

Similarly, correlation analysis of prediction performance is also conducted on the experimental validations, the comparison results of which are shown in Figure 4-9. Three cases are randomly selected to present the performance of seismic response prediction. The overall prediction results match well with the real responses. Specifically, the quartiles CI indices of training and testing set of CNN are (0.93, 0.98, 0.99) and (0.90, 0.97, 0.98), respectively. Remarkably, the quartiles CI of training and testing set of the proposed SSM-CNN are (0.94, 0.99, 1.00) and (0.90, 0.98, 0.99), respectively, suggesting a superior CI outcome in contrast to the CNN. The quantifiable CI indices demonstrate the effectiveness of both established CNN and SSM-CNN in seismic response prediction and confirm the superiority of SSM-CNN compared to

CNN without physical mechanism embedded.

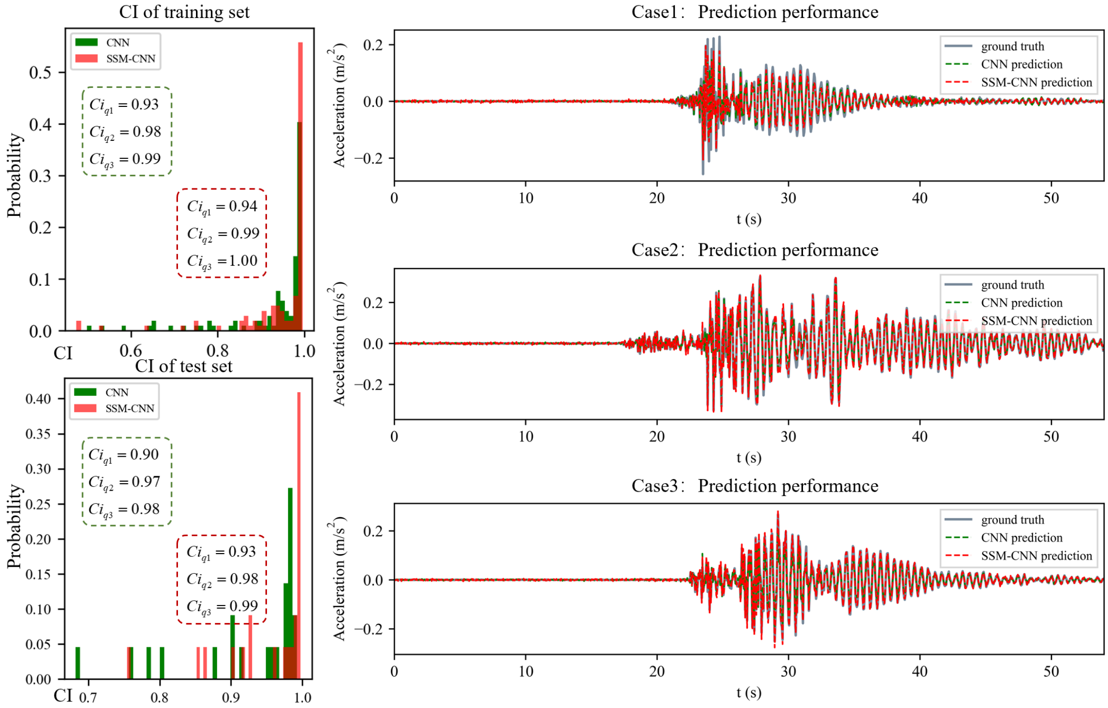

(a) Correlation analysis

(b) Cases comparison of prediction performance

Figure 4-9. Comparison of prediction performance: (a) correlation analysis; (b) cases of prediction history

4.3.3 Model generalization analysis

The two randomly-selected earthquake records as denoted in Table 4-2 which have never been involved in the model training and validating procedure are used to dig into the model generalization ability. Specifically, the CI indices of the two cases predicted by SSM are 0.12 and 0.38, and those of SSM-CNN are 0.30 and 0.49. Frankly speaking, neither the prediction performance of SSM nor SSM-CNN trained with scarce dataset could be regarded as satisfactory in terms of the low CI values. This phenomenon exhibits a similar deficiency in state-of-the-art related work by Liao et al. (2023). The model generalization ability of surrogate models for seismic response prediction proposed in this study needs further improvement in the future work with larger training set as well as specific optimization strategies. Nonetheless, as clarified in the model sensitivity analysis in Section 4.2.3, the low CI values of prediction results in low-intensity cases doesn't mean that the surrogate models are invalid. The proposed SSM-CNN with novel physics informed exhibits superior performance than conventional CNN, which confirms the enhancing effectiveness of the devised parameter-free physics-informed mechanism.

4.4 Summary

This chapter proposes a parameter-free PINN named SSM-CNN for rapid seismic response prediction. The purely data-driven surrogate model leverages the powerful capability of deep 1D CNN and SSM to build the mapping relationship between seismic ground motions and structural responses. An innovative parameter-free physics-informed mechanism is propounded by construing the differential nexus of state variables that are derived from the state-space representation of initial acceleration measure. The physics-informed mechanism is embedded into the 1D CNN to constrain training. Two groups of field-record datasets of earthquake events with different sources from PEER and CESMD are utilized for numerical and experimental validation, respectively. The prediction results verify the effectiveness and superiority of the proposed method in seismic response prediction. Unlike conventional physics-informed strategies that rely on structural parameters such as stiffness or mass matrices, the proposed parameter-free SSM-CNN allows better interpretability and adaptability of the surrogate models for seismic response prediction.

CHAPTER 5 SEMI-SUPERVISED LABEL PROPAGATION FOR STRUCTURAL CONDITION ASSESSMENT

In the monitoring of existing in-service structures, obtaining sufficient measured data with explicit labels corresponding to specific conditions is usually costly and even inaccessible. Meanwhile, unlabeled data, particularly from intact structures (IS), are continuously generated. SSL approaches become a promising solution to deal with the imbalanced data distribution in vibration-based structural condition assessment.

Two key challenges in this workflow can be summarized as extracting DSFs from unlabeled data and propagating labels from the known to the unknown.

This chapter proposes a novel semi-supervised approach for structural condition assessment. This approach integrates self-supervised learning, UL and SSL techniques. It leverages labeled data from IS as a foundation while require no labels for different damage scenarios (DSs), thus enabling an improved applicability to class-imbalance data. In essence, this method can be viewed as a label propagation (Iscen et al., 2019) process from partially known labels to unlabeled data and is therefore called a semi-supervised label propagation approach.

5.1 Semi-supervised label propagation

The proposed label propagation method consists of three main steps: DSF extraction, optimized clustering, and damage classification, as depicted in Figure 5-1. Specifically, vibrational signals representing the IS state are utilized to train DAE in a self-supervised schema. After signal representation learning, the DAE reconstructs the signal for unlabeled samples, and DSFs are defined based on the quantification of signal reconstruction errors. An optimized clustering algorithm is then employed to analyze the extracted DSFs, assigning pseudo-labels to the unlabeled data that correspond to different DSs. Finally, the DSFs and pseudo-labels are utilized as the inputs and outputs of classifier models in a supervised learning paradigm. The trained classifiers can be utilized to predict damage levels for unknown signals.

The remainder of this section will provide a detailed explanation of each of the three main steps.

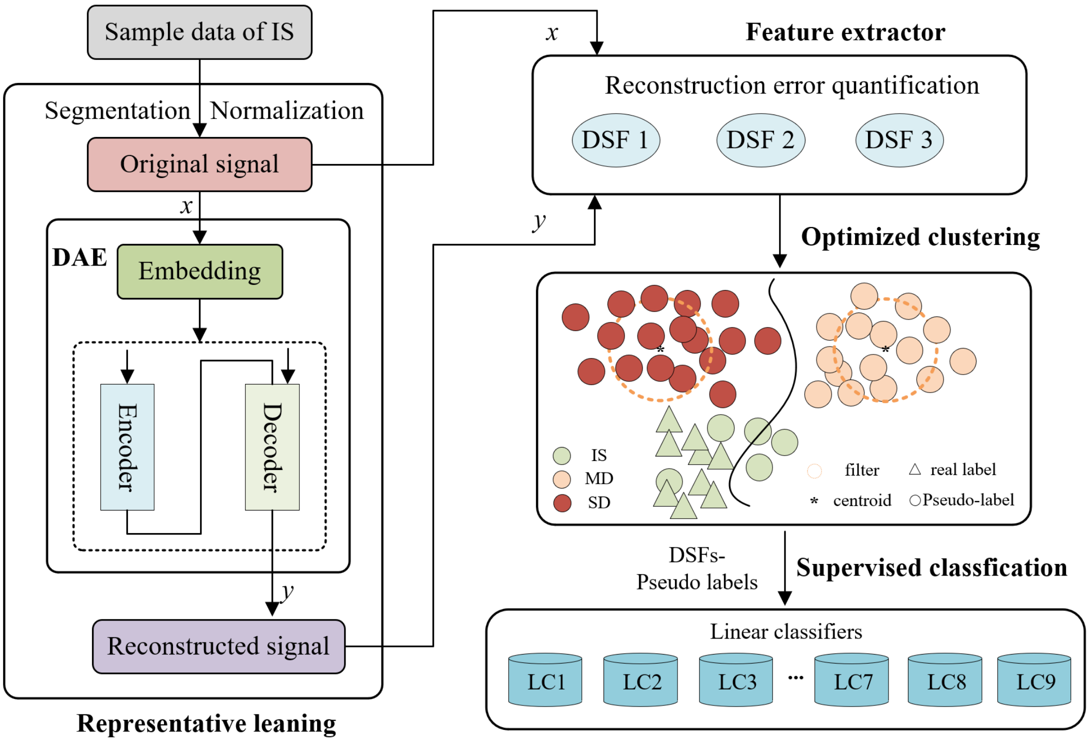

Figure 5-1. Workflow of the proposed semi-supervised label propagation method

5.1.1 DSFs extraction based on signal reconstruction

5.1.1.1 Vibration signal reconstruction by DAE

A DAE is a special type of self-supervised neural network that is trained to duplicate its input to output via repeated backpropagation. It comprises two major parts, namely encoder and decoder, both of which are stacked up with several hidden layers, as shown in Figure 5-2.

Given a signal series x_j, the encoder first encodes the signal into a lower dimensional latent representation h_i. Then the decoder decodes the latent representation back from its encoded form to a reconstructed output y_i with equal dimension with input.

$$h_i = f(W_{ij}x_j + c_1) \tag{5.1}$$

$$y_j = g(\hat{W}_{ji}h_i + c_2) \tag{5.2}$$

where f and g denote the activation functions, such as ReLU, SoftMax and Sigmoid function for the encoder and decoder, respectively. W_{ij} denotes the weight matrix connecting the input x_j to the hidden state h_i; $\hat{W}_{ji}$ denotes the weight matrix connecting the hidden state h_i to the output y_j; c_1 and c_2 are the biases between the input and hidden layers of the encoder and decoder, respectively.

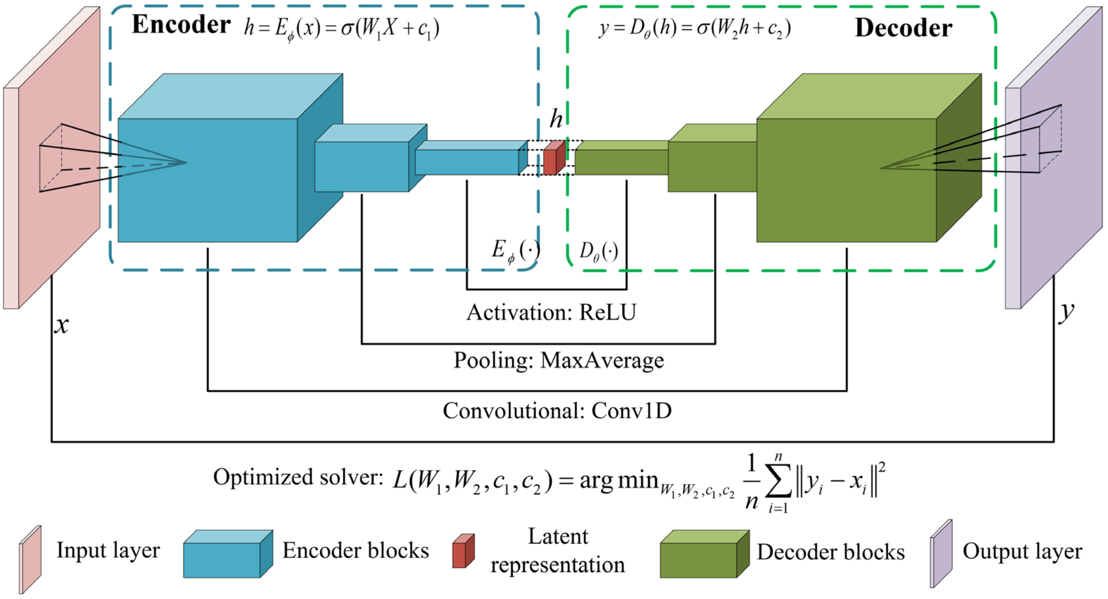

Figure 5-2. Architecture of the proposed DAE

A DAE learns to encode and decode the data while minimizing the reconstruction error $L(\bullet)$ through backpropagated optimization of weight matrices and biases, where MSE is commonly used as the cost function:

$$L(W, \hat{W}, c_1, c_2) = \arg\min_{W,\hat{W},c_1,c_2} \frac{1}{n}\sum_{i=1}^{n}\|y_i - x_i\|^2 \tag{5.3}$$

where n represents the size of input; and x_i and y_i represent the input and output of the i-th iteration, respectively.

Self-supervised representation learning on signals can prompt DAE to learn an internal representation via encoding and decoding input data. When using IS samples to train DAE, the model learns the unique potential features of IS data. When the trained DAE is used to reconstruct signals, IS samples can obtain better reconstruction performance due to their similar damage-associated characteristics. While the DAE is used to reconstruct samples from DSs, reconstruction errors will significantly increase. In other words, a DAE trained by IS samples can hardly learn an effective encoding-decoding paradigm adapted to data from DSs. Thus, the DSFs can be quantitatively defined according to reconstruction errors.

5.1.1.2 DSFs extraction

Given that the differences in vibration characteristics resulting from changes in structural damage states are sometime more pronounced in the frequency domain than in the time domain, the original time-domain vibration signals are processed using DFT to obtain their amplitude spectrum. The resulting data are then normalized and utilized as both the inputs and outputs for training the DAE model.

To quantify the reconstruction errors, three indicators namely MSE, original-to-reconstructed signal ratio (ORSR) and cross correlation coefficient (CORR) are defined as DSFs in this study. Thereinto, MSE is a classic index to quantify the reconstruction loss via measuring the similarity between the original and reconstructed data.

Inspired from the conception of SNR that compares the level of a desired signal to the level of background noise, a similar indicator namely original-to-reconstructed signal ratio (ORSR) is proven as an effective measure to quantify the discrepancy between the original and reconstructed signals (Wang & Cha, 2020). It is defined as the ratio of the cumulative square of the magnitudes of the original signal X to that of the reconstructed one Y in dB, which can be calculated as follows:

$$ORSR = 10\log_{10}\frac{\sum_{i=1}^{n} x_i^2}{\sum_{i=1}^{n} y_i^2} \tag{5.4}$$

When assessing information between two separate time series, CORR is commonly utilized to track the similarities in the movement of two factors over time, which can be expressed as follows:

$$\rho = \frac{\sum_i (X_i - \bar{X})(Y_i - \bar{Y})}{\sqrt{(X_i - \bar{X})^2 (Y_i - \bar{Y})^2}} \tag{5.5}$$

where $\bar{X}$ and $\bar{Y}$ denotes mean values of the original and reconstructed signals, respectively. The CORR can range between − 1.0 and +1.0. It quantifies how much one data series correlates with a shifted version of another series.

The three DSFs mentioned above are used to quantify the reconstruction error. Compared to a single feature index, using a combination of three indices to form the DSF vector provides a more comprehensive and systematic description of the differences between the reconstructed signal and the original signal from various perspectives. This approach facilitates the subsequent clustering of pseudo labels for DSFs and aids in downstream damage classification tasks. Additionally, it should be noted that there are multiple metrics for measuring vector differences. In addition to the three metrics selected in this chapter, other metrics can be also explored in future work.

5.1.2 Optimized fuzzy clustering

It should be noted that only DSFs of IS are assigned to labels at present stage, while those of unknown DSs are unlabeled. Therefore, the next stage is to assign pseudo labels to the unlabeled data containing the DSs, that is, to analyze the distribution characteristics of DSF through fuzzy clustering techniques to preliminarily characterize the structural damage condition. Fuzzy clustering is a classic algorithm of UL, in which the clusters are identified via similarity measures such as distance, connectivity, and intensity. Unlike building high-dimensional mapping relationships via input-output pairs in supervised learning, fuzzy clustering aims to learn a mapping between the components of the input-output pairs so-called clusters (Pedrycz, 2021).

In this chapter, the fuzzy C-means algorithm (FCM) (Bezdek et al., 1984), one of the most widely used clustering algorithms is adopted for optimized design. Given a dataset with N points and an expected cluster number of c, the workflow of FCM can be summarized and formulized as follows:

Step 1: Assume an initial clustering pattern and calculate the centroid m_0 of points in each cluster Γ_i ($i = 1, 2, \ldots, c$)

$$m_i = \frac{1}{N} \sum_{y \in \Gamma_i} y \tag{5.6}$$

Step 2: Calculate the clustering function J_e as clustering criterion, which is defined as the summed Euclidean distance of sample points to their respective cluster centroids:

$$J_e = \sum_{i=1}^{c} \sum_{y \in \Gamma_i} \left\| y - m_i \right\| \tag{5.7}$$

Step 3: Assign each sample to the cluster closest to the representative point according to the principle of minimum distance and recalculate the centroids continuously. Adjust each sample class to minimize the clustering criterion function J_e

$$\Gamma_c^{(t)} = \{ y_i : \left\| y - m_i^{(t)} \right\| \le \left\| y - m_{\sim i}^{(t)} \right\|, \forall i = 1, 2, \ldots, c \} \tag{5.8}$$

Step 4: Repeat Step 3 until the iteration calculation converges.

Using the above approach, FCM divides the sample space into clusters of a specified number of categories through fuzzy clustering. Pseudo-labels that can characterize different DSs can be assigned through clustering features of DSFs. This strategy is a common operation in multiple related studies for SSL methods (Silva et al., 2021; Wang et al., 2020; Rastin et al., 2021).

Particularly, during the extraction of DSFs, the DSF vector points (3D spatial points corresponding to the vectors) associated with different damage states may inevitably overlap. As a result, the clustering outcomes will exhibit a certain "fuzzy" region. This phenomenon is generally more pronounced in regions distant from the cluster centroids. Consequently, the pseudo-labels assigned to samples within this area based on the clustering results are likely to incur significant errors. These inaccurate pseudo-labels can adversely affect the performance of the subsequent damage classifiers, ultimately reducing the accuracy of the final predictions.

Therefore, this section devises an optimized clustering algorithm based on the classic FCM for semi-supervised damage assessment that considers the accuracy of pseudo-labels, as shown in Figure 5-3.

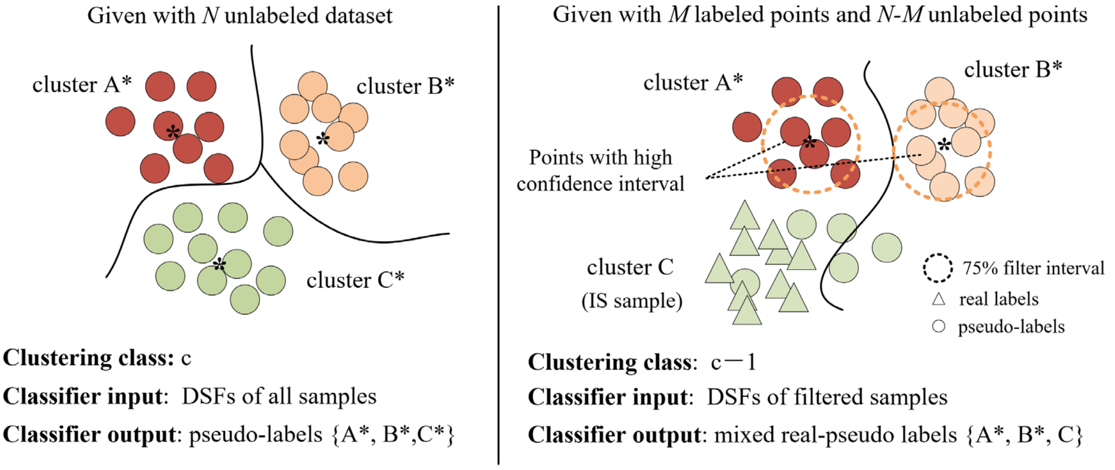

(a) FCM algorithm for UL paradigm (b) Optimized FCM algorithm for SSL paradigm

Figure 5-3. Optimized FCM for SSL paradigm

In the traditional unsupervised FCM, all samples are clustered into c categories to serve as training data for damage classifiers. In the proposed SSL clustering method, the unlabeled data, excluding the IS sample data, undergoes cluster analysis with a specified number of clusters ($c-1$) to perform pseudo-label assignment on the unknown samples. Additionally, an attention mechanism based on the centroid distance metric is introduced to eliminate fuzzy sample points that are far from the cluster center.

Specifically, based on the results of the FCM calculations, the distance of each sample point from the centroid is computed. The points that fall within the top 75% in each cluster are selected as high-confidence points. Subsequently, the DSF vectors of the labeled IS samples and the high-confidence samples, corresponding to their true or pseudo-labels, are utilized as the inputs and outputs for training the damage classifier. In this way, the accuracy of the generated pseudo-labels can be feasibly enhanced, thus benefiting the classification performance of damage classifiers.

5.1.3 Damage classification

Taking several labeled data of only IS as premise, the pseudo-labels of the other data points can be obtained through the proposed optimized FCM. Then all the samples have been attached with a pseudo-label, which could be further utilized to train a classifier in a supervised way.

To single out the appropriate classifiers, nine prevalent ML algorithms are investigated in this study, namely Gaussian Naïve Bayes (Nguyen & Do, 2020), K-nearest Neighbors (Houshmand et al., 2022), Logistic Regression (Hess & Hess, 2019), SVC (Jun, 2021), Decision Tree (Quinlan et al., 1986), Random Forest (Mohapatra et al., 2020), AdaBoost (Wang & Sun, 2021), Gradient Boosting (Sigrist, 2021) and MLP classifier (Santos et al., 2021). These ML models can be directly implemented through the open-source Python ML library Scikit-learn (Pedregosa et al., 2011) and are not described in detail in this section.

After the training is completed, given a test sample, the signal is reconstructed using the trained DAE. The DSF vector derived from the signal reconstruction error is input into the trained damage classifiers for prediction. Thus, the fundamental principles and overall process of the proposed semi-supervised label propagation method have been outlined. The following sections will present numerical and experimental validations on a shear wall structure.

5.2 Numerical validations

5.2.1 Numerical simulation of a two-story shear-wall structure

The elastic-plastic response of a two-story reinforced concrete shear wall structure under different seismic loads is simulated using ABAQUS. The structural dimensions match the subsequent shaking table test model. The density, Young’s modulus and Poisson’s ratio of concrete is 2400 kg/m^3, 37000 MPa and 0.2, respectively. Tensile strength and compressive strength of the concrete are set as 2.99 MPa and 30 MPa, respectively. The cubic element C3D8R with eight nodes and three degrees of freedom per node is used to model concrete. The linear truss element T3D2 is used to model longitudinal and transverse reinforcements. The numerical model is constructed, and a preliminary modal analysis is conducted according to the standard modeling process. These contents are not directly related to the verification of the algorithm's effectiveness and thus not discussed in detail in this section. The ground motion input is stepwise applied according to the seismic levels: 7-degree frequent occurrence (i.e., 35 gal), 7-degree fortification (i.e., 100 gal), and 7-degree rare (i.e., 220 gal). After a group of tests with each level, white noise excitation with a peak amplitude of 50 gal is applied to the structure model to obtain its modal properties.

Notably, the degree of structural damage is generally divided according to the maximum inter-story drift ratio as stipulated in related standards. However, it should be clarified that obtaining such parameters is often challenging in field measurement. And it is also impractical to construct multiple structural entity models with different DSs and conduct separate shake-table tests in experimental validations. Therefore, this chapter uses the cumulative damage state of the structure, resulting from stepwise loading of earthquake motions, as the classification standard for structural damage severities. To coincide with the subsequent experimental cases in Section 5.3, the numerical validation in this section uses the same strategy to define the structural damage labels, as shown in Figure 5-4.

Without loss of generality, the response data under white noise excitation after experiencing a 7-degree frequent earthquake is labeled as IS. The response data following cumulative exposure to a 7-degree fortification earthquake is labeled as damage status 1 (DS1), while the response data after exposure to a 7-degree rare earthquake is labeled as damage status 2 (DS2). Particularly, the defined IS, DS1 and DS2 only suggest comparative damage severity, which are not rigorous quantification. Nonetheless, considering the essential objective of this chapter, that is to develop a semi-supervised label propagation method, this definition of damage levels will make little degradation to the validation reasonability and is thus deemed acceptable.

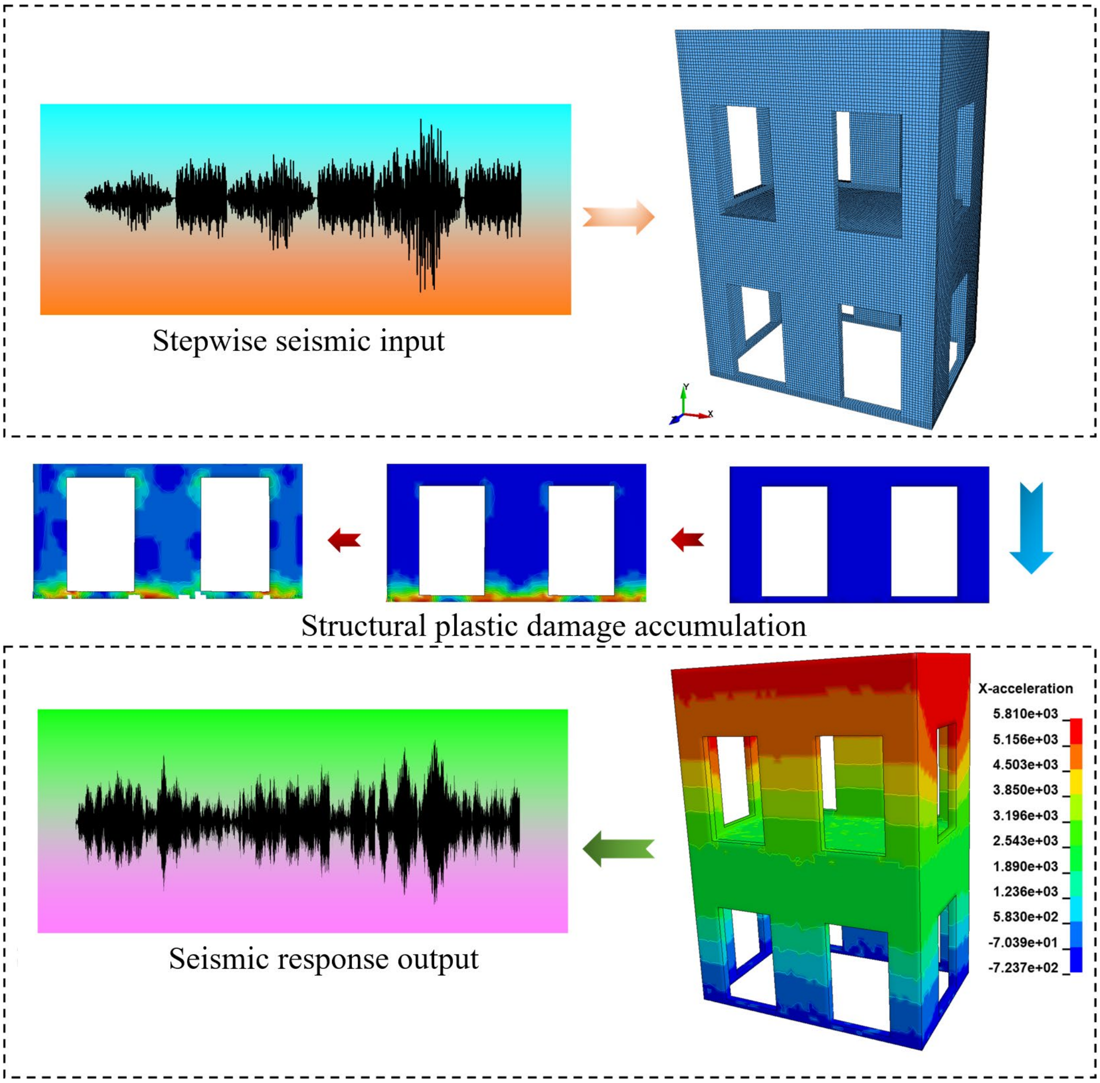

Figure 5-4. DS definition based on stepwise damage accumulation

5.2.2 Data acquisition and DSFs extraction

Without loss of generality, the acceleration response of the point on upper window beam in X direction (i.e., strong axis) are randomly selected to perform the purely data-driven condition assessment via single channel. The original vibration signal is divided into fixed-length segments, each containing 256 points with a sampling frequency of 256 Hz. After performing DFT with an identical length of the signal, the symmetric portion of the signal is normalized, resulting in a frequency-domain magnitude series containing 128 points. Using this method, a total of 400 segments of IS signals, along with 100 segments each of damage DS1and DS2 are obtained.

300 segments of IS samples are initially used to train the DAE in a self-supervised learning schema. In this DAE, the encoder consists of four fully connected layers with dimensions of 128, 64, 48 and 32, respectively. Correspondingly, the decoder also includes four fully connected layers with dimensions of 32, 48, 64 and 128. The activation function is defined as ReLU, the loss function is defined as MSE, and the learning rate for the Adam optimizer is set to 0.001. The maximum number of training epochs is set to be 500.

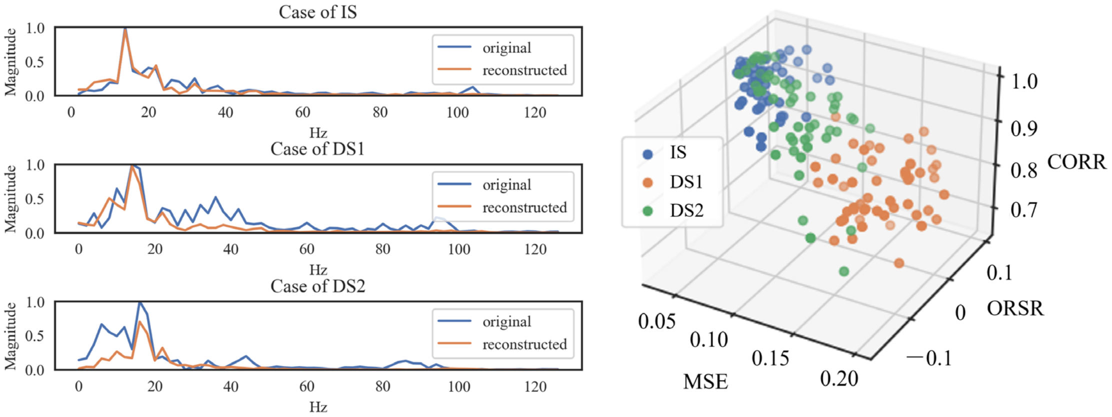

(a) DAE-based signal reconstruction

(b) Distribution of DSFs

Figure 5-5. Signal reconstruction and distribution of DSFs in numerical case

Figure 5-5(a) illustrates the reconstruction results for the three classes of signals. The IS signal exhibits the best reconstruction performance, while the more severely damaged signal (DS2) shows the poorest reconstruction performance. This difference indicates that the DAE, trained with IS data, has effectively learned the inherent characteristics of this type of data and can accurately reconstruct similar data. In contrast, a greater degree of damage correlates with an increased reconstruction error. This observation provides preliminary support for the feasibility of the proposed DSF extraction approach based on reconstruction error.

The spatial distribution of the obtained DSF vectors is shown in Figure 5-5 (b). The DSF vectors exhibit clustering characteristics related to damage levels. This clustering facilitates subsequent pseudo-label assignment using the optimized clustering analysis. Notably, the damage labels are presented solely to illustrate the effectiveness of the extracted DSFs. In this section, all data except for the IS labels are unknown and serve as a reference benchmark for evaluating final prediction results. Thus, the proposed algorithm aims to identify different DSs within this mixed data set.

5.2.3 Damage classifiers training and testing

To minimize the influence of erroneous labels from ambiguous points, only the top 75% points closest to the centroids are utilized to train classifiers. This process resulted in a total of 250 samples, comprising 100 IS samples and 150 DS samples. All 250 samples with pseudo-labels are utilized to train the classifiers, while model testing is conducted on a randomly selected subset of 75 samples with real labels.

The confusion matrices for the predictions on the testing dataset are presented in Figure 5-6. Among the nine classification algorithms tested, three of them, i.e., Decision Tree, Random Forest and Gradient Boosting achieved a notably high accuracy of 0.95. This numerical simulation validates the proposed semi-supervised label propagation method for structural condition assessment, and its applicability is further confirmed through subsequent experimental case studies.

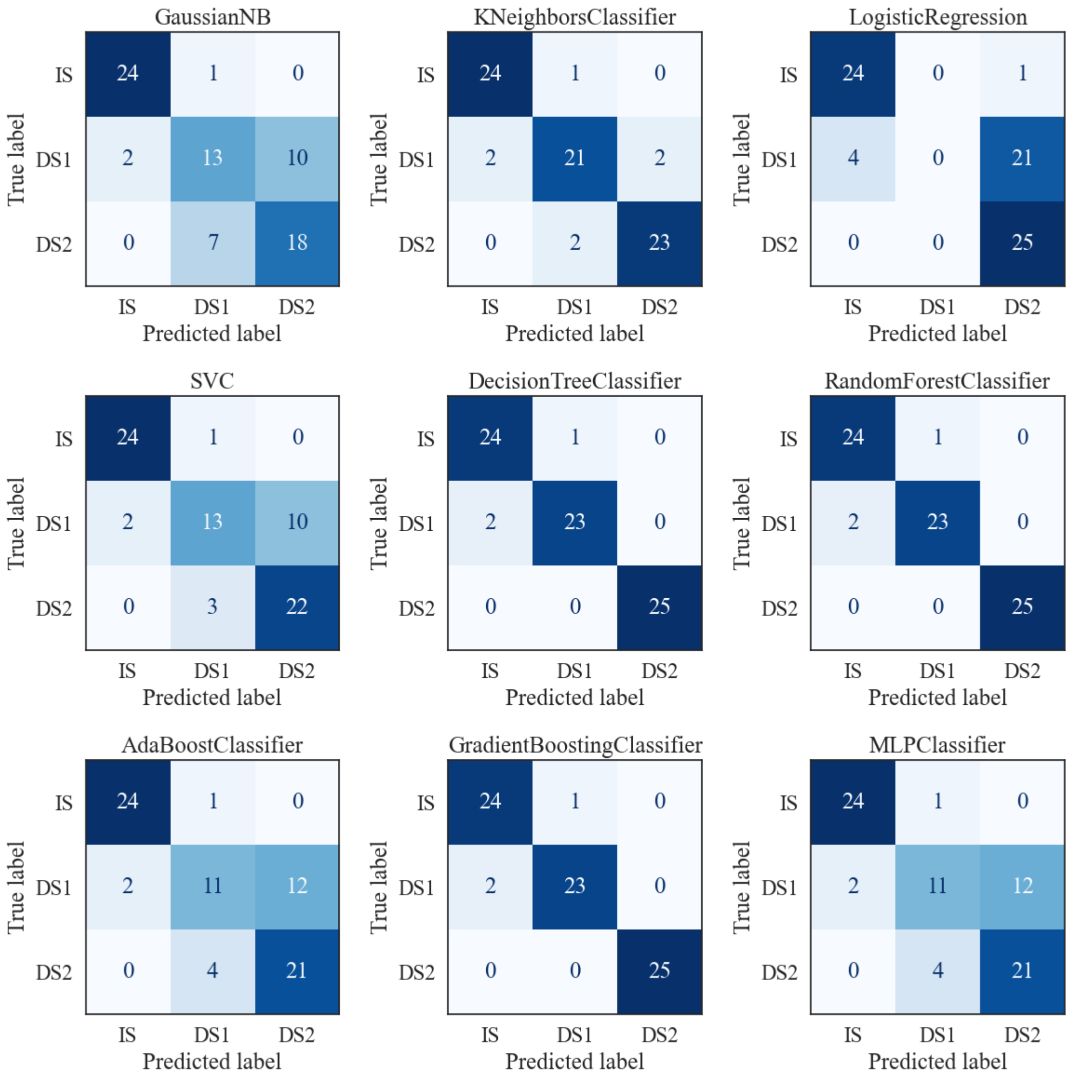

Figure 5-6. Confusion matrices of prediction results using nine classifiers

5.3 Experimental validations

5.3.1 Experimental setup

A full-scale two-story shear wall structure model is adopted to conduct experimental validation in this section. To obtain structural acceleration response of different post-earthquake damage scenarios, a shaking table test was performed on the MTS shaking table of the State Key Laboratory of Disaster Reduction in Tongji University, Shanghai, China, as shown in Figure 5-7.

The total height of the model on the shaking table is 6.9 m, including a two-story, 6.4 m-high shear wall structure and a 0.5 m-high RC foundation beam. The outer dimension of the foundation beam is 5.96 m × 3.66 m, and the shear wall structure is 4.72 m × 3.22 m. The total mass of the structure is about 52.92 t including the dead load around 49.02 t, and the live load 3.90 t deployed by additional mass. A total number of 30 accelerometers were deployed to measure the acceleration response of the structure. Amongst them, the sensor A2-1Y deployed atop the model is first selected to conduct the purely data-driven structural condition assessment.

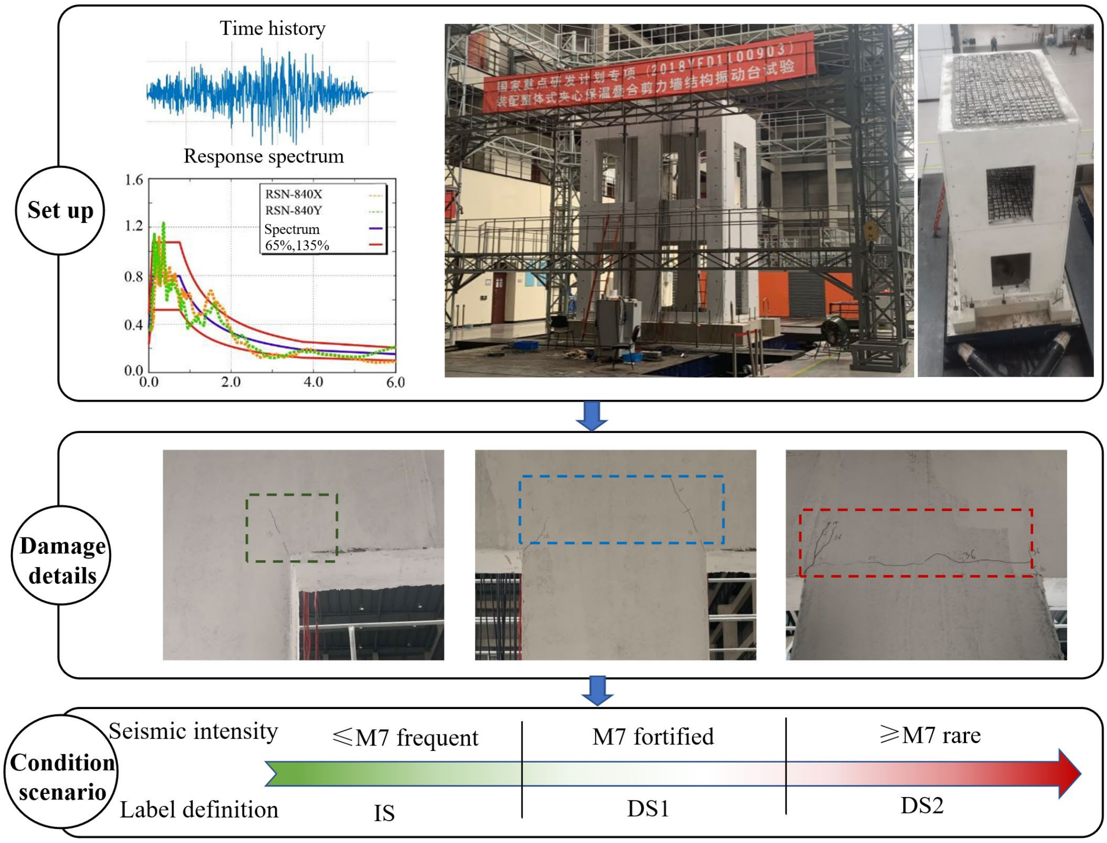

Figure 5-7. Shaking table test and DSs definition

Following the standard shaking test procedure, the input acceleration amplitudes were increased from small to large according to the fortification requirements to simulate the effect of frequent, fortified and rare earthquakes on the structure. Consistent with the previous numerical validation in Section 5.2, the structural damage state is defined according to the cumulative damage of the earthquake subjected to stepwise loading. That is, the damage state of the model structure is divided into IS, DS1 and DS2, which correspond to the structural states after earthquakes with an intensity of less than 7-degree frequent, 7-degree fortification and exceeding 7-degree rare respectively.

5.3.2 Data acquisition and DSFs extraction

After each group of seismic wave inputs in shaking table tests, a white noise force with a peak amplitude of 50 gal is applied to the model structure to measure the acceleration response. This force pattern has been shown to effectively excite multiple structural modes. The acceleration signals measured by one out of ten accelerometers are first investigated, while the other channels are utilized to perform parallel studies subsequently. Each segment has a sampling frequency of 256 Hz and a duration of 1.0 second.

Following the same procedure for training and testing DAE as in numerical validation, reconstructed signals associated with different DSs are produced. On this basis, three DSFs, namely MSE, ORSR and CORR are obtained. The distribution characteristics with corresponding real damage labels are presented in Figure 5-8. Overall, the DSFs exhibit a satisfactory clustering pattern. The MSE values of IS present a distribution with less mean value than that of DSs, while the CORR values of IS present a larger mean value, indicating a better reconstruction quality. As for the ORSR, a higher percentage of IS samples are around zero value, which suggests better reconstruction performance of IS signals. The distribution characteristics highlight the underlying mechanism between reconstruction errors and damage severities. Hence, the feasibility of allocating the three DSFs for damage condition detection is validated at a preliminary stage.

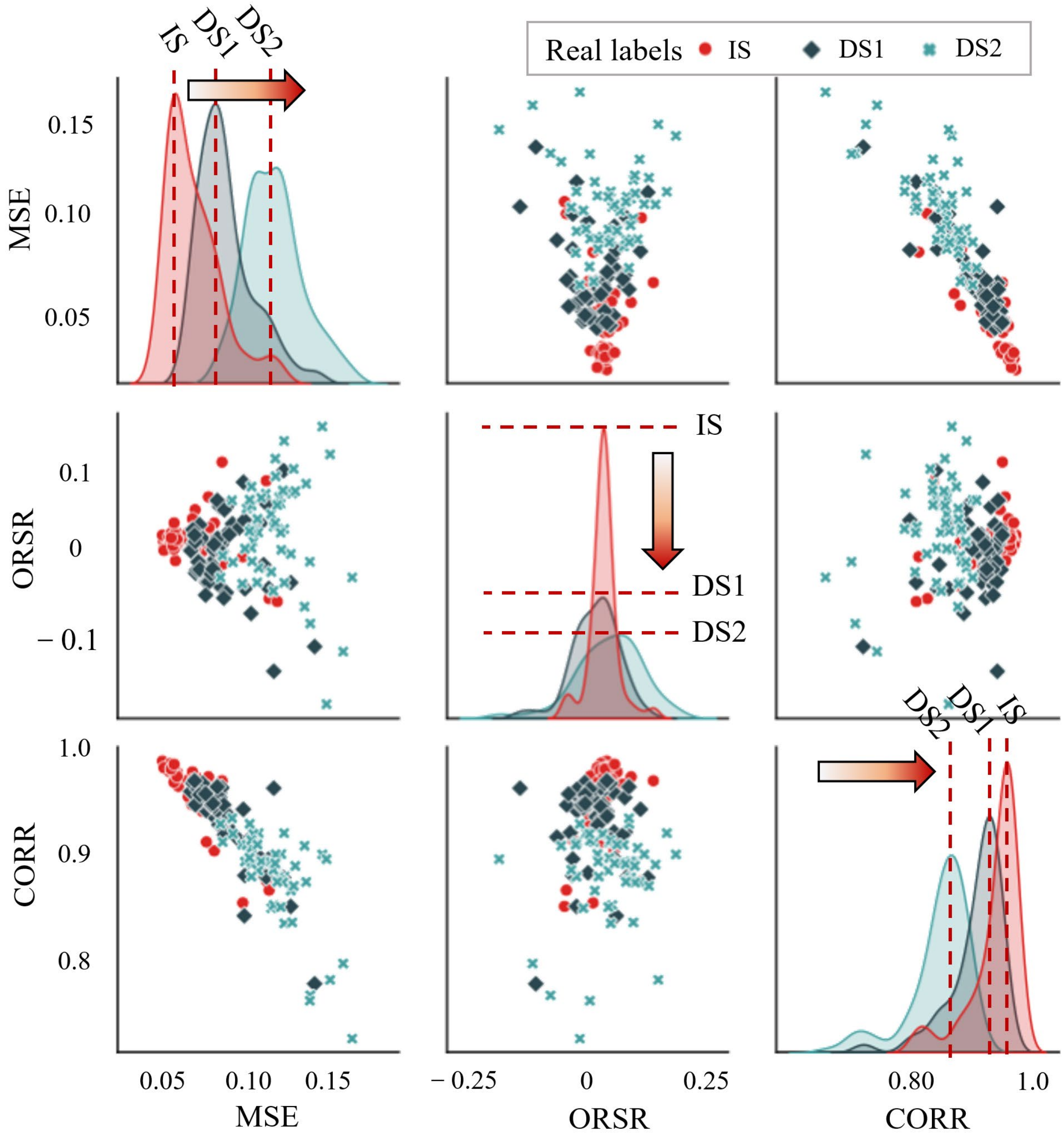

Figure 5-8. Pair-up distribution of DSFs associated with real labels

5.3.3 Damage classifiers training and testing

Taking several labeled data of IS as premise, pseudo-labels of the other data points are assigned through the proposed optimized fuzzy clustering method. Figure 5-9 depicts the pair-up distribution of the extracted DSFs for experimental case study. Compared with the true labels as shown in Figure 5-8, the pseudo-labels demonstrate consistency, particularly for those points situated near the centroid of each cluster. Since then, the semi-supervised damage condition task has been effectively transformed into a conventional supervised problem, which can be directly addressed using readily accessible classification algorithms.

All 250 samples with pseudo-labels are utilized to train the classifiers, while model testing was conducted on a randomly selected subset of 75 samples with real labels. The random forest classifier emerges as the most suitable classification model among the nine algorithms tested, achieving an accuracy of 0.85.

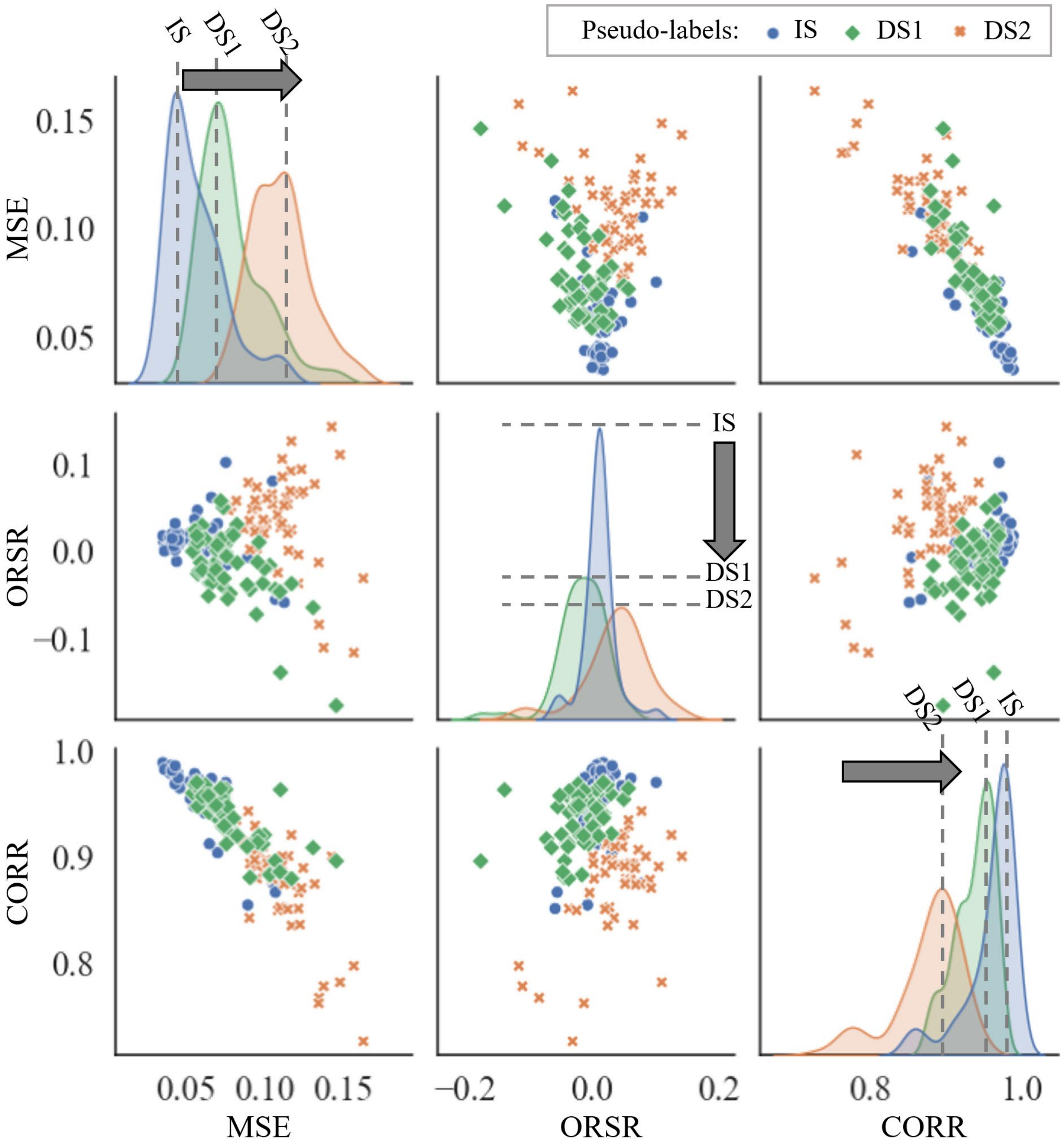

Figure 5-9. Pair-up distribution of pseudo-labels for the experimental case study

Table 5-1. Prediction accuracy summary of ten channels of sensors

Case	**Sensor**	**Direction**	**Accuracy**	**Case**	**Sensor**	**Direction**	**Accuracy**
1	A2-1Y	Y	0.85	6	A2-1X	X	0.89
2	A2-2Y	Y	0.79	7	A2-2X	X	0.95
3	A2-3Y	Y	0.84	8	A2-3X	X	0.89
4	A2-4Y	Y	0.87	9	A2-4X	X	0.80
5	A2-5Y	Y	0.84	10	A2-5X	X	0.85
Average accuracy				0.86			

To further validate the robustness of the proposed method, all ten channels of accelerometers deployed on top of the model structure are examined individually. The final prediction accuracy results are summarized in

Table 5-1. The average accuracy attained is 0.86, with the random forest classifier demonstrating the best performance consistently across all cases.

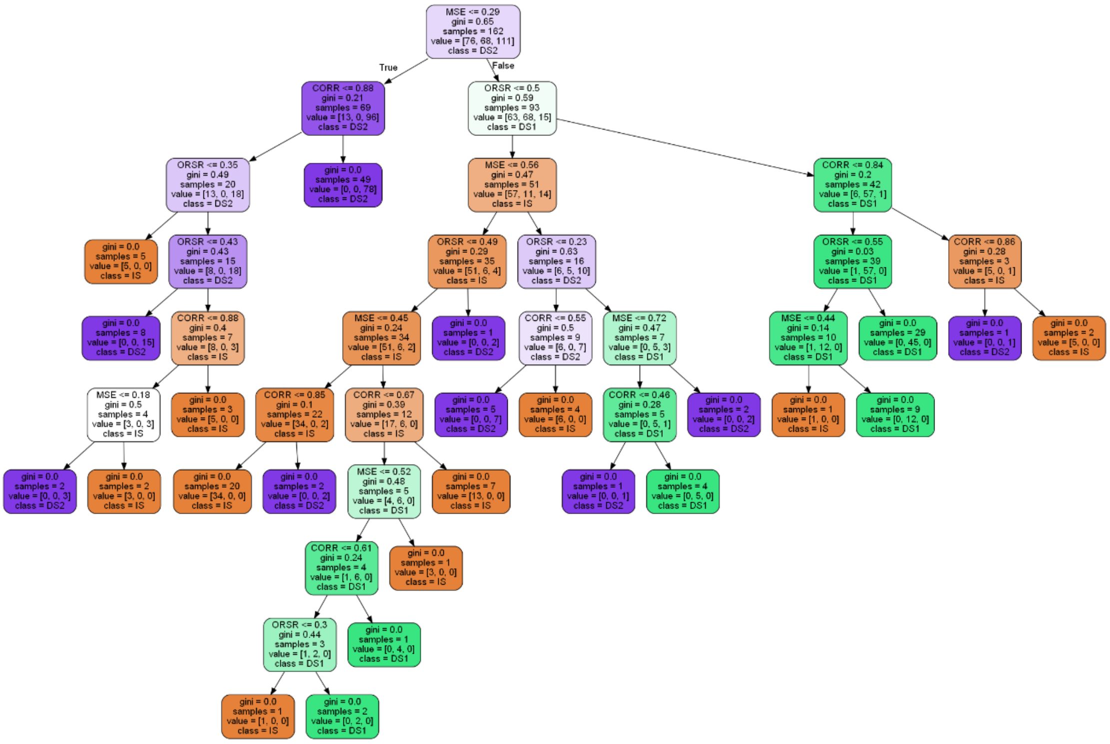

Figure 5-10. Visualization of decision trees in random forest

As the name suggests, a random forest comprises of numerous individual decision trees ensembled as an entirety. Featured as an example of a “black-box” algorithm, each individual tree makes a class prediction, and the class with majority votes becomes final prediction. Particularly, it is possible to understand how the algorithm operates by visualizing the trees within the random forest. Figure 5-10 depicts the visualization results of decision trees in the trained random forest classifier for Case 1, here solely for presenting the "tree" architecture. Given an acceleration time series, three DSFs can be obtained via the data processing with the trained DAE. Based on these values, the corresponding structural condition can be analytically identified in accordance with the decision trees of the random forest.

5.4 Summary

In this chapter, an innovative semi-supervised label propagation method is proposed for structural condition assessment. In this method, DAE is established to perform the representation learning of vibration signals. Three specified indicators, namely MSE, ORSR and CORR are defined as DSFs to quantify the reconstruction errors. An optimized fuzzy clustering technique is devised based on the classic FCM algorithm, which can improve the accuracy of assigned pseudo-labels, thus allowing for better performance of the damage classifiers.

Both numerical simulations and laboratory shaking table test of a full-scale shear wall structure are conducted to validate the method. Nine prevalent ML classification algorithms are investigated, among which random forest classifier turns out to be the most appropriate model with a prediction accuracy of 0.95 in numerical validation and an average accuracy of 0.86 in the experimental case study. As a stringent semi-supervised approach, the proposed method can perform structural condition assessment in a relevantly reliable accuracy without any labels of DSs, which indicates a vast applicability in data-driven structural condition assessment given limited training data labels.

CHAPTER 6 ZERO-SHOT KNOWLEDGE TRANSFER FOR STRUCTURAL CONDITION ASSESSMENT

Due to the stringent data availability and knowledge transfer paradigm, quite few studies have been presented thus far to achieve a zero-shot knowledge transfer toward structural condition assessment. This chapter presents a novel zero-shot knowledge transfer approach through multi-channel 1D CNN integrated with DAE-based DA. Unlike normal GAN-based strategies, the proposed DA module is devised as translating the unseen samples in the target domain to a mimic latent representation via a pretrained DAE using purely source data, thus achieving rigorously zero-shot learning schema.

6.1 The proposed zero-shot knowledge transfer framework

The overall workflow of the proposed zero-shot knowledge transfer framework is depicted in Figure 6-1.

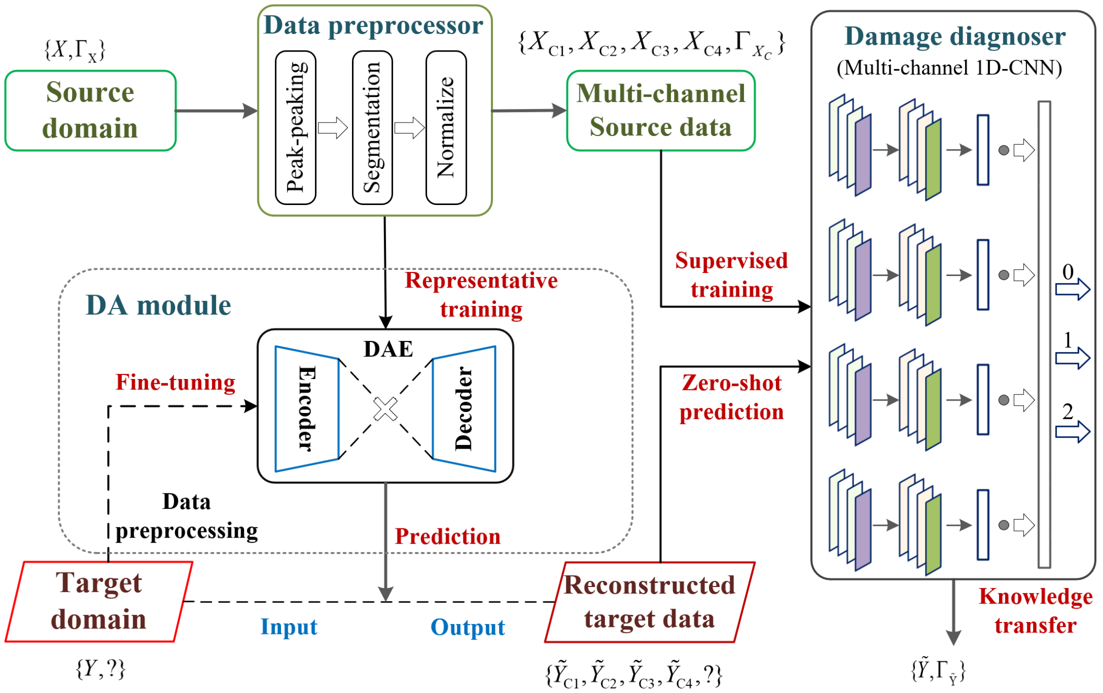

Figure 6-1 Overview of the proposed zero-shot knowledge transfer framework

The framework comprises two data source branches, i.e., the source domain and target domain, and consists of three major modules, namely data preprocessor adaptive for seismic vibration signals, DAE-based DA module, and damage diagnoser assembled by multi-channel 1D CNN. In this framework, the target-domain data is reconstructed using a DAE trained by the source-domain data, allowing for a similar latent space to the source-domain data. Thus, the damage diagnoser trained by the source-domain data in a supervised learning paradigm could be readily utilized to perceive damage-informed knowledge on the obscure target-domain data. The three main modules in the proposed zero-shot knowledge transfer approach are elaborated subsequently.

6.1.1 Data preprocessor adaptive for seismic vibration signals

Seismic vibration data often exhibit non-stationary characteristics, manifesting as time-varying amplitude, frequency-dependent contents, and transient variation profiles (Yu et al., 2022). Appropriate preprocessing is essential for accurately analyzing and interpreting the data, such as data cleaning, resampling, segmentation, baseline correlation, time-frequency domain transformation, normalization techniques, etc. Specific process adapted to the seismic vibration data needs to be implemented.

In this section, a stepwise process including peak-adjacent segmentation and normalization is devised to better suit seismic vibration signals, which are detailed as follows.

- **Peak-adjacent segmentation**

In most historical records or sensing vibrational signals, the majority of long-duration signals are manifested as ambient-excitation perturbation with low amplitudes. In this circumstance, the SNR of the measurement is probably quite low, which can pose substantial challenges to effective feature extraction and data interpretation.

Thus, in this study, a peak-adjacent segmentation strategy is devised to ensure determining the high-SNR partition series while eliminating the negative effect caused by the low-SNR partitions, as shown in Figure 6-2. The peak point of the entire series is first recognized, and a slice length L is then cut out as the valid partition on this center

Particularly, the slice length L needs to be designated manually according to the raw data length and excitation duration, as long as ensuring that the segment covers multiple completed periods of structural vibration. Thus, the selected partition can be resampled via regular segmentation process such as window sliding.

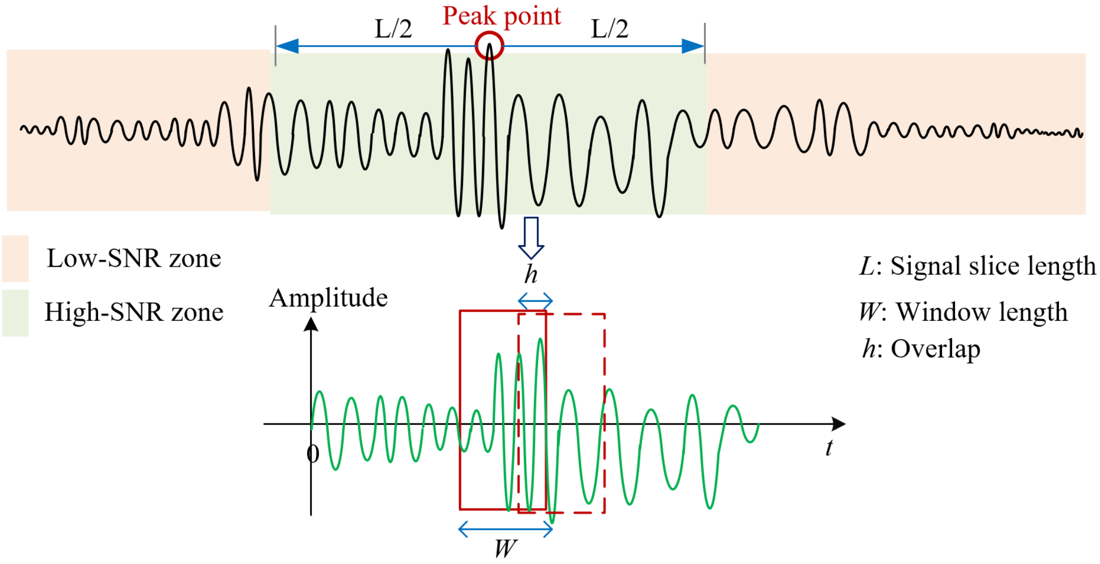

Figure 6-2. Schematic diagram of peak-adjacent data segmentation

- **Normalization**

Normalization involves scaling the input features to a fixed range to ensure no single feature disproportionately influences the results. Normalization can improve the convergence and stability of some machine learning algorithms, particularly those that use gradient-based optimization.

In this study, the raw acceleration signals are scaled into a fixed range of −1 to 1, considering the compatibility with the activation function of the ML models employed. The mathematical equation can be expressed as follows:

$$y' = y / \max(abs(y)) \tag{6.1}$$

where $\max(abs(\cdot))$ refers to the maximum absolute value of the input vector.

6.1.2 Damage diagnoser: Multi-channel 1D CNN

As classic feed-forward neural networks, CNN has demonstrated its efficacy in a variety of computer vision and machine operation tasks (Ghose et al., 2020; Yuan et al., 2021; Zhao et al., 2022). The conventional CNN is designed to handle 2D data such as images and videos. Nonetheless, 1D and 3D CNN are employed in certain scenarios. Recently, 1D CNN has exhibited exceptional performance in processing 1D signals, such as vibrational time series. The reduced computational complexity of 1D CNN compared to 2D CNN makes it particularly suitable for real-time operations.

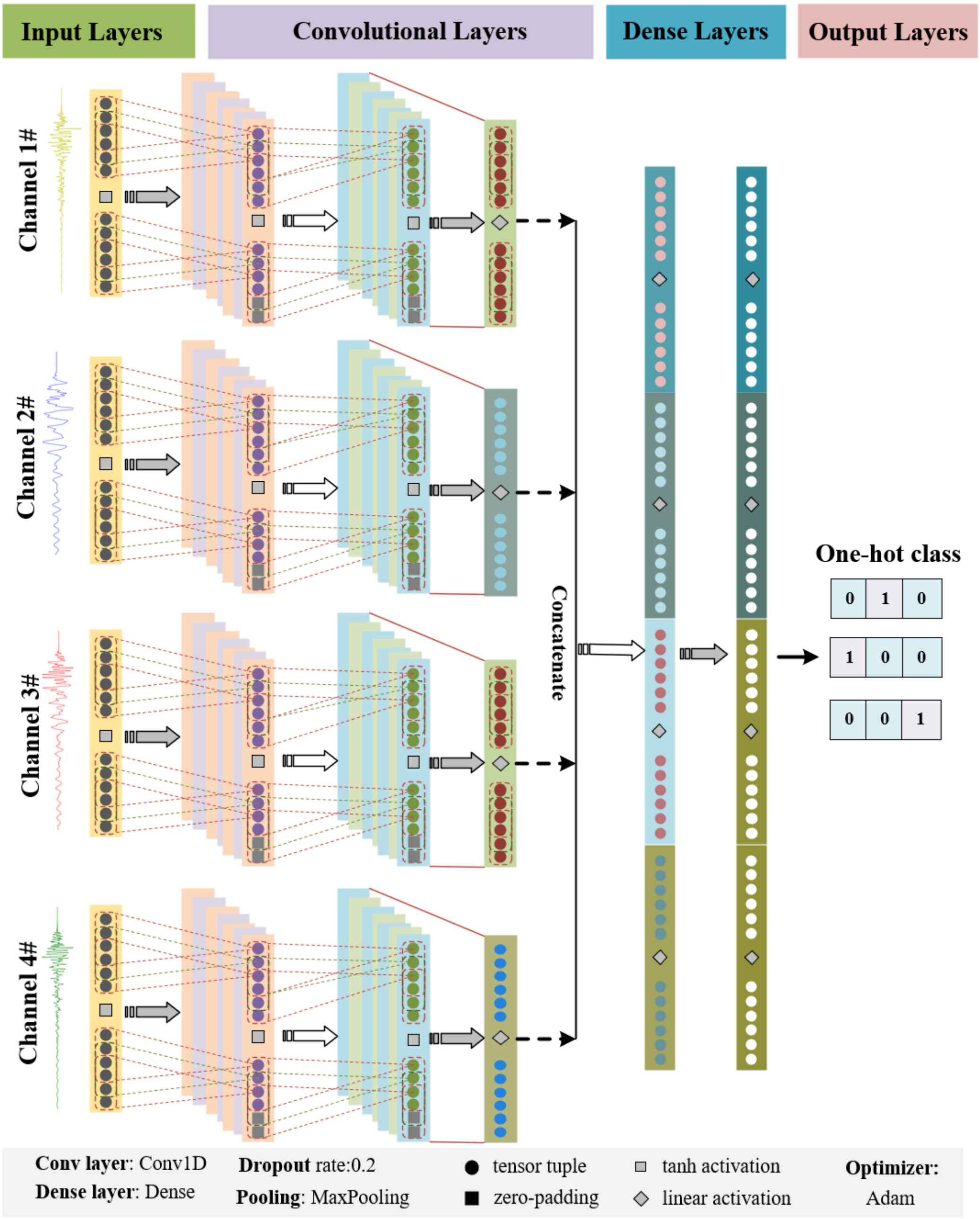

Figure 6-3. Architecture of the proposed multi-channel 1D CNN for damage diagnosis

A multi-channel network is designed by considering multiple input channels simultaneously, which allows for richer, more comprehensive feature extraction, thus leading to improved performance in structural damage diagnosis. The key idea behind a multi-channel CNN is to apply separate sets of filters to each input channel and to extract relevant features independently, as shown in Figure 6-3.

These feature maps are subsequently combined to capture the interdependencies and relationships among different input channels via concatenating the feature maps along the channel axis, resulting in a tensor that depicts the multi-channel feature representation. In the present study, vibration signals collected by sensors at different floors of a building structure are defined as the input of multiple channels, which are further elaborated in the validation sections.

6.1.3 DAE-based DA

The primary objective of the DA module is to minimize the discrepancy between the unseen target domain and the source domain, especially in terms of joint probabilistic distribution between feature space and labels. In general GAN-based DA approaches, unlabeled data are involved in adversarial training. However, in zero-shot knowledge transfer, the gap bridging issue shifts from domain "adaptation" to domain "translation", that is, the zero-shot target data are translated into a similar feature space associated with the well-deliberated source domain.

Inspired by the powerful capability of the representative learning of DAE, the proposed DA method utilizes the source domain data, more specifically, the vibration signals containing multiple damage states regardless of labels at this stage. As a unique self-supervised learning type, a DAE is designed to reproduce the input to output by learning to encode and decode the data while minimizing the reconstruction error through backpropagation. Particularly, given a tuple x_j, the input is first encoded into a lower dimensional representation space h, which is further encoded into initial dimension as a reconstruction output $\tilde{x}_j$. This encoding-decoding process can be described as follows:

$$h_i = \varphi_E(w_{ij}^E x_j + b^E) \tag{6.2}$$

$$\tilde{x}_j = \varphi_D(w_{ji}^D h_j + b^D) \tag{6.3}$$

where φ denotes the activation functions; w is the weight matric; b is the bias; and the subscripts E and D refer to the hidden layers of the encoder and decoder, respectively. In the present study, the MSE is defined as the error loss function. Thus, the optimization of the weight matrices and biases can be expressed as follows:

$$\Gamma(w^E, w^D, b^E, b^D) = \underset{\{w^E, w^D, b^E, b^D\}}{\arg\min} \frac{1}{L} \sum_{j=1}^{L} \left\| \tilde{x}_j - x_j \right\|^2 \tag{6.4}$$

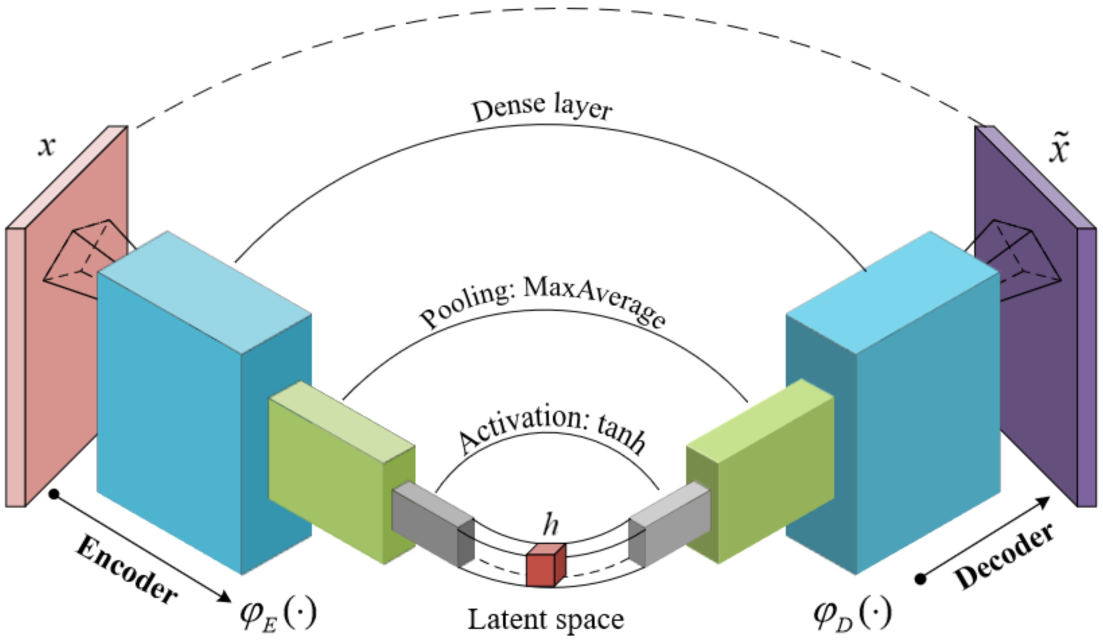

Figure 6-4. Architecture design of the proposed DA-oriented DAE

The architecture design of the proposed DA-oriented DAE is presented in Figure 6-4. The fully-connected layers are allocated for kernels of encoding and decoding, while the pooling layers (i.e., Moxaverines pooling) and activation function (i.e., tanh) are embedded. The labels (i.e., multi-class categories) are performed on one-hot encoding to avoid the problem of ordinality and thus improve the model performance by providing more information to the model about the categorical variable. The Adam optimizer (D. Kingma & J. Ba, 2014) with a learning rate of 0.001 is utilized to update network weights iteratively based on the training data. The parameters, such as the numbers of neurons and epochs, can be determined by specific data input, which are elaborated in the subsequent validation sections.

After training the DAE with sufficient source data, the limited, unlabeled, and imbalanced target data are fine-tuned with less training epochs than the pre-training phase. In this study, the epochs of pre-training and fine-tuning are set to be 500 and 50, respectively. In this manner, the pretrained DAE model can reconstruct the target test data into similar feature space associated with the source domain, owing to its prior abundant representative learning on the source data.

Hereby, the underlying design philosophy and innovative mechanism of the proposed method is demonstrated, and the three major modules are elaborated. A data preprocessor adaptive to seismic vibration signals, a damage diagnoser via multi-channel 1D CNN, and a DAE-based DA module are devised and integrated in the proposed zero-shot transfer learning approach, which is promising in knowledge transfer for structural damage diagnosis with superior adaptability and reliability.

Particularly, considering the practical data availability in engineering practice, where a series of numerical models with multi-level fidelity can be established and associated with certain real-word structure as is, the damage on the target prototype structures can be diagnosed using the knowledge derived from the source numerical data. In this context, two kinds of gaps exist in knowledge transfer: the gap between multi-level fidelity numerical models (e.g., the simple and refined), and the gap between the numerical models and real-world structures. Consequently, these two gap paradigms pose substantial challenges to the knowledge transfer for structural damage diagnosis.

To this end, two knowledge transfer schemas, namely, from a simplified model (low fidelity) to a refined model (high fidelity), and from a numerical model to an experimental structure, are investigated to verify the proposed method. One noteworthy point of the first validation phase is that the gap between the simplified and refined numerical models can mimic the inherent offset in numerical models compared to real-world structures to some extent. In this regard, investigating the capability of the proposed method in transferring knowledge from a simplified model to a refined model is reasonable for validation and facilitates the understanding and evaluation of proposed zero-shot knowledge transfer approach. Therefore, the two-phase validations are performed subsequently to evaluate the effectiveness and performance of the proposed method thoroughly.

6.2 Numerical validations upon benchmark models

6.2.1 Data acquisition for cross-domain damage quantification

Given the inherent challenges in comparing numerous methods documented in the existing literatures, this study applies the proposed method to tackle a benchmark problem in SHM, specifically targeting the quantification of structural damage severity. The problem was proposed by the IASC-ASCE Structural Health Monitoring Task Group. It adopts two analytical models of a four-story, two-bay by two-bay steel-frame shear building to emulate representative damage patterns (DPs) to be identified (Johnson et al., 2004). The simplified model has 12 degree-of-freedom (DOF), and the refined model has 120-DOF.

Specifically, the simplified model restricts all movements except for two horizontal translations and one rotation per floor, where Euler–Bernoulli beam elements are used. Therefore, the refined model only requires that the floor nodes have identical horizontal translations and in-plane rotations. Euler–Bernoulli beam elements are used for columns and floor beams, while truss elements are adopted for the braces without bending stiffness, as shown in Figure 6-5(a).

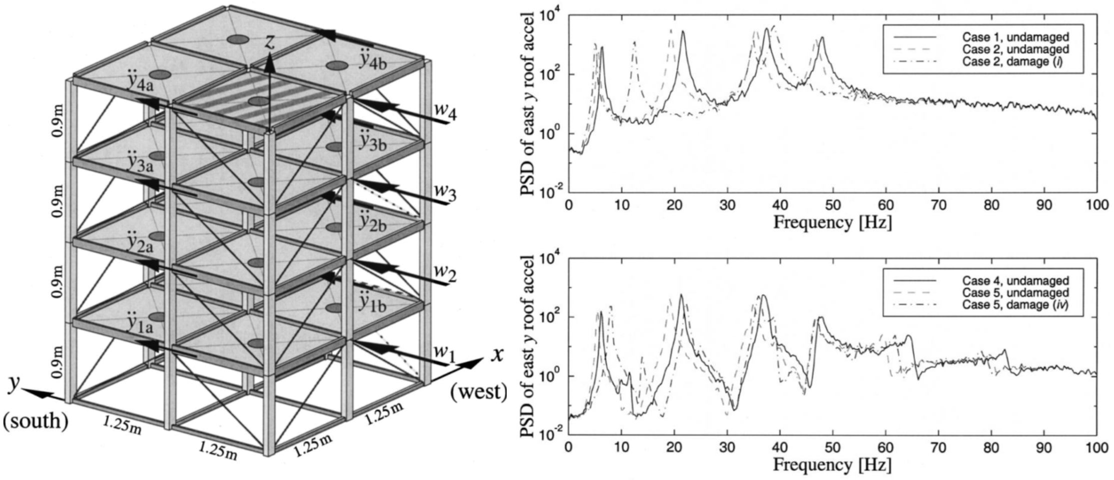

(a) The benchmark model

(b) Cases of acceleration PSD

Figure 6-5. Benchmark structure and power spectral densities of acceleration (Reproduced from the benchmark study (Johnson et al., 2004))

Table 6-1. Definition of damage severity and description of damage patterns

Damage pattern	Damage description	Re-defined damage severity
Undamaged	No damage	Intact structure, (IS)
DP1	No stiffness in all the 1st floor braces	Severe damage, (SD)
DP2	No stiffness in all the 1st, 3rd floor braces	
DP3	No stiffness in one 1st floor braces	Moderate damage, (MD)
DP4	No stiffness in one 1st, 3rd floor braces	
DP5	No stiffness in one 1st, 3rd floor braces, and one beam-column connection weakened	

In the introduced benchmark models, various DPs are defined through removing braces or weakening certain beam-column connection, which are then redefined into three damage severities according to their stiffness loss extent in this study, namely, intact structure (IS) with no damage applied, moderate damage (MD), and severe damage (SD), as summarized in Table 6-1. Typical acceleration power spectral densities for several cases and DPs are presented in Figure 6-5(b). The percentage loss of stiffness of different DPs compared with the undamaged scenario is presented in Table 6-2. Accordingly, three damage severity groups (i.e., labels to be identified) are redefined with analogous stiffness degradation obeying customary practice in the related literatures (Das & Saha, 2018; Shi et al., 2022; Tronci et al., 2023), which is considered reasonable and acceptable without loss of generality.

Table 6-2. Percentage loss in stiffness of DPs compared with the intact model (Recalculated from the benchmark study (Johnson et al., 2004))

Story	DOF	IS (Intact)	SD (Severe damage)		MD (Moderate damage)		
		Undamaged	DP1	DP2	DP3	DP4	DP5
1	x	0	45.24%	45.24%	0.00%	0.00%	0.00%
	y	0	71.03%	71.03%	17.75%	17.75%	17.75%
	θ	0	64.96%	64.96%	9.87%	9.87%	9.87%
2	x	0	0	0	0	0	0
	y	0	0	0	0	0	0
	θ	0	0	0	0	0	0
3	x	0	0	45.24%	0	11.31%	11.31%
	y	0	0	71.03%	0	0.00%	0.00%
	θ	0	0	64.96%	0	9.15%	9.15%
4	x	0	0	0	0	0	0
	y	0	0	0	0	0	0
	θ	0	0	0	0	0	0

Notes: x, y, and θ represent the DOF in the x, y and rotational directions, respectively.

Table 6-3. Natural frequencies (Hz) of the simplified and refined models (Reproduced from the benchmark study (Johnson et al., 2004))

Mode No.	Undamaged		DP1		DP2	
	12-DOF	120-DOF	12-DOF	120-DOF	12-DOF	120-DOF
1	9.41(y)	8.59 (y)	6.24 (y)	5.47 (y)	5.83 (y)	4.96 (y)
2	11.79 (x)	9.18 (x)	9.91 (x)	7.37 (x)	9.52 (x)	6.68 (x)
3	16.53 (θ)	14.58 (θ)	11.84 (θ)	9.69 (θ)	11.13 (θ)	8.70 (θ)
4	25.60 (y)	23.45 (y)	21.58 (y)	19.31 (y)	14.93 (y)	12.34 (y)
5	32.07 (x)	25.95 (x)	28.99 (x)	22.77 (x)	24.98 (x)	17.79 (x)
6	38.85 (y)	36.81 (y)	37.56 (y)	34.18 (θ)	28.78 (θ)	21.56 (θ)

Notes: x, y, and θ represent the DOF in the x, y and rotational directions, respectively.

To calculate the response of the analytical models, a MATLAB-based finite element analysis code is used via the modal superposition approach. Thereinto, a discrete-time integration algorithm is adopted by assuming the excitation is constant over a time step. The excitations are described as filtered Gaussian white noise through a sixth-order low-pass Butterworth filter with a cutoff frequency of 100 Hz. 10% Gaussian noise of the acceleration responses in terms of root mean square is added to the analytical response data to simulate the measurement noise (Shi et al., 2022).

Hence, the acceleration data of the benchmark structure are produced using a consistent parameter configuration, including a damping ratio of 0.01 and a time interval of 0.01 s. The response signals with a duration of 10,000 s (i.e., 1 million points) of each undamaged and damaged pattern are simulated. Without loss of generality, the acceleration data of the four floor points of the medium east column are designated as the input of multi-channel 1D CNN. Considering the natural frequency of the models, the signal segment is defined as a 100-point length covering several completed vibrational periods. Particularly, as sufficient data can be generated by analytical models, the raw data are segmented without window overlapping. Thus, 10,000 samples of the structural responses associated with each damage severity are obtained, which are then utilized to perform numerical validations.

6.2.2 Knowledge transfer from the simplified to refined models

As mentioned above, an uncertain gap between the simplified models and the refined models might exist, manifested as different dynamic properties and thus hindering the knowledge transfer effectively. The natural frequencies of the two models in the undamaged and damaged scenarios are compared, in Table 6-3. The first six natural frequencies of the models have significant differences. In this context, the proposed method is utilized to tackle the zero-shot problem of transferring knowledge from the simplified to refined models for damage severity quantification.

To comply with the input segment length of 100, the three units of three encoded layers in DAE are set to be 100, 64, and 48 successively, whereas those of the decoded layers are set to be 48, 64, and 100 inversely. The source domain data consisting of all the damage labels are utilized to train the DAE in a self-supervised paradigm. The number of pre-training epochs at this stage is set to be 200, with an early stopping (Yao et al., 2007) module with 50-epoch patience monitored by validation loss embedded to alleviate over-fitting through stop training when the monitored metric stops improving.

The damage diagnoser, that is, multi-channel 1D CNN, detail architecture catering to the data in this section is presented in Figure 6-6. Given an input with a length of 100, the first Conv1D layer is embedded with 32 filters and a kernel size of 4, and the second Conv1D layer is embedded with 16 filters and a kernel size of 4.

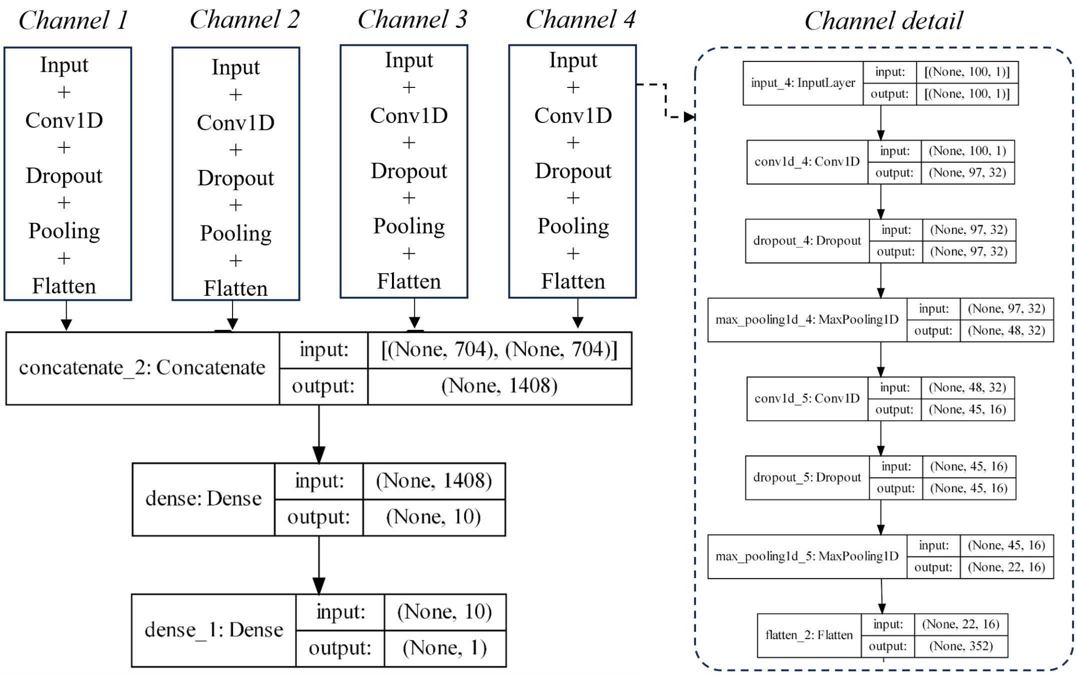

Figure 6-6. Architecture of designed multi-channel 1D CNN for damage diagnosis

Particularly, to represent the label imbalance of real data distribution better, a random data split method is devised to divide the source-domain data into training set and validation set, while the test set is assigned by the unseen target-domain data, as schematically illustrated in Figure 6-7. Unlike conventional data splitting practice via dividing the samples at a certain split ratio, the original sample data are first fully permutated randomly and then divided partially with certain splitting ratio. In this way, both the training and validation set of the source domain and the test set of the target domain could extensively comply with the practical circumstance where the data distribution is always label-imbalanced with minute prior information.

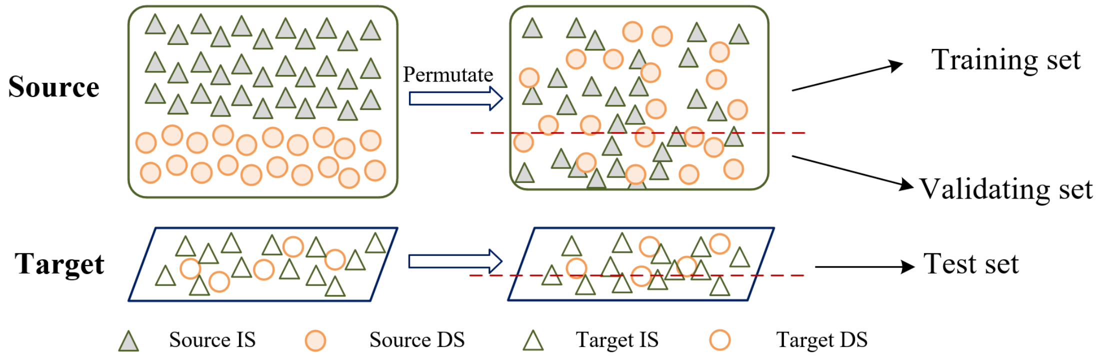

Figure 6-7. Schematic illustration of random data split considering label imbalance

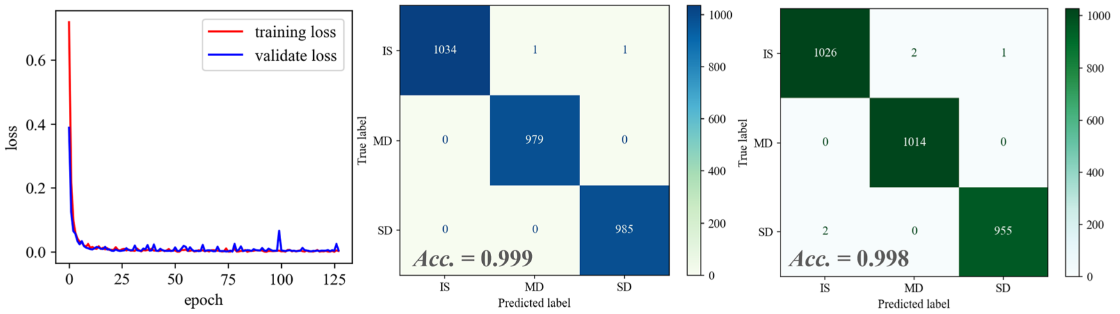

(a) Training loss function (b) Confusion matrix of validation (b) Confusion matrix of test

Figure 6-8. In-domain multi-class damage classification: training loss and confusion matrices

The multi-channel 1D CNN is trained and validated by the source-domain data processed by the data processer to build a mapping nexus between the multi-channel vibration signals and the associated damage severity labels. Figure 6-8(a) presents the convergence of training loss function. The damage diagnosis model converges at a very beginning epoch and remains stable until stopped by the early-stopping module. The ultimate validation and test performances are shown in Figure 6-8(b) and Figure 6-8(c). The two confusion matrices reveal the overall prediction accuracy, that is, the in-domain validation and testing accuracy exceed 0.998. Thus, the proposed multi-channel 1D CNN is competitive in in-domain damage quantification as a multi-class classifier.

After the DAE (i.e., DA module) and multi-channel 1D CNN (i.e., damage diagnoser) are well trained by the source-domain data, the unseen target-domain test samples are utilized to perform the task of zero-shot knowledge transfer toward damage quantification. Figure 6-9 depicts the cross-domain prediction results of with and without intervention by the proposed DAE-based DA method. After translation by the DA module, the cross-domain prediction accuracy increases from 0.626 to 0.820, improving the performance by 31.0%.

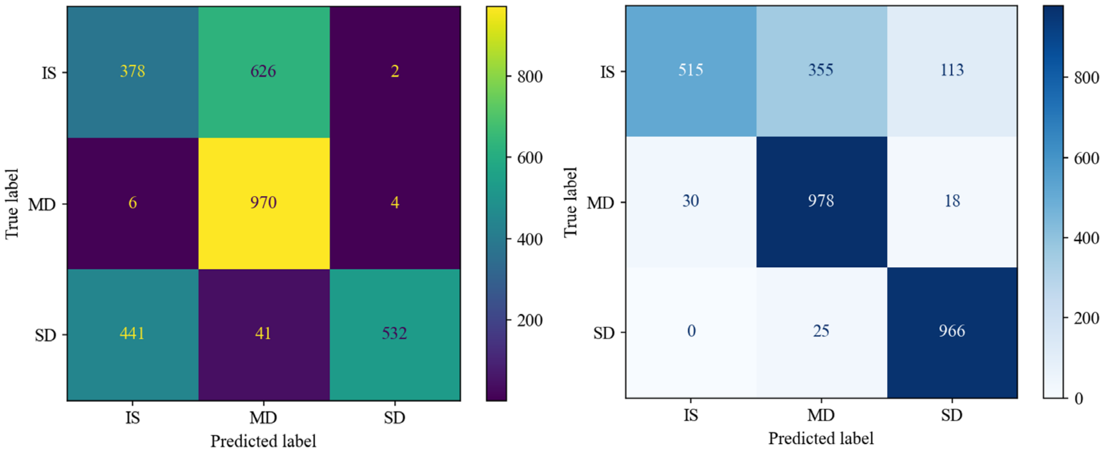

(a) Without DA: ***Acc.* = 0.626**   (b) With DA: ***Acc.* = 0.820**

Figure 6-9. Cross-domain zero-shot knowledge transfer results

Moreover, as a damage severity quantification issue, the false negative (FN) rate is a quite substantial indicator to evaluate the model performance because a misjudgment asserting a severe damage scenario (i.e., negative) as moderate damage or especially undamaged scenario (i.e., positive) might result in catastrophic mismanagement. The annotation of popular FN rate adapted to binary classification is extended to multi-class damage severity classification with a reasonable denotation, which can be defined as follows:

$$\mathrm{FN}=\frac{False\_undamaged\,/\,less\_damaged}{Damaged\_calls}=\frac{False\_MD}{MD\_calls}+\frac{False\_IS+False\_MD}{SD\_calls} \tag{6.5}$$

The FN values of the ultimate prediction performance are also compared in this study, as summarized in Table 6-4. The FN rate has been reduced from 0.441 to 0.054, reaching around 1/8 of the original value. Hence, the superiority of the proposed zero-shot TL algorithm with novel DA technique over those without DA embedding is verified.

Table 6-4. Performance comparison of cross-domain damage quantification

	Accuracy (the higher the better)	**FN rate** (the lower the better)
Without DA	0.626	0.441
With DA	0.820	0.054
Comparative improvement	31.0%	1/8

*Note: The improving percentage is calculated as: (0.820–0.626)/0.626, and 0.054/0.441.

6.3 Experimental validations on shake table tests

6.3.1 Data acquisition for cross-domain damage detection

After a seismic event, performing extensive damage analysis and detailed severity inspections for each structure may be neither feasible nor practical. Alternatively, binary damage detection provides a rapid decision-making tool by reducing the complexity of classifying structures into two categories, namely, damaged or not damaged, to help engineers and authorities prioritize and respond promptly based on the initial assessments. Thus, a cross-domain binary damage detection task is performed in this chapter to substantiate the proposed method. In this case, the knowledge extracted from numerical models (i.e., source domain) are utilized to perceive the damaged/undamaged status of an experimental structure (i.e., target domain).

The experimental measurement of a shake table test based on a blind calculation competition is introduced as the target domain data. On this basis, a numerical FEM is established using OpenSees (V2.5.0) to perform seismic response simulation as the source domain. Detail data acquisition and knowledge transfer results are demonstrated subsequently.

6.3.2 Shake table tests: Target domain

The shake table test data from the blind calculation competition under the auspice of the 10th National Conference on Earthquake Engineering of China are used in this study. The object of this experiment is a two-span, three-story reinforced concrete frame structure. The structure is designed with 7-degree seismic fortification (0.1 g) and Category IV site category requirements. The shake table tests are performed at the State Key Laboratory of Disaster Reduction in Civil Engineering, Tongji University, Shanghai, China, as shown in Figure 6-10.

Figure 6-10. On-site photo of the scaled frame structure and shake table tests

The structural plane size is 4.14 m×3.4 m, and the height is 2.6 m. The design, production and test methods of the specimens refer to similar local and international test experiences and comply with the relevant specifications, including the Code for Design of Concrete Structures (GB 50010-2010, 2015), the Code for Seismic Design of Buildings (GB 50011-2010, 2010), and the Building Code Requirements for Structural Concrete (ACI 318-11, 2011). The main materials used in the model design are C40 concrete and steel wire or bars with diameters ranging from 1.60 mm to 8 mm.

According to the requirements, the input acceleration amplitude increases in ascending order to simulate the response of the structure under different earthquake levels, specifically ranging from frequent, mortified, to rare earthquake. Considering the dynamic characteristics of the structure itself and in accordance with the seismic regulations, two actual earthquake records, namely, EI Centro wave, EC8 wave, and an artificially simulated acceleration time history curve (Shanghai wave, SHW2) were selected as the excitation input of the shaking table in all three earthquake levels.

Without loss of generality, the structural responses under the excitation of frequent-level earthquakes are regarded as healthy status, whereas the responses excited by the mortified- and rare-level earthquakes are labeled as the damage status. The reasonability of such simplified definition has been clarified in Section 5.2.1. The structural responses with a sampling frequency of 256 Hz of the middle columns at the base-level and three floor-levels are selected as the input of the multi-channel 1D CNN.

6.3.3 Numerical simulation: Source domain

FEM is developed using OpenSees (V2.5.0) to simulate the structural seismic response and obtain sufficient source data associated with multiple damage scenarios. The model configuration is established according to the prototype drawings, as depicted in Figure 6-11(a). The beams and columns are divided into three sections. The shorter parts at both ends are taken as the length of the refined zone, as shown in Figure 6-11(b).

According to the model construction drawing dimensions, the beam dimensions are 60 mm×130 mm and 80 mm×130 mm; the column dimensions were 90 mm ×120 mm (bottom floor) and 90 mm ×100 mm (the second and third layers). The beam and column components all use the DispBeamColumn unit in OpenSees, and the cross-section adopts fiber cross-section, in which the concrete fiber cross-sectional area is 10 mm × 10 mm, and the steel fiber area is defined according to the drawing value (that is, the reinforced area and the non-reinforced area are considered). The concrete components are modeled by the Concrete01 elements, and its mechanical parameters (elastic modulus, yield strain, yield strength, failure strain, and strength) were measured from material tests. The steel bars are modeled by the Steel01 elements, and their mechanical parameters (elastic modulus), yield strength, modulus after yield and initial modulus ratio) were measured from material tests.

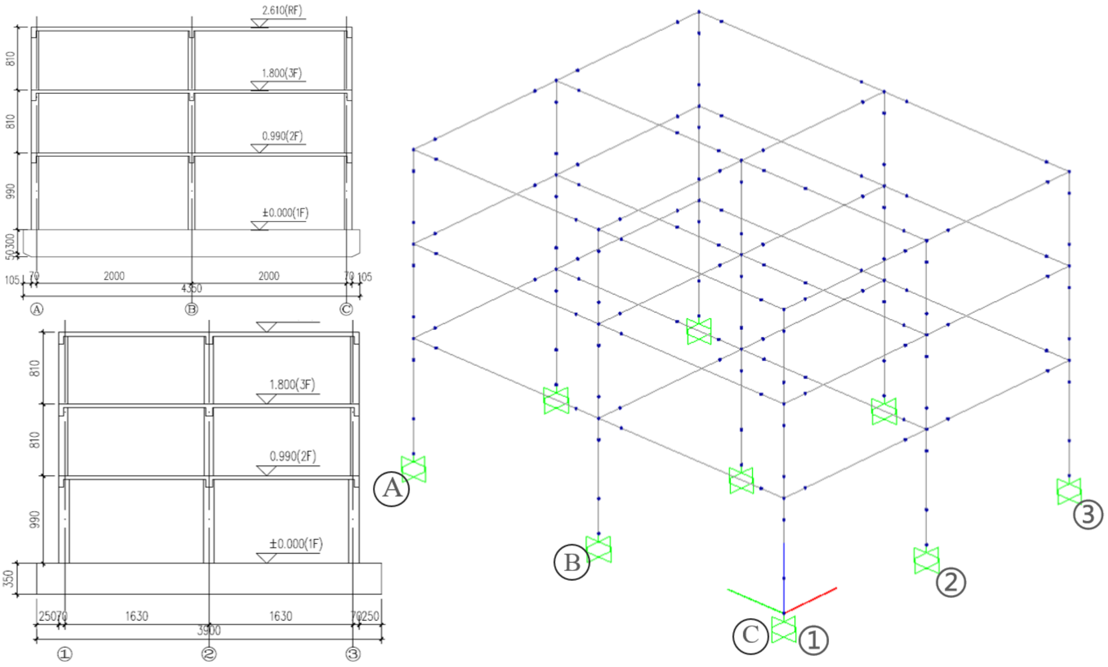

(a) Configuration details (b) OpenSees FEM model

Figure 6-11. Established OpenSees FEM model for seismic simulation

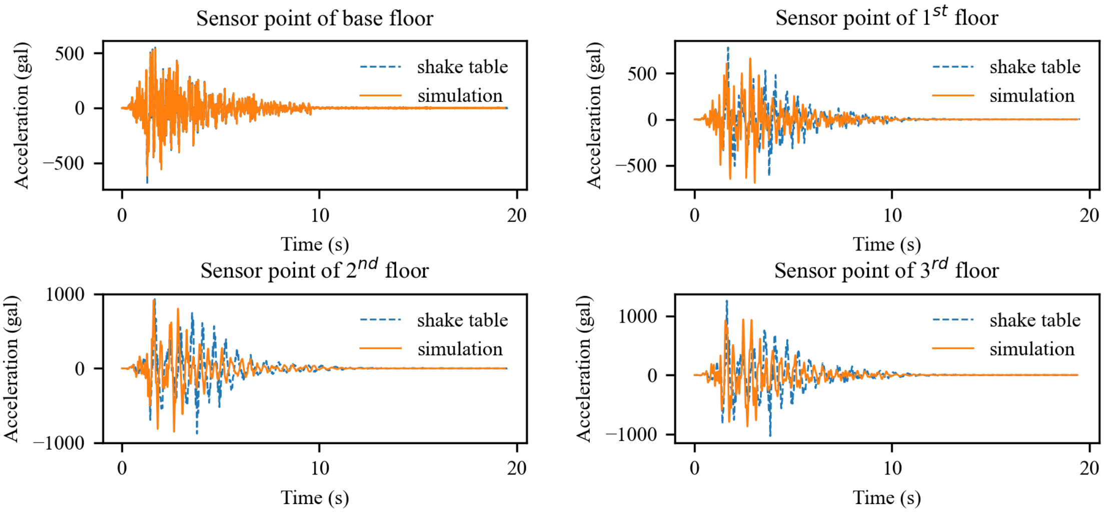

Figure 6-12. Comparison of simulation responses and shake table test measurement

The structural responses under the excitation of series of multi-level earthquake ground motions are simulated. The numerical results and shake table tests are compared, as shown in Figure 6-12. The overall simulation responses agree with those of the shake table tests, though the local curves of some channels exhibit deviation. Hence, the fidelity of the established FEM model is reasonable for simulation and consistent with the nature of the inherent gap between the simulation and the real-world structures.

6.3.4 Knowledge transfer from the numerical to experimental

The raw response data are processed by the peak-adjacent segmentation technique to thus eliminate the inference of noise tails that hinder effective data digging. The selected partition tests are segmented into a length of 256 with an overlapping of 64. The preprocessed data are ready for the subsequent task of damage detection.

Correspondingly, the detailed architecture of DAE is adjusted to comply with the input signal length. In this section, the units of three encoded layers in DAE are set to be 256, 128, and 64 successively, whereas those of the decoded layers are set to be 64, 128, and 256 inversely. The DAE is pretrained by the source domain data with 500 epochs and finetuning by the unseen target-domain data with 50 epochs. The epoch ratio of finetuning to pretraining is guided by the basic principle that the number of finetuning epochs should be much less than the number of pretraining epochs and determined by multiple parallel experiments. More insightful work could be conducted correspondingly in related future work, while this study will not go into detail on this issue.

Figure 6-13 depicts one case of signal reconstruction results, where the original target data associated with the IS and DS are translated into a similar space to the source domain. As a high-dimensional representation, even though this kind of discrepancy after translating is obscure, the mimicking is beneficial for the DA, as verified subsequently. Then, the training loss function and in-domain prediction performance are given in Figure 6-14. After the convergence of validation loss, the damage detector reaches a satisfactory in-domain prediction accuracy of 0.96, which also further confirms the effectiveness of the proposed multichannel 1D CNN in vibration-based damage detection.

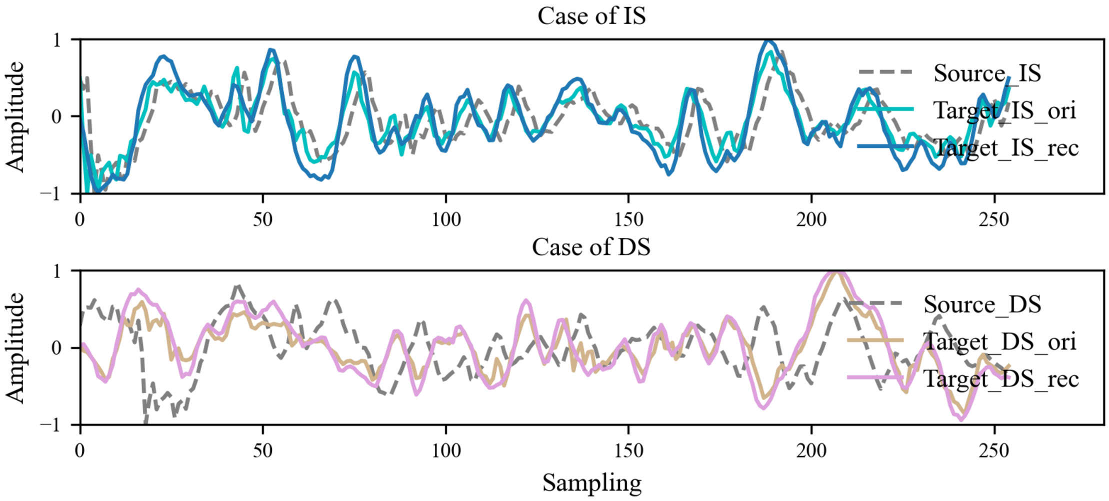

Figure 6-13. DAE-based signal reconstruction of the target domain

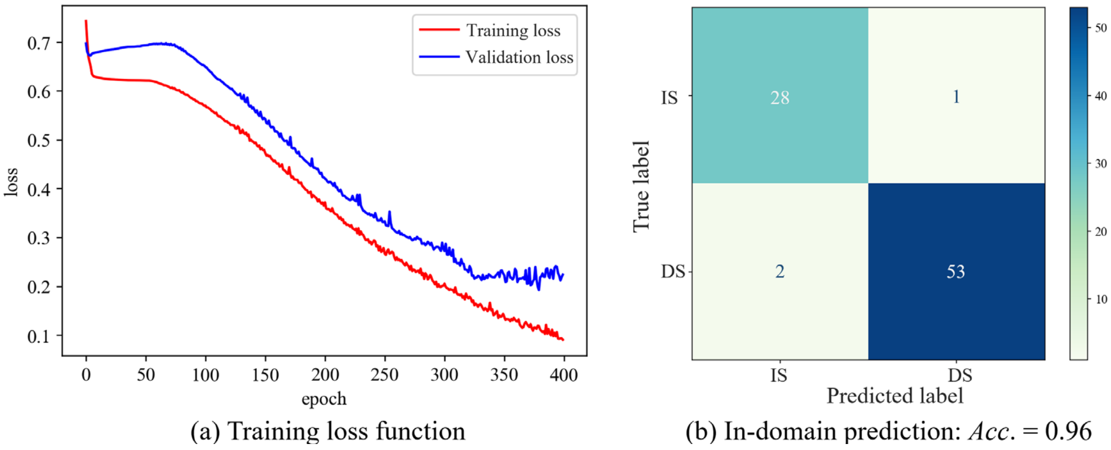

(a) Training loss function

(b) In-domain prediction: *Acc.* = 0.96

Figure 6-14. In-domain binary damage detection: training loss and confusion matrix

The cross-domain prediction performances with and without DA are compared in Figure 6-15. As a stringent zero-shot TL issue, the proposed multichannel 1D CNN exhibits a powerful capability of knowledge transfer toward damage detection with or without DA module embedded. Moreover, compared with conventional transfer learning without DA method as summarized in Table 6-5, the overall prediction accuracy increases from 0.792 to 0.833 with a 5.2% improvement, and the FN rate decreases from 0.240 to 0.167, reaching 2/3 of the original value. The capability and superiority of the proposed zero-shot knowledge transfer approach embedded with novel DAE-based DA module are validated.

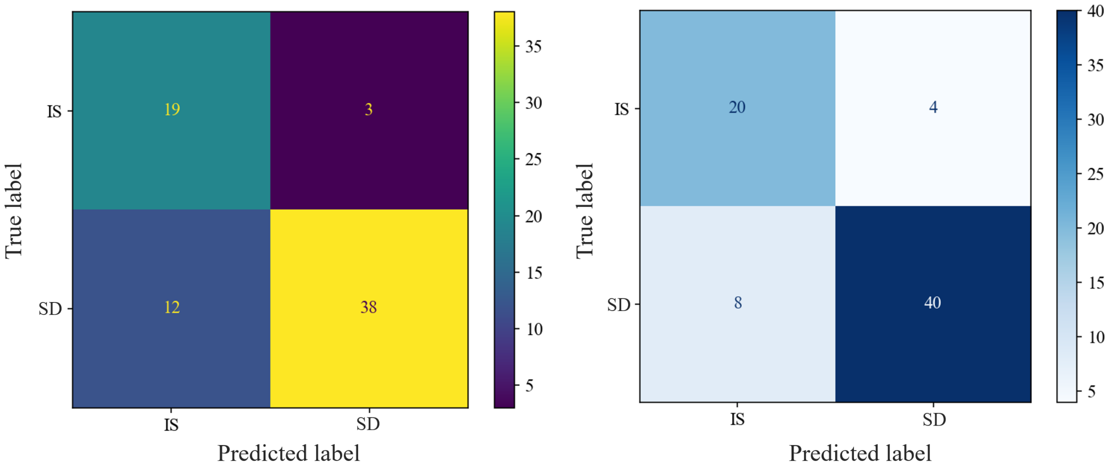

(a) Without DA: ***Acc.* = 0.792** (b) With DA: ***Acc.* = 0.833**

Figure 6-15. Cross-domain zero-shot damage detection results

Table 6-5. Performance comparison of cross-domain damage detection

	Accuracy (the higher the better)	**FN rate** (the lower the better)
Without DA	0.792	0.240
With DA	0.833	0.167
Comparative improvement	5.2%	2/3

*Note: the comparative improving percentage was calculated as: (0.833−0.792)/0.792 and 0.167/0.240.

6.4 Summary

6.4.1 Limitations and discussions

On the one hand, in the two-paradigm validations of this study, the detection/classification task and simulated damage scenarios in the target domain are the same as those in the source domain, which might be inconsistent with the real circumstance where the classes of target domain are probably unknown. Nonetheless, the main objective of this chapter is to address the data scarcity problem in the scope of TL-based structural damage diagnosis. In this context, a zero-shot TL approach is developed without any target-domain data (neither vibration themselves nor labels). In future work, more in-depth studies will be conducted by jointly considering the data scarcity and class imbalance from one domain to the other. To our best knowledge, this study is the first attempt to realize multi-class zero-shot knowledge transfer in cross-domain structures. However, only numerical models are utilized for validation. Realizing multi-class zero-shot knowledge transfer in engineering practice remains challenging due to the substantial system complexity and inevitable noise disturbance. Further investigations will be pursued using real-world case studies.

On the other hand, the scope of zero-shot knowledge transfer toward structural damage diagnosis comprises a hierarchy across levels of increasing complexity to accomplish knowledge transfer: i) from homogeneous numerical to numerical models, ii) from homogeneous numerical/experimental to experimental structures, iii) from heterogeneously numerical to numerical models, and iv) from heterogeneously numerical/experimental to experimental structures. Homogeneous and heterogeneous refer to the structural type of coherence between the source domain and the target domain, such as buildings, bridges, and dams. With a scientific focus on rapid data-driven structural damage diagnosis with enhanced applicability, this chapter primarily addresses the issue of the first two levels of task implementation, within the scope of transferring knowledge among homogeneous structures. Performing zero-shot knowledge transfer among heterogeneous prototype structures remains challenging due to the substantial discrepancy and gap in terms of configuration complexities, dynamic properties, response transmitting mechanisms, and as-in environmental conditions. More structural static information (structural geometry, configuration, and material properties, etc.) should be comprehensively considered with the dynamic structural responses for domain-invariant, damage-discriminative feature extraction in the future work.

6.4.2 Concluding Remarks

This chapter presents a novel zero-shot knowledge transfer approach for structural condition assessment through multichannel 1D CNN integrated with DAE-based DA. In this framework, three modules, namely, data preprocessor adaptive to seismic vibration signals, DAE-based DA module, and damage diagnoser via multichannel 1D CNN, are devised and integrated. Unlike the normal GAN-based strategies, the DA module in the proposed method seamlessly translates the unseen samples of the target domain to mimic latent representation via a pretrained DAE using sole source-domain data, thus realizing zero-shot knowledge learning schema. The term “zero-shot” in this study refers to the zero-shot data sample from the target domain, rather than the “zero-shot” class. To the best of our current knowledge, this framework represents the first attempt to tackle the challenge of zero-shot knowledge transfer in cross-domain building structures, enabling the diagnosis of multiclass damage severity (beyond binary detection) without relying on labels or even the data of the target buildings.

Two representative paradigms of knowledge transfer, namely, multiclass damage classification across two benchmark models and binary damage detection across a laboratory shake table model and corresponding FEM model are performed to substantiate the knowledge transferability of the proposed method. Both examples confirm the capability and superiority of the proposed method in zero-shot knowledge transfer for structural damage diagnosis among homogeneous structures. It results in higher prediction accuracy and lower FN rates. The proposed knowledge transfer framework can be extended from present zero-shot to few-shot learning paradigm for performance enhancement and adapt to various data availability scenarios.

CHAPTER 7 CLASS-IMBALANCE REWEIGHTED ACGAN-BASED DATA AUGMENTATION FOR STRUCTURAL CONDITION ASSESSMENT

This chapter proposes an innovative class-imbalance reweighted auxiliary classifier GAN (Re-ACGAN) to augment structural vibration data aiming at advancing structural multiclass damage identification. The model is established with improved architecture design based on the classical image-oriented auxiliary classifier GAN (ACGAN) structure (Odena et al., 2017) to effectively adapt to 1D vibration data. The proposed Re-ACGAN incorporates two novel class-conditional reweighting mechanisms to adeptly address the class imbalance issue and three diverse execution workflows integrating DAug-based damage classification for performance enhancement. To the best of the authors' current knowledge, this work is the first to achieve advancing vibration-based multiclass damage identification, jointly considering class-conditional DAug and class-imbalance reweighting.

7.1 Related works and preliminary knowledge

7.1.1 1D CNN-based damage classification

Recently, CNNs have shown superior performance in vibration-based structural damage identification due to powerful image classification and recognition capabilities. By automatically learning the spatial and temporal features of signals, high-dimensional abstract feature representations can be extracted. Dang et al. (2021) utilized a 2D CNN to identify structural damage via converting vibration signals into a time-frequency spectrum through STFT. Similarly, Zhang et al. (2022b) establish a CNN for bolt looseness damage detection using CWT to generate time-frequency images from vibrational signals. To fully utilize the image feature extraction capability of CNNs, extensive progress has been made in using time-frequency domain transformation to convert 1D structural vibration signals into 2D images and extracting high-dimensional features to achieve damage identification. This augmentation in data dimensionality often requires a large amount of image data for training, leading to substantially increased computational costs and hardware requirements.

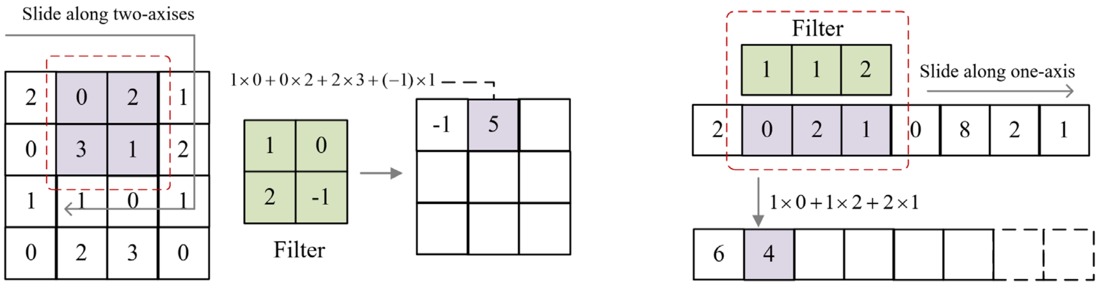

(a) Two-dimensional convolution

(b) One-dimensional convolution

Figure 7-1. Schematic of 2D and 1D convolution processes

In comparison to 2D CNN, which performs convolution operations in two directions, 1D CNN only performs convolution in a single direction, without the need for expanding data dimensionality. Figure 7-1 presents the schematic of 2D and 1D convolution processes. Different from 2D CNN, a 1D convolutional layer moves along the time axis of the input data (or the length of the sequence) through a filter (or convolution kernel) to extract local features of the sequence. Each slide computes the dot product (sum after element-wise multiplication) between the filter and the covered input data, producing one element of the output feature map. For a 1D input signal x and a convolution kernel w of length K, the output y of the convolution operation can be calculated as follows:

$$y[n]=\sum_{k=0}^{K-1} w[k]\cdot x[n+k]\,, \tag{7.1}$$

where $y[n]$ is the value of the output feature map at position n, $w[k]$ is the weight of the convolution kernel at position k, and $x\ [n+k]$ is the value of the input signal at position $n+k$. In this manner, convolutional layers can effectively extract and learn local features in the input data while maintaining the specific input data structure.

In this context, 1D CNN is gaining increased interest for structural damage identification (Hong & Kim, 2023; Kiranyaz et al., 2021; Pandey et al., 2022). Abdeljaber et al. (2017) first introduced 1D CNN for damage classification and verified its effectiveness on a 5 m × 6 m flat steel frame model. Zhou et al. (2022b) proposed a hybrid method using finite element model and 1D CNN for damage detection on a typical high-pile wharf. Ahmadzadeh et al. (2024) proposed a damage classification framework integrating 1D CNN and a long short-term memory (LSTM) model. In this method, the features extracted by 1D CNN were then fed into the LSTM layers to establish a mapping nexus associated with damage patterns. The proposed model was validated to be applied effectively to some cases with different damage patterns.

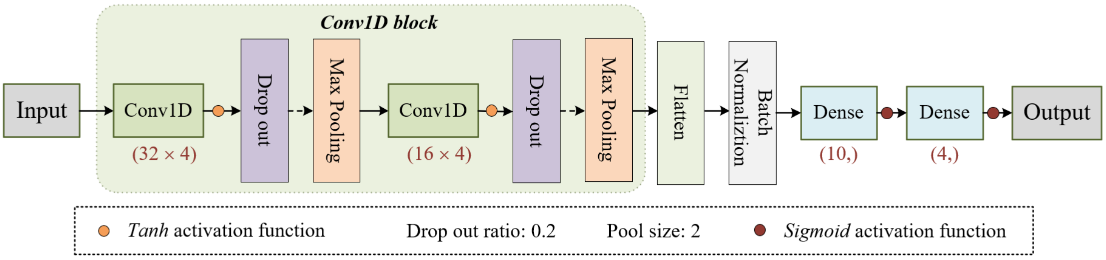

Figure 7-2. Architecture of the 1D CNN-based classifier

Therefore, the 1D CNN is utilized to perform as a baseline model for vibration-based structural damage classification in this study. Figure 7-2 presents the architecture of the established 1D CNN-based classifier. In this model, the input is fed into duplicated blocks consisting of 1D convolution layers (i.e., Conv1D), drop out layers, and pooling layers (i.e., max pooling). The obtained latent space is then concatenated by flatten layers and passed into two dense layers connected to the model output. The activation functions connected with Conv1D layer are defined as Tanh function (i.e., hyperbolic tangent function), and that connected to the dense layer are defined as Sigmoid function (i.e., logistic function). The kernel sizes of convolutional filters and units of dense layers are designated according to the input and output dimensions, which will be demonstrated in subsequent validation sections.

With sufficient training samples, the well-designed classifier is expected to be capable of accurately discriminating against diverse damage patterns. However, while dealing with data scarcity for training, the prediction performance can be extensively degraded. Thus, this study aims to advance the prediction performance of the damage classifier via DA from given limited and class-imbalance samples.

7.1.2 Basic ACGAN

The ACGAN, a variation of the GAN architecture, has been introduced to enhance the quality of generated images and provide better control over the characteristics of the generated samples. Odena et al. (2017) introduced the ACGAN framework and demonstrated its effectiveness in generating high-quality images conditioned on specific class labels. ACGAN provides insights into how the addition of an auxiliary classifier to GAN architecture enables better control over the generated samples and improves the overall quality of the generated images.

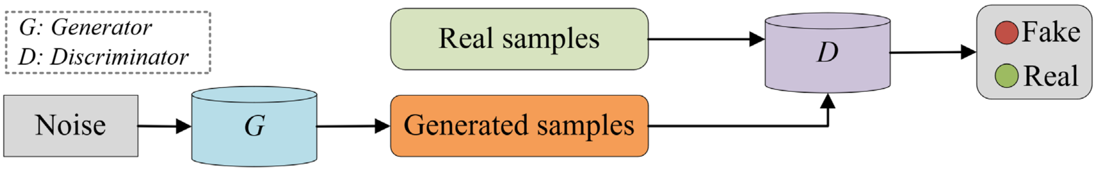

(a) GAN

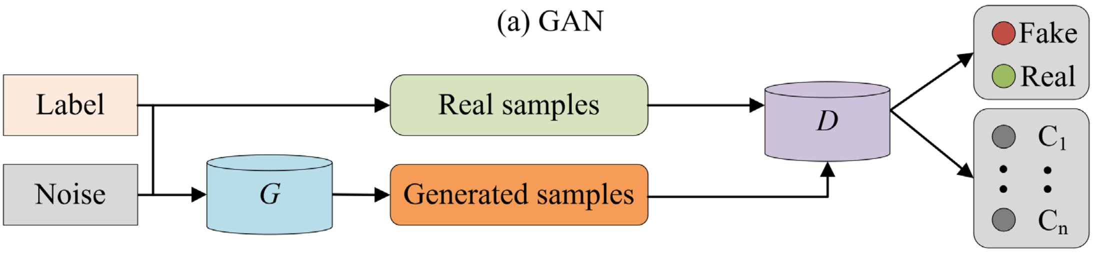

(b) ACGAN

Figure 7-3. Structure of (a) GAN and (b) ACGAN

In a traditional GAN, the generator's sole objective is to produce realistic-looking images, and the discriminator's task is to distinguish between real and fake images. However, the ACGAN extends this framework by adding an auxiliary classifier to the discriminator, as shown in Figure 7-3. This classifier not only determines whether an image is real or fake but also classifies the images into different categories. Specifically, the generator G takes random noise z and a class label y as input and generates samples $\hat{x} = G(z, y)$. The discriminator D takes a sample x from the dataset along with its corresponding class label y and tries to classify whether x is real or fake ($D(x)$) and, in parallel, predicts the class label ($D_y(x)$).

Thus, the objective functions for training ACGAN are composed of two parts: the log-likelihood of the correct source L_S and the log-likelihood of auxiliary classification L_C. The adversarial loss encourages G to generate realistic samples that can fool D, which is defined as (Odena et al., 2017)

$$L_S(G,D) = E_{x\sim p_r(x)}[\log D(x)] + E_{z\sim p(z),y\sim p_r(y)}[\log(1-D(G(z,y)))] \tag{7.2}$$

where $p_r(x)$ is the real data distribution; $p(z)$ is the noise distribution; and $p_r(y)$ is the distribution of class labels. $D(x)$ $p_r(x)$ denotes the probability that D discriminates x from the true sample distribution $p_r(x)$ as true. $D(G(z, y))$ represents the probability of D judging the generated sample to be true.

The auxiliary classification loss is used to train D to classify the samples into different classes. It is defined as the cross-entropy (CE) loss between the predicted class probabilities ($D_y(x)$) and the true class labels y, as shown as follows (Odena et al., 2017):

$$L_C(G,D) = E_{x\sim p_r(x)}[\log D_y(x)] + E_{z\sim p(z),y\sim p_r(y)}[\log D_y(G(z,y))] \tag{7.3}$$

Therefore, the training process of ACGANs involves jointly optimizing G and D along with the auxiliary classifier. G aims to maximize $L_C - L_S$, whereas D aims to maximize $L_C + L_S$. The ACGAN uses this additional classifier to regulate the generation process. Thus, in addition to generating realistic images, G also learns to control the characteristics of the generated samples based on specified categories. This adversarial training process ensures that G not only produces realistic images but also aligns them with the desired categories.

Nonetheless, as primarily designed for generating high-dimensional image data, using ACGANs for augmenting 1D vibration data to advance damage classification poses an adaptability problem that needs to be addressed for effective implementation. The primary issue casts on the complexity of data representation due to limited contextual information of vibration data. Vibration series often exhibits temporal dependencies and contextual information that are crucial for damage classification. ACGANs, in their conventional form, may not effectively capture the temporal dynamics and dependencies present in 1D time series data. Incorporating mechanisms to model temporal dependencies, such as RNN or CNN with temporal convolutions, may be promising for enhancing the model's ability to learn from 1D vibration data. Therefore, this study devises the Re-ACGAN based on a modified architecture from the classical image-oriented ACGAN to effectively adapt to vibration data.

7.2 Proposed methodology

7.2.1 Overall framework of the proposed method

Figure 7-4 depicts the overall framework of the proposed method. In this framework, three major modules are included, namely, the DAug module, execution workflow module, and classifier module.

Specifically, the DAug module plays as the research focus of the present study, where an innovative Re-ACGAN model is devised with special class-imbalance reweighting mechanism. The classifier module refers to the 1D CNN-based classification network. This baseline model has been elaborated in Section 7.1.1. The execution workflow module consists of three types of execution workflow integrating DAug-based damage classification. The multiple workflow design aims to explore the influence of different execution strategies and various distribution percentages between real and synthetic data on eventual prediction performance. The remaining contents in this section will elaborate the three modules in detail.

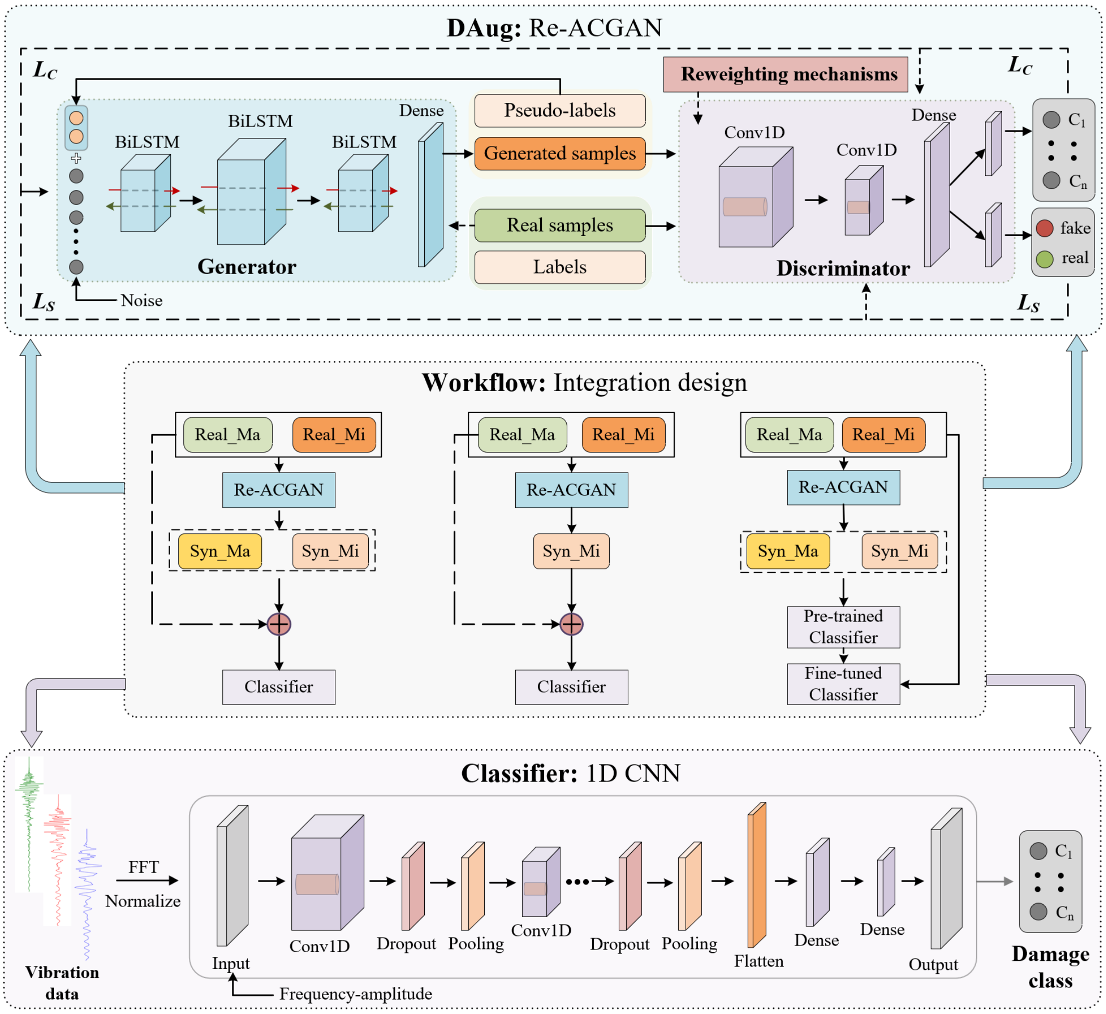

Figure 7-4. Overall framework of the proposed method

Given the fact that the frequency spectrum of vibration signals exhibits intuitive discrepancies due to damage, the time-domain vibration data segments are initially transformed into the frequency domain via FFT. The obtained amplitude spectrums are then normalized into a range of 0 to 1. Therefore, the real samples in the proposed framework refer to the normalized frequency-domain amplitudes of corresponding acceleration segments.

7.2.2 Improved DAug network design based on ACGAN

Optimized from the conventional ACGAN framework designed for image generation, which typically integrates various operational layers directly, such as convolutional, normalization, and activation layers, the proposed network establishes the discriminator based on bidirectional LSTM (BiLSTM) architectures and the generator based on 1D CNN. Structurally, this model does not significantly differ from existing models. However, this modification to the conventional image-oriented ACGAN formulation is beneficial to enhance the adaptability to 1D vibration data.

7.2.2.1 Generator: BiLSTM

LSTM networks are a special type of RNN architecture specifically designed to address the vanishing gradient problem. They can learn long-term dependencies in sequential data, making them well-suited for tasks, such as natural language processing, speech recognition, and time series prediction (Yu et al., 2019). LSTMs achieve this by introducing a memory cell and three gates, namely, forget, input, and output gates, which regulate the flow of information through the cell. The equations governing the behavior of an LSTM cell are as follows (Hochreiter & Schmidhuber, 1997):

$$f_t = \sigma_g(W_f \cdot [h_{t-1}, x_t] + b_f) , \tag{7.4}$$

$$i_t = \sigma_g(W_i \cdot [h_{t-1}, x_t] + b_i) , \tag{7.5}$$

$$\tilde{C}_t = \tanh(W_C \cdot [h_{t-1}, x_t] + b_C) , \tag{7.6}$$

$$C_t = f_t * C_{t-1} + i_t * \tilde{C}_t , \tag{7.7}$$

$$o_t = \sigma_g(W_o \cdot [h_{t-1}, x_t] + b_o) , \tag{7.8}$$

$$h_t = o_t * \tanh(C_t) , \tag{7.9}$$

where f_t is the forget gate output; i_t is the input gate output; $\tilde{C}_t$ is the candidate cell state; C_t is the cell state; o_t is the output of output gate; h_t is the hidden state; x_t is the input at time step t; σ_g is the Sigmoid activation function; W_f, W_i, W_C, and W_o are weight matrices; and b_f, b_i, b_C, and b_o are bias vectors.

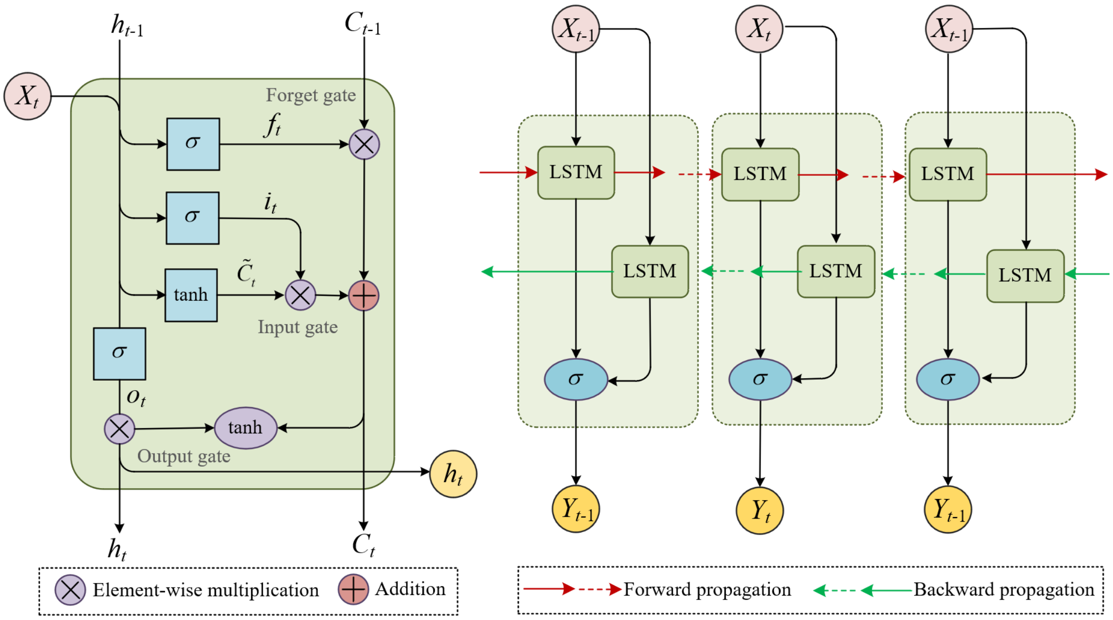

(a) Architecture of classical LSTM network

(b) Architecture of BiLSTM network

Figure 7-5. Architecture of classical LSTM and BiLSTM networks

Although LSTMs can effectively capture dependencies in sequential data, they are unidirectional, which indicates that they process the input sequence in one direction (either forward or backward). However, many tasks benefit from considering context from past and future information. BiLSTMs address this limitation by processing the input sequence in forward and backward directions simultaneously. The key idea is to concatenate the hidden states from BiLSTMs at each time step, effectively capturing information from both past and future context (Graves & Schmidhuber, 2005). Figure 7-5 presents the architecture of the classical LSTM and BiLSTM networks schematically.

Mathematically, the hidden state of the BiLSTM (h_t) at time step t is obtained by concatenating the hidden states of the forward LSTM (h_t^f) and the backward LSTM (h_t^b), as shown as follows:

$$h_t = [h_t^f, h_t^b]. \tag{7.10}$$

This concatenated hidden state h_t contains information from past and future context and can be used for downstream tasks, such as sequence classification, tagging, or generation.

In this study, a generator model is established based on the BiLSTM. Figure 7-6 presents its model architecture. In this model, the input is fed into duplicated blocks consisting of BiLSTM layers. The obtained latent space is then concatenated by flatten layers and passed into a dense layer connected to the model output. The activation functions connected with the BiLSTM layer are defined as a leaky rectified linear unit (LeakyReLU) function, and that connected to the dense layers are defined as a Sigmoid function.

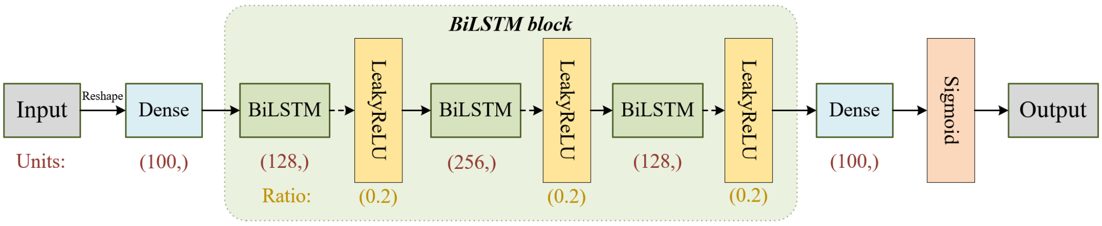

Figure 7-6. Architecture of the generator

7.2.2.2 Discriminator: 1D CNN

As demonstrated in the damage classifier context in Section 7.1.1, 1D CNN has been proven to be capable of effectively extracting damage-sensitive features from vibration data. Thus, the discriminator in the proposed method is also developed based on 1D CNN, which is consistent with the baseline classifier model. Figure 7-7 presents the architecture of the discriminator.

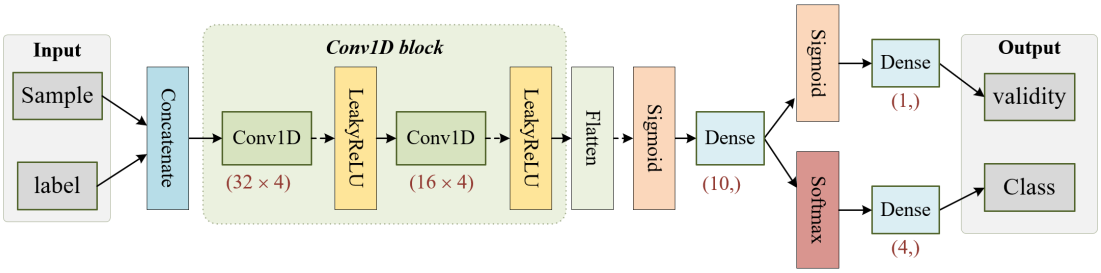

Figure 7-7. Architecture of the discriminator

Particularly, the model input layer consists of sample data and corresponding class labels, which are concatenated together and then fed into the Conv1D blocks. The kernel size of the first Conv1D layer is 32 × 4, and the second one is 16 × 4. LeakyReLU activation functions are embedded for connection. The high-dimensional latent space is then flattened and passed to a dense layer with a size of 10 through a Sigmoid activation function. Subsequently, two branches of output are established in parallel. The first branch outputs the sample authenticity (i.e., real/fake) via a dense layer with units of 1, and the other branch outputs the predictive class label in terms of one hot encoding vector via a dense layer with 4 units (i.e., number of classes).

7.2.3 Class-imbalance reweighting mechanisms

In the training objective of ACGAN, the auxiliary classification loss is typically computed using CE loss, which treats each class equally. However, in the presence of class imbalance, this can lead to unbalanced loss contributions, where the loss from minority classes has less effect on the overall training objective compared to majority classes. This can hinder the model's ability to effectively learn from minority class samples (Thabtah et al., 2020). To mitigate the class-imbalance issue in the conventional ACGAN, two classical strategies are considered in the proposed Re-ACGAN, namely, dynamic class reweighting (DCR) and extended focal loss.

7.2.3.1 DCR

DCR is a typical technique used to address the class-imbalance issue, where certain classes have significantly fewer samples than others in the training dataset. This technique involves assigning different weights to the classes during the training process, dynamically adjusting the weights based on their frequency or importance. It aims to mitigate the influence of class imbalance by giving more emphasis to underrepresented classes, thereby improving the model's ability to learn from minority classes and achieve improved performance on imbalanced datasets.

In this study, an automatic DCR module is designed and embedded into the sampling in each training epoch. The basic idea is to adjust class weights based on their frequencies in the training dataset, giving higher weights to less frequent classes. Table 7-1 summarizes the stepwise flowchart of its implementation. With this modification, the class weights will be dynamically calculated based on the distribution of classes in the training data for each epoch. This approach can help adapt the model's training to changes in class distribution during training.

Table 7-1. Flowchart of DCR process

Step	**Given**: (*y_true*, *y_pred*)	**Interpretation**
1:	$f_c = \sum_{i}^{N} 1 \vert (y\_true[i] = c)$	Calculate class frequencies for each class
2:	$\omega_c = \frac{N}{K \times f_c}$	Calculate class weights
3:	$l[i] = CE\left(y_{true[i]}, y_{pred[i]}\right) \times w_c$	Compute weighted CE loss
4:	$L = \frac{1}{N} \sum_{i=1}^{N} l\,[i]$	Compute mean of all weighted losses

*N is the total number of samples in an epoch (i.e., batch size); K is the total number of classes.

7.2.3.2 Extended focal loss reweighting

Focal loss, introduced by Lin et al. (2017b), is a type of loss function commonly used in DL models, particularly in tasks with class imbalance or when the dataset contains a large number of easy-to-classify examples. It aims to address these challenges by down-weighting the loss assigned to well-classified examples. It introduces a modulating factor that reduces the contribution of easy examples to the total loss, focusing on hard-to-classify examples.

Initiatively, focal loss is proposed for dense object detection in a binary classification form, typically defined as (Lin et al., 2017b):

$$FL(p_t) = -(1 - p_t)^{\gamma} \cdot \log(p_t)\,, \tag{7.11}$$

where p_t is the predicted probability of the correct class; and γ is the focusing parameter that modulates the rate at which easy examples are down-weighted. The term $(1 - p_t)^{\gamma}$ reduces the loss for well-classified examples (where p_t is close to 1), effectively focusing on hard examples. When $\gamma = 0$, the focal loss reduces to the standard CE loss.

Figure 7-8 plots a series of focal loss associated with predicted probability for different focusing parameters. In comparison to CE loss, focal loss pays more attention to those poorly classified samples (probably the minority classes) during training, thereby improving the model's ability to recognize and generate such underrepresented data samples.

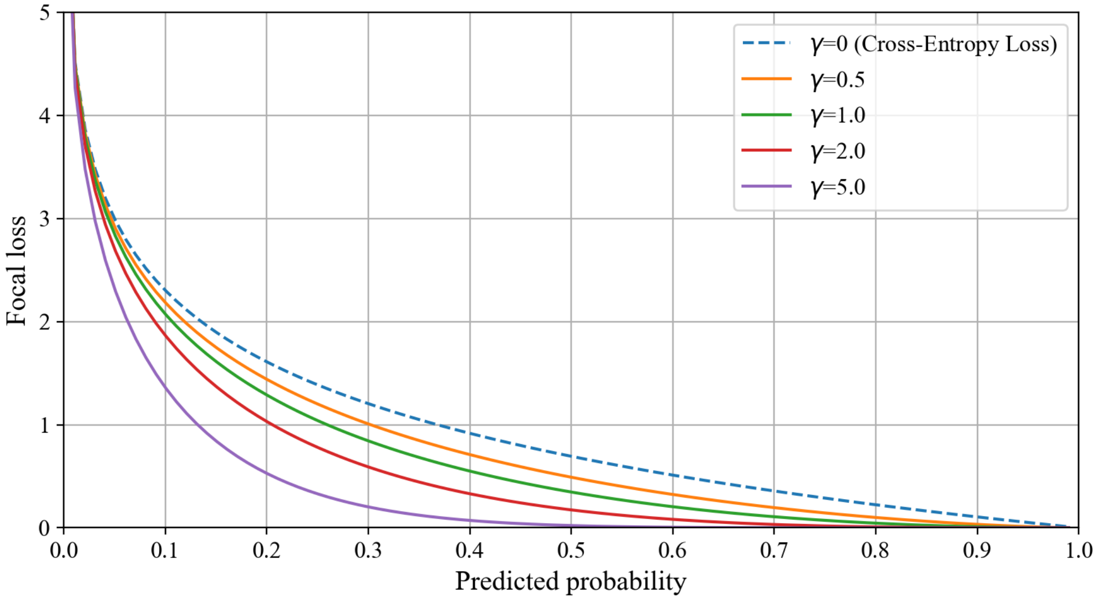

Figure 7-8. Focal loss for different focusing parameters

In this study, the initial binary focal loss is extended to multiclass form, which is expressed as follows:

$$FL(p_t, y) = -\sum_{c=1}^{C} \alpha \cdot y \cdot (1 - p_t)^{\gamma} \cdot \log(p_t)\,, \tag{7.12}$$

where the class balancing factor α ranges from 0 to 1; the focusing parameter γ is a nonnegative constant; y is the one hot encoded label vector of ground truth; and C is the number of classes.

The DCR process and extended focal loss serve as an alternative strategy to mitigate class imbalance issues, and they are investigated and embedded into the model in parallel in the Re-ACGAN. The two key parameters of the focal loss are initialized as $\alpha_c = 0.05$ and $\gamma = 2.0$. Further parametric sensitive analysis will be conducted subsequently.

7.2.4 Workflow design for DAug-based structural damage identification

The proposed DA model can be a promising tool for augmenting dataset of high quality and representative of the minority class, but suspicious bias exists inevitably in generated data compared to the real ones. Making reasonable use of generated data properly for advancing classifier training is crucial. In other words, the distribution percentages between real and synthetic samples can result in different prediction performance. Thus, this section devises three execution workflows integrating Re-ACGAN-based DA and 1D CNN-based classification, as depicted in Figure 7-9.

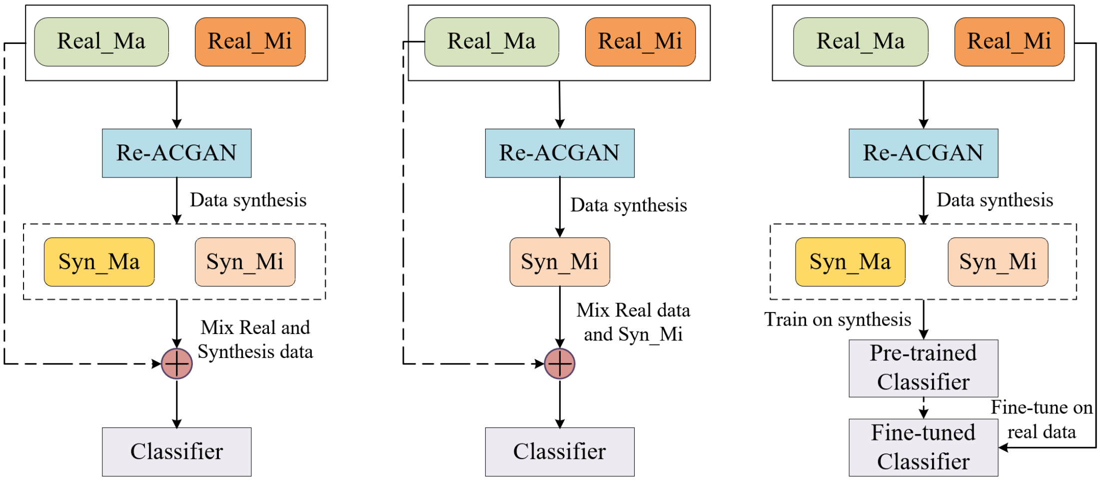

(a) MDA-GAN: Mixed DA (b) PDA-GAN: Partial DA (c) TL-GAN: transfer learning

*Real_ and Syn_ denotes real and synthetic data. _Ma and _Mi denotes the majority and minority data, respectively.

Figure 7-9. Execution workflows for DAug-based damage identification

Specifically, the first type mixes real and synthetic data of majority and minority classes for hybrid training on the downstream classifier. The mixed DAug procedure is denoted as MDA-GAN, as shown in Figure 7-9(a). Given that the samples of majority data (i.e., healthy status) are sufficient, the second type only utilizes the trained Re-ACGAN for augmenting the data of the minority class. The classifier will be trained by the real data and generated minority data. This partial DAug procedure is denoted as PDA-GAN, as shown in Figure 7-9(b). Eventually, different from directly training the classifier with mixed data, the third one pretrains the classifier using synthetic data and then fine-tunes it by real data. This TL-based procedure is denoted as TL-GAN, as shown in Figure 7-9(c). In this study, the training epochs of fine-tuning is set the same as the pretrained one.

In this parallel approach, the multiple workflow design enables a comprehensive analysis of the influence of distribution percentages between real and synthetic data on prediction performance. This approach integrates DAug and TL strategies to improve classification performance with class imbalance and limited data availability.

7.3 Benchmark validations: Numerical and experimental

7.3.1 Benchmark structures and experimental setup

The International Association for Structural Control (IASC) and the American Society of Civil Engineers (ASCE) provided the SHM benchmark structures (from this point forward, IASC–ASCE benchmark structure), and they claimed a two-phase SHM benchmark problem. The first phase involves simulated data from a numerical model (Johnson et al., 2004), and the second phase involves experimental data obtained from the test structure at the University of British Columbia in August 2002 (Dyke et al., 2003). In this study, the numerical and experimental data of the benchmark structure are investigated for comprehensive validations, as shown in Figure 7-10.

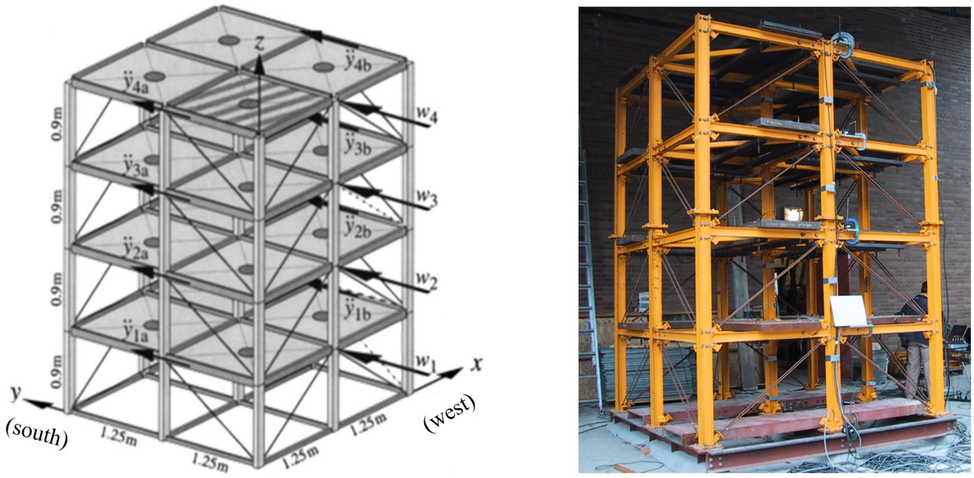

(a) Phase I: numerical model

(b) Phase II: experimental model

Figure 7-10. Two phases of benchmark structures: numerical and experimental

7.3.1.1 Phase I: Numerical data

The numerical model, as shown in Figure 7-10(a), consists of a four-story, two-bay by two-bay steel frame with a story height of 0.9 m. Euler–Bernoulli beam elements are used for numerical modeling of beams and columns, and link elements are used for support without bending stiffness. The floor slabs are considered completely rigid, with symmetric mass distribution. Acceleration sensors are installed in the *x*- and *y*-directions at each level of the frame. Using provided finite element analysis codes in MATLAB, the response of the analytical model can be calculated via the modal superposition method and a discrete time integration algorithm. The load excitation is Gaussian white noise filtered through a sixth-order low-pass Butterworth filter with a cutoff frequency of 100 Hz. The structural damping ratio is set to 0.01, and the sampling frequency is 100 Hz. Moreover, the 10% root mean square Gaussian noise is added to the acceleration response to simulate measurement noise. The simplified model in this benchmark (i.e., the symmetric model with 12 degrees of freedom) is chosen, with the load applied to all floors. The measurement point is selected as the outermost columns in the *y*-axis direction atop the structure.

7.3.1.2 Phase II: Experimental data

The experimental model is a follow-up to the previous numerical one. The model configuration remains the same. A data acquisition system was used to acquire 16 channels of data in each test. In this study, the data of random shaking tests induced by the electrodynamic shaker with moving mass are used for experimental validation. The chosen sensor point is the same as that in the numerical case. More details regarding the experiments can be referred to the official description (Dyke et al., 2003).

7.3.1.3 Label definition and data preparation

The current quantification of structural damage based on the earthquake intensity assessment specification developed by seismologists includes five seismic damage levels for buildings, namely, intact, slight damage, moderate damage, severe damage, and destruction (Sun & Li, 2021). This study divides the degree of damage based on the stiffness reduction of different damage conditions in the benchmark models to set data labels. Consistently, it is divided into four levels of damage (except destruction): healthy status (HS), light damage (LD), moderate damage (MD), and severe damage (SD). Particularly, the four damage severity labels are executed in a one hot encoding format to avoid ordinal issues. In this manner, the discrete features are mapped into a Euclidean space, thereby enhancing model performance by providing information about the categorical variables to the model.

Structural damage of the numerical benchmark model is simulated by removing or weakening braces and weakening specific beam–column nodes, resulting in six damage scenarios, as shown in Table 7-2. In the experimental study, structural damage is similarly simulated via removing braces or weakening connections. The damage configurations of the experimental benchmark are not exactly consistent with that of the numerical one. The first six cases associated with different configurations are introduced in this study. The classification of damage severity of the experimental benchmark is presented in Table 7-3.

Table 7-2. Definition of damage patterns and classification of damage severity of the numerical benchmark (reproduced from Johnson et al. (2004))

Item	Damage patterns	Damage severity
0	No damage	HS
1	Remove all 1st floor braces	SD
2	Remove all 1st and 3rd floor braces	
3	Remove one 1st floor braces	MD
4	Remove one 1st and 3rd floor braces	
5	Remove one 1st and 3rd floor brace, and weaken one 1st floor connection	
6	Reduce 1/3 stiffness of one 1st floor brace	LD

In numerical and experimental cases, a total number of 60 samples associated with each class are prepared as the training data, and 20% of that (i.e., 12 samples) are prepared as the validation set. In addition, another 30 samples associated with each class are prepared for the test set. Each sample is a 100-point time series. In practical circumstances, HS samples are usually far more than samples from damage scenarios. The proposed method only uses identical numbers of HS data as damaged ones for Re-ACGAN training to eliminate initial class imbalance.

Table 7-3. Definition of damage patterns and classification of damage severity of the experimental benchmark (reproduced from Dyke et al. (2003))

Item	Damage patterns	Damage severity
1	Fully braced	HS
2	Remove 1st floor braces in one bay on the southeast corner	LD
3	Remove braces on all floors in one bay on the southeast corner	MD
4	Remove 1st and 4th floors braces in one bay on the southeast corner	
5	Remove all braces on the east side	SD
6	Remove braces on all floors on the east side and 2nd floor braces on the north side	

7.3.2 Results and analysis of numerical cases

As demonstrated in Section 7.2.4, three execution workflows have been designed for DAug-based structural damage identification. For concise writing, this section only details the training and prediction process of the first workflow (i.e., MDA-GAN workflow) and compare the final prediction results with the other two workflows. In the MDA-GAN workflow, the Re-ACGAN is trained by 60 samples of each class and then utilized to augment a total of 600 class-conditional samples generated for mixed training on the classifier.

7.3.2.1 Re-ACGAN training and DAug

The process of training the Re-ACGAN involves iteratively improving two models that work in tandem: the generator *G* and the discriminator *D*. *G* takes random noise and class labels as input and generates synthetic data. *D* evaluates the authenticity of the data and classifies it. During adversarial training, both *G* and *D* are updated in alternating fashion.

In the present study, the Re-ACGAN is constructed using the TensorFlow 2.10.1 DL framework and programmed using Python 3.9.12. A parallel computing platform and programming model, namely CUDA (Manavski & Valle, 2008), is introduced for general computing on graphical processing units (GPUs) to speed up computing by harnessing the power of GPUs. The learning rate parameter of the Adam optimizer is set to 0.001. Particularly, the loss function on sample authenticity (real/fake) is defined as binary CE, whereas the multiclassification loss of damage labels is calculated by the customized reweighted loss, including DCR loss or focal loss. The total epoch number is set to be 500. In each epoch, the Re-ACGAN is trained on batch samples with a batch size of 16. The whole training process is a balancing act between *G* and *D*. Over time, both models improve, resulting in a *G* capable of producing high-quality synthetic data with class conditions. Detailed training philosophy can be referred to Section 7.1.2.

To compare the two class-imbalance reweighting mechanisms, Figure 7-11 presents the training loss of Re-ACGAN models embedded with DCR and focal losses. Notably, in the DCR reweighted model, the total loss receives a smooth convergency at early epoch, whereas the focal loss reweighted model fails to converge at a stable total loss. The classification loss of the two models achieves convergence, where the DCR reweighted model converges faster. The comparison results suggest that the DCR reweighting mechanism can facilitate superior capability of producing high-quality class-conditional synthetic data. The downstream comparison on eventual prediction performance can further confirm this claim.

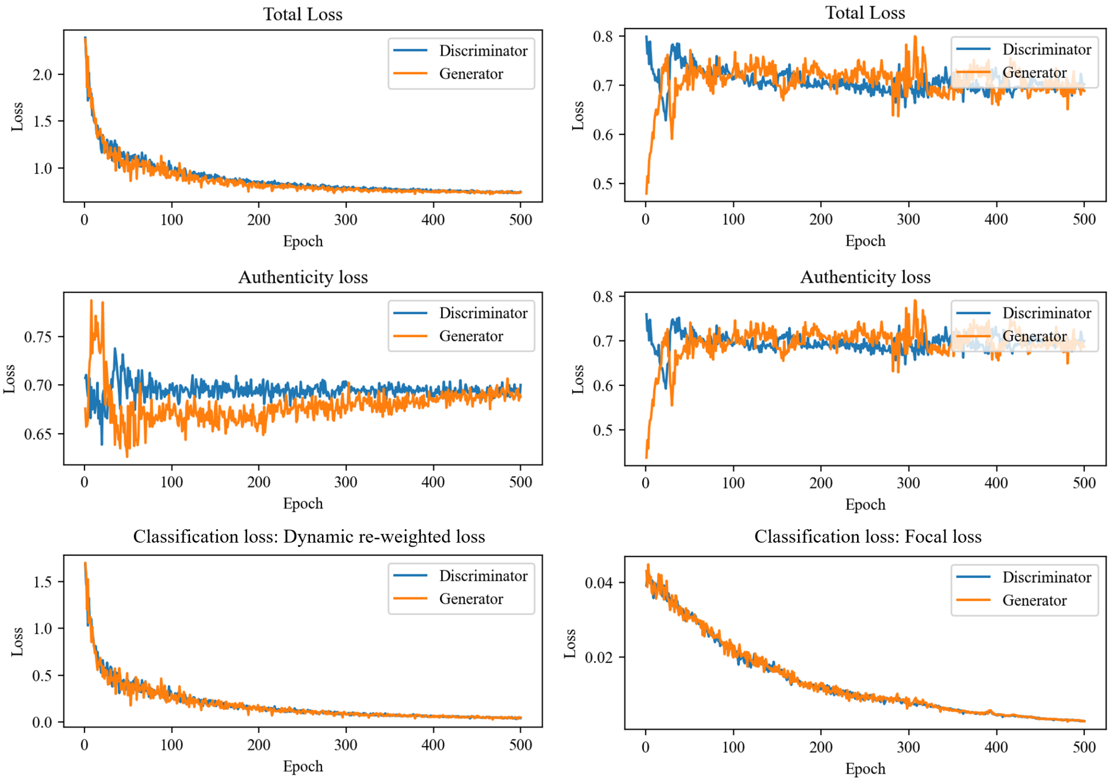

(a) Loss function with dynamic class re-weighed loss (b) Loss function with focal loss

Figure 7-11. Training loss of Re-ACGAN with different class-imbalance reweighting mechanisms

7.3.2.2 Performance comparison on damage classification

Preliminarily, the classification performance of the 1D CNN-based classifier trained by limited 60 samples is compared with the proposed DA-based damage classification to verify its effectiveness. The 1D CNN-based classifier is built in the same environment using TensorFlow. The training epoch is set to be 500. An early-stopping callback module (Yao et al., 2007) is introduced to prevent overfitting and improve the generalization ability models. Its monitoring indicator to determine the stop is defined as the validation loss, and the patience parameter is set to be 50. In this manner, the callback monitors the validation loss during training, and training is halted if no improvement is observed in the validation loss for 50 consecutive epochs, and the model’s weights are restored to the best state observed during training.

Figure 7-12 depicts the training history of the damage classifier without DAug.

Neither the loss function nor accuracy function obtain convergence. The confusion matrices of prediction performance are presented in Figure 7-13. Given the limited training samples, the classifier performs poorly in identifying different damage conditions. The early-stopping callback module stops the iteration process due to nonconvergence. Therefore, the prediction accuracy on the test dataset is only 0.767.

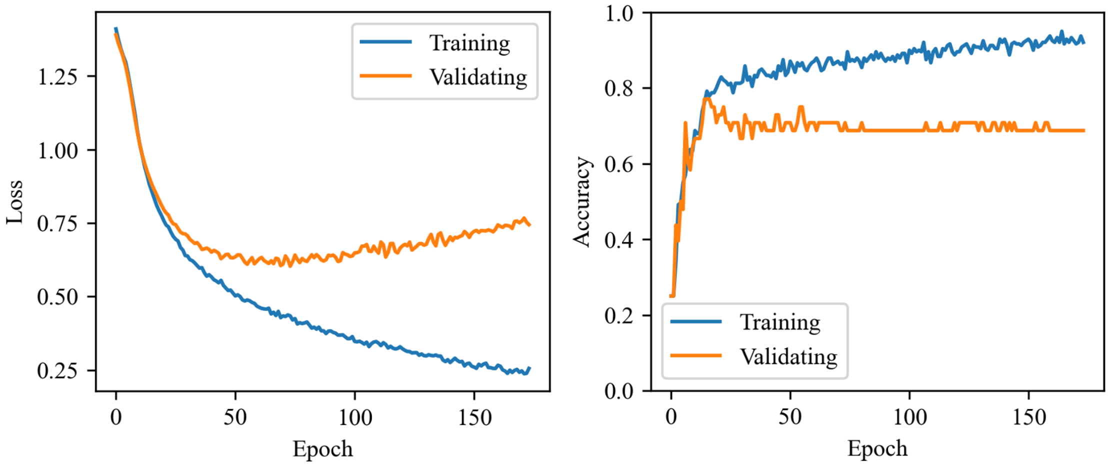

(a) Training loss history (b) Training accuracy history

Figure 7-12. Training history of the classifier without DAug: (a) loss history; (b) accuracy history

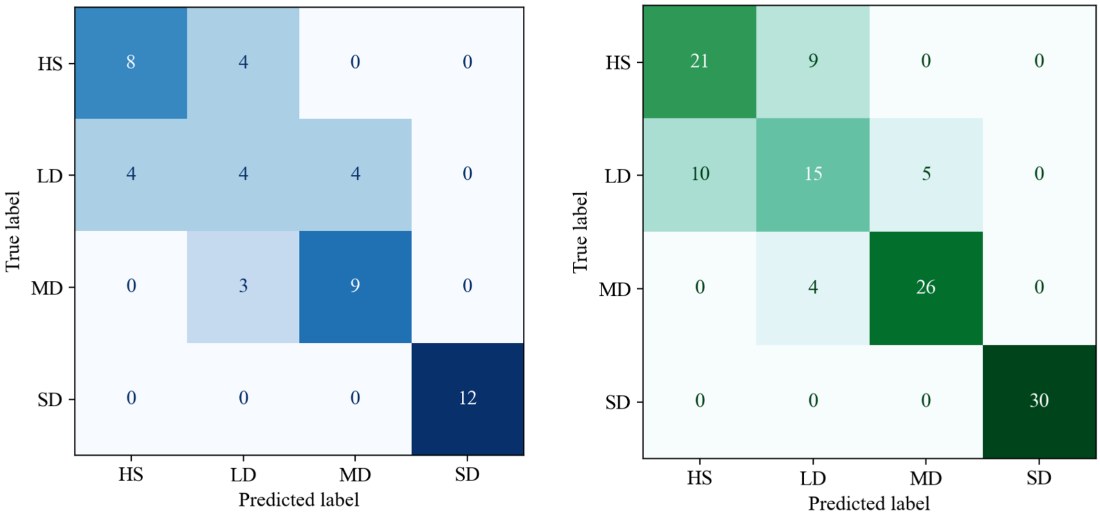

(a) Validation accuracy: 0.687 (b) Test accuracy: 0.767

Figure 7-13. Confusion matrices of the classifier without DAug: (a) validation set; (b) test set

Comparatively, using the trained Re-ACGAN to augment 600 synthetic samples for each class, the classifier is then trained by the mixed real and generated data, followed by the MDA-GAN workflow. Figure 7-14 depicts the training history of the classifier after DAug. The loss and accuracy functions reach a stable convergence soon at the beginning of epochs. Figure 7-15 depicts the confusion matrices of the classification performance after DAug. Overall, the ultimate prediction accuracy increases from 0.767 to 0.850 after DAug.

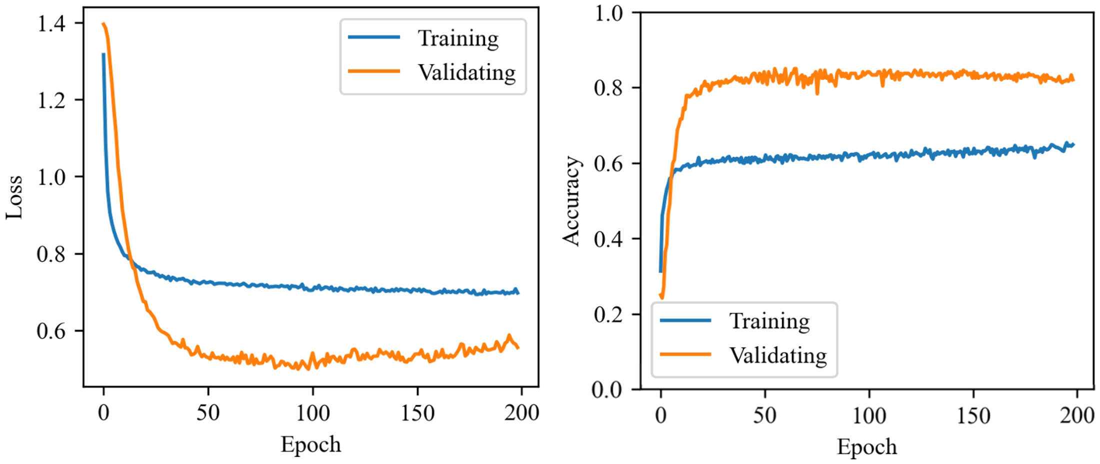

(a) Training loss history (b) Training accuracy history

Figure 7-14. Training loss and accuracy history of the classifier after DAug

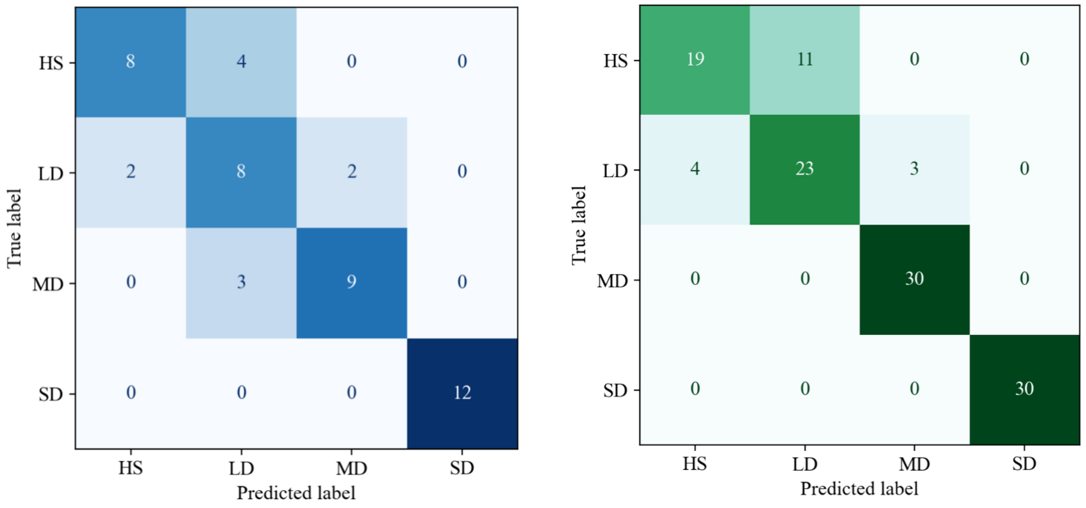

(a) Validation accuracy: 0.771 (b) Test accuracy: 0.850

Figure 7-15. Confusion matrices of the classifier after DAug: (a) validation set; (b) test set

7.3.3 Results and analysis of experimental cases

Similarly, in the example of experimental shake tests, the classifiers trained by the original limited dataset and the augmented dataset generated by the trained Re-ACGAN are utilized to perform the damage classification task. In addition to the data source, all the setup remains consistent to that of the numerical case. Figure 7-16 presents the training and test results of the classifier before and after DAug. In this case, the classifier converges before and after the DAug process.

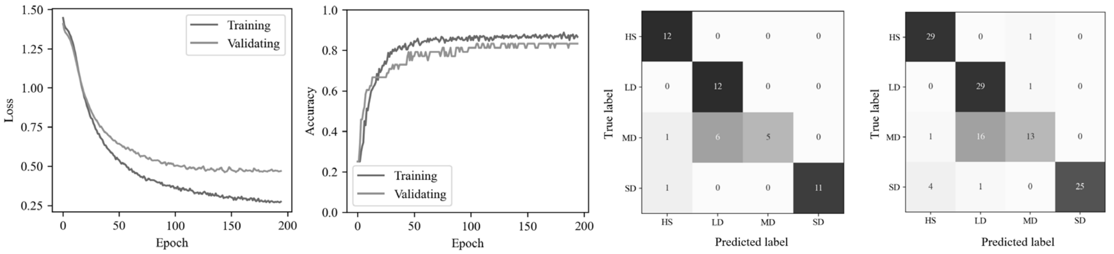

(a) Loss history (b) Accuracy history (c) Validation matrix (d) Test matrix

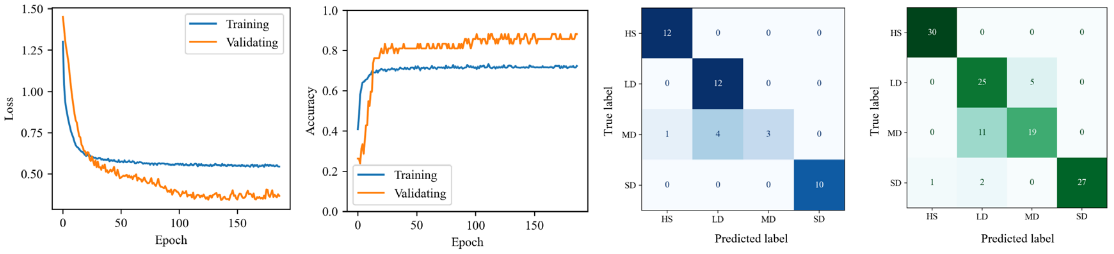

(e) Loss history (f) Accuracy history (g) Validation matrix (h) Test matrix

Figure 7-16. Details of training and test of the classifier: (a–d) before DAug; (e–f) after DAug

Table 7-4. Performance comparison of damage classification before and after DA

	Numerical case		Experimental case	
	Val_accuracy	Test_accuracy	Val_accuracy	Test_accuracy
Before DA	0.687	0.767	0.833	0.800
After DA	0.771	0.850	0.881	0.842
Improvement	12.2%	**10.8%**	5.8%	**5.3%**

*Notes: Val_accuracy and Test_accuracy refer to the prediction accuracy on the validation and test sets, respectively.

The quantification performance comparison is summarized in Table 7-4. In both cases, the DAug process exhibits substantial improvement on the validation and prediction accuracy. After DAug, the eventual prediction accuracies of the two cases achieve a satisfactory value around 0.85. Particularly, the test accuracy results in a comparative improvement of 10.8% in the numerical case, increasing from 0.767 to 0.850, and 5.3% enhancement in the experimental case, increasing from 0.800 to 0.842.

On the one hand, the overall results confirm the effectiveness of the proposed Re-ACGAN in advancing the damage classification implementation. On the other hand, a higher degree exceeding 10% of performance improvement is obtained in the numerical case, whereas that in the experimental case only exhibits a slight advancement with around half degree. Such discrepancy might be attributed to the noise interference in real-world measurement, which can affect the extraction and representation of damage-sensitive feature on the vibration signals, thereby degrading the quality of synthetic data generated by the Re-ACGAN model. The issue is beyond the scope of the present study, and specific exploration can be further conducted in future work.

7.3.4 Performance of improvement tricks

In this section, ablation experiments are conducted to further investigate the performance of the proposed improvement tricks for network training, including two class-imbalance reweighting mechanisms and three execution workflows. Table 7-5 summarizes the prediction results of multiple parallel experiments by Re-ACGAN models with different combinations of reweighting mechanism embedding and workflow execution.

Overall, the MDA-GAN outperforms consistently across parallel reweighting mechanisms, with the highest accuracy of 0.850 in the numerical case and 0.842 in the experimental one. The PDA-GAN exhibits the poorest prediction accuracies across the three workflows, even though it achieves an accuracy of 0.850 in an experimental case embedded with the focal loss. In this workflow, the DAug only generates damage samples, whereas all the HS samples are derived from the real ones. After observation of the prediction confusion matrices, relatively few LD samples are misidentified as HS. The phenomenon indicates that all real HS samples dominate over the generated damage samples, thereby leading to a biased representation of multiclass damage status in the synthetic dataset. Here, the related confusion matrix figures are omitted for short paragraphs because simple consciousness is followed. Nevertheless, to avoid possible knowledge loss of representative features due to biased data generation of synthetic samples, the DAug model can better augment the training data associated with all classes and then mix with the available real data for joint classifier training. The TL-GAN workflow exhibits similar performance compared to MDA-GAN across different reweighting embeddings. Particularly, it achieves the highest prediction accuracies with DCR embedding in both cases, with 0.850 in the numerical cases and 0.858 peaking in the experimental cases.

Table 7-5. Performance comparison of prediction accuracies by models with different reweighting mechanisms and workflows

	MDA-GAN		**PDA-GAN**		**TL-GAN**	
	Numerical	Experimental	Numerical	Experimental	Numerical	Experimental
None	0.800	0.842	0.742	0.800	0.800	0.825
DCR	**0.850**	**0.842**	**0.783**	0.825	**0.850**	**0.858**
Focal	0.825	0.833	0.733	**0.850**	0.816	0.833

*Note: None, DCR, and Focal refers to no reweighting, DCR-based reweighting, and focal loss reweighting, respectively.

With a particular insight upon reweighting mechanisms, the proposed DCR method outperforms the focal loss-based reweighting. Embedded with the DCR module, almost all the three workflows in both cases reach a comparatively superior performance, with only one exception in the experimental case reweighted by the focal loss. For the models without reweighting modules, the prediction results are less satisfactory. The ablation experimental results confirm the effectiveness of proposed reweighting methods compared to that without consideration of class-imbalance issue.

Substantial improvement in damage classification precision is promisingly expected after the integration of reweighting strategies, especially the DCR method.

As mentioned in Section 7.2.3.2, the two key parameters of focal loss are initially set according to typical practice, where the class balancing factor α is set to 0.05, and the focusing parameter γ is set to 2.0. To understand the functional ability of focal loss-based reweighting, parametric sensitivity analysis is also conducted in this section. Representatively, the proven superior models compiled in the TL-GAN workflow (denoted as the TL-GAN model) are selected. Figure 7-17 presents the precision results of models reweighted by focal loss associated with different parameters. The precision of the predictions shows slight sensitivity upon the two paramaters in focal loss. When fixing α to 0.05, focal loss with $\gamma = 5.0$ achieves the highest precision of 0.842 in the numerical and experimental cases. When fixing γ to 2.0, focal loss with $\alpha = 0.5$ has the highest precision of 0.842 in the numerical case and 0.833 in the experimental case. Particularly, no general linear relationship is observed explicitly between the values of two parameters and prediction precisions. To determine the optimized setting parameters, specific exploration may need to be pursued in each domain-specific task implementation.

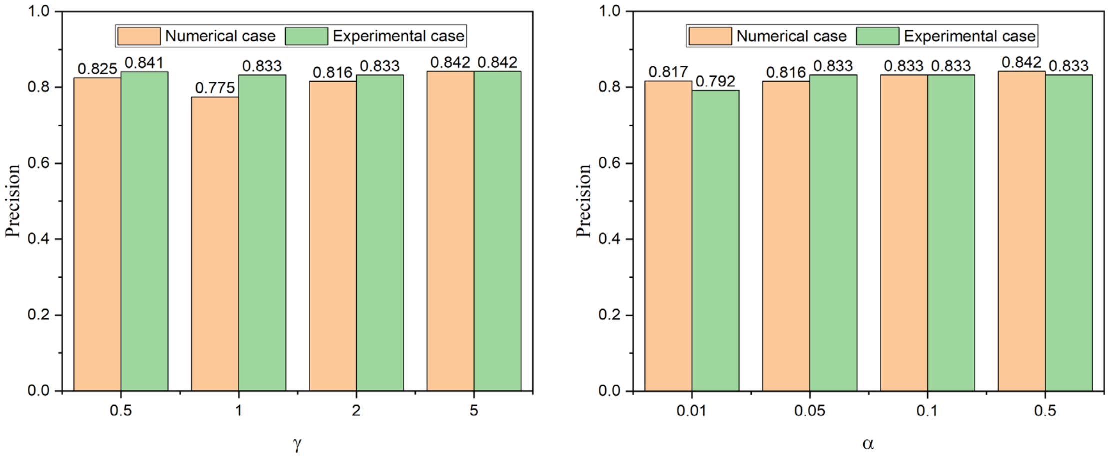

(a) Fixed α=0.05 (b) Fixed γ=2.0

Figure 7-17. Parametric sensitivity analysis of focal loss in TL-GAN model

7.3.5 Generated data quality evaluation using t-distributed stochastic neighbor embedding (t-SNE) visualization

To identify multiclass damage using limited sample data, the capability of the proposed Re-ACGAN in enhancing prediction precisions has been well substantiated. To further delve into the quality of generated data, this section performs the data visualization using t-SNE (Van der Maaten & Hinton, 2008) on the original and generated data. The technique is a variation of SNE (Hinton & Roweis, 2002) used for dimensionality reduction, primarily to visualize high-dimensional data in a low-dimensional space. In this manner, the t-SNE process helps reveal the underlying structure of the data in a visually interpretable form, enabling the discovery of patterns and structures that may not be easily discernible in the original space.

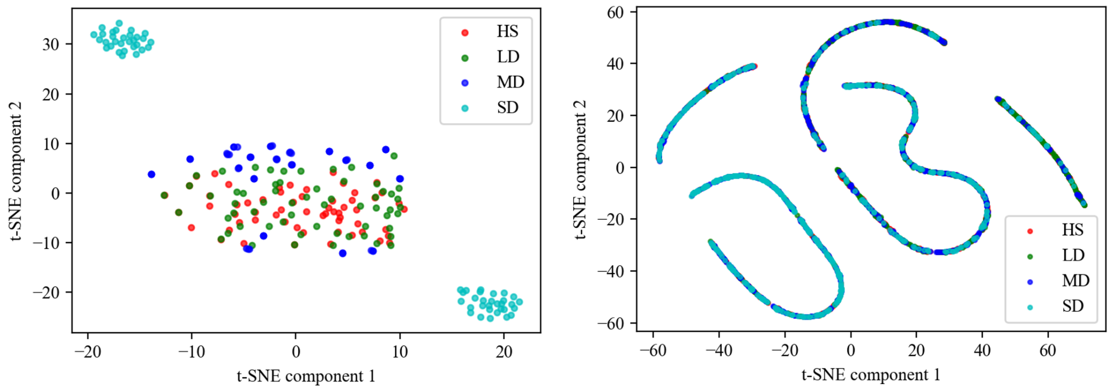

(a) Real data (b) Synthesis without re-weighting

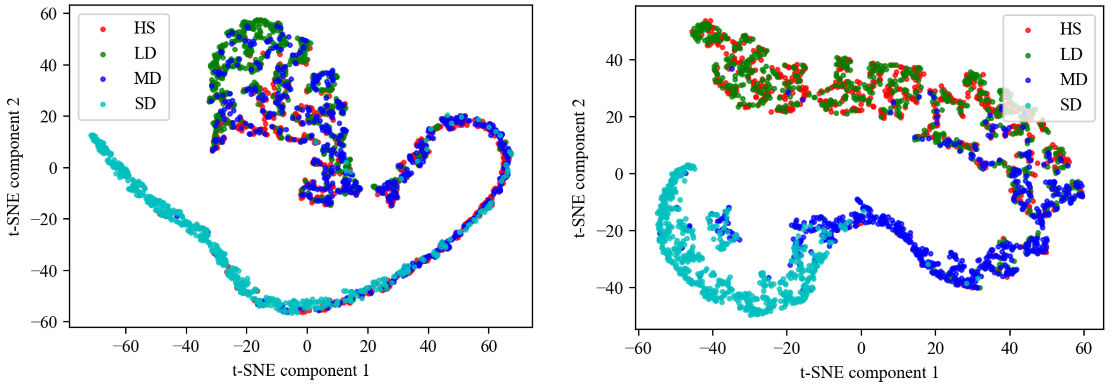

(c) Synthesis with DCR re-weighting (d) Synthesis with focal loss re-weighting

Figure 7-18. Data visualization using t-SNE of real and synthetic data

This study visualizes the real and synthetic data associated with corresponding damage labels into 2D using t-SNE, as depicted in Figure 7-18. In the original real data, the clusters associated with damage labels are explicitly observed in Figure 7-18(a), where MD and SD samples are distributed separately from HS samples. The distribution of LD samples is mixed with HS ones, indicating the inherent difficulty in distinguishing LD. This pattern visualization aligns with the physical significance of the data. Upon examining the synthetic data from the ACGAN without the reweighting module in Figure 7-18(b), although more clusters are visible, confusion persists among different damage classes, indicating the potential for enhancing the quality of data synthesis. Figure 7-18(c) and Figure 7-18(d) depict the 2D visualization of synthetic data generated by Re-ACGAN with DCR and focal loss reweighting, respectively. After the introduction of class-imbalance reweighting modules, the synthetic data exhibit improved cluster structures and obvious class-conditional distribution. In the two reweighting mechanisms, the SD and MD samples are successfully separated from the dataset. Particularly, in synthetic data with DCR reweighting module, substantial discrepancies are also obtained among the distribution of the LD and HS samples, enabling accurate identification on the nuance damage. Visual insight into the underlying patterns of generated data can account for the superior improvement performance of DCR, as verified in parallel ablation experiments. It emphasizes underrepresented classes and mitigates the dominance of majority classes, thereby ensuring a balanced dataset representation. The results provide an evident and deep understanding of how the proposed reweighting mechanisms improve network training.

7.4 Summary

This chapter develops the Re-ACGAN to augment structural vibration data for structural damage identification. The classical image-oriented ACGAN is modified to adapt to vibration data effectively, where the discriminator is established based on BiLSTM and the generator based on 1D CNN. In the proposed Re-ACGAN, two novel class-conditional reweighting mechanisms, namely, DCR and focal loss-based reweighting, are incorporated to adeptly address the class imbalance issue. In addition, three execution workflows, namely MDA-GAN, PDA-GAN, and TL-GAN for DAug-based damage classification are integrated into the framework for performance enhancement.

Numerical and experimental studies on the IASC–ASCE benchmark structure validate the effectiveness of the proposed DAug network in enhancing the precision of multiclass damage identification. Given only a total number of 60 training samples of each class, the DAug improves the damage identification precision by 10.8% in the numerical case and 5.3% in the experimental case. Three execution workflows integrating DAug-based damage classification are comprehensively investigated. The parallel experiments indicate that the MDA-GAN outperforms PDA-GAN and TL-GAN, achieving the highest prediction accuracies exceeding 0.85 with DCR embedding in both cases.

The precision results of ablation experiments on the Re-ACGAN unequivocally demonstrate the efficacy of the proposed reweighted mechanisms over those without addressing class imbalance. For a qualitative assessment of the generated data quality, t-SNE visualization results reveal that the introduction of class-imbalance reweighting modules improves cluster structures and class-conditional distribution in synthetic data. This provides compelling evidence and a profound understanding of how the proposed reweighting mechanisms contribute to enhancing data synthesis.

To the best knowledge of the authors, this study is the first to jointly consider class-conditional DAug and class-imbalance reweighting for advancing vibration-based multiclass damage identification. In future work, class-conditional DAug in the time-frequency domain and latent space using other DGMs can be further investigated. DAug-based TL approaches jointly considering DAug and domain adaptation are also promising future opportunities for advancing structural damage identification.

CHAPTER 8 CONCLUSIONS AND FUTURE WORK

8.1 Main research results

Vibration-based approaches assisted by ML techniques have been asserted as one of the most dominant roles in real-time SSDA. However, the issues of data noise, data loss and data scarcity of vibrational measurement pose significant obstacles in their applications. This study aims to tackle these challenges through exploiting advanced methodologies integrating physics-based and ML algorithms. In-depth research is conducted on corresponding tasks, including vibration signal denoising, seismic response prediction and structural condition assessment. The developed methods are validated using diverse data sources and objective structures in both numerical and experimental schemas. The main conclusions are as follows:

(1) To address the data noise issue in vibration measurement, a novel signal denoising network has been established for automatic vibration signal denoising. Artificial noise injection and time-frequency domain transformation are embedded to respectively address the pseudo-clean signal definition and high-dimensional feature extraction. The effectiveness and superiority of the proposed method are validated using field measurement of a super skyscraper, the 632-meter-tall Shanghai Tower. Moreover, the original and denoised signals are utilized to estimate the modal frequencies. The results verify the capability of the proposed denoising method in enhancing modal identification, thus enabling preliminary evaluation of structural integrity.

(2) To address the data loss issue in structural seismic response acquisition, a parameter-free PINN has been developed for rapid seismic response prediction. A novel physics-informed mechanism is devised by construing the differential nexus of state variables derived from initial acceleration responses. Applications to a numerical mass-spring-damper system and a real-world building demonstrate the effectiveness and superiority of the proposed method in seismic response prediction compared to

conventional ML regression models. The merit of this method is that it attains physics-informed embedding without reliance on structural dynamics parameters (such as stiffness or mass matrices), thus allowing for better applicability and interpretability of the surrogate response prediction models.

(3) Considering data scarcity in structural condition assessment, three different approaches namely semi-supervised label propagation, zero-shot knowledge transfer and class-conditional DAug algorithms have been developed to address this issue.

The semi-supervised label propagation method is devised by integrating self-supervised representation learning, optimized unsupervised fuzzy clustering and supervised classification algorithms. A numerical study and full-scale shaking table tests of a shear wall structure confirm the effectiveness of the devised DSF extraction strategy via DAE-based signal reconstruction and the optimized FCM algorithm in pseudo-label assignation. In tandem with damage classifiers, the proposed method can realize structural condition assessment without any labels of DSs in a semi-supervised paradigm.

In addition, a zero-shot knowledge transfer framework with novel DA mechanism is proposed for cross-domain structural condition assessment. In the proposed DA technique, the target-domain data are reconstructed using DAE trained by the source-domain data in a self-supervised way, thus reducing the domain bias for cross-domain prediction. Two representative cross-domain knowledge transfer paradigms are performed to validate the method. The prediction results after embedding DA exhibit higher precisions and lower FN rates for structural condition assessment. The merit of this method is that it achieves DA without training on vast target-domain data, thus allowing for a rigorous zero-shot TL paradigm catering for those situations where unlabeled data are limited in target-domain structures.

Moreover, an innovative class-imbalance reweighted Re-ACGAN has been developed to augment vibration data. It incorporates two class-conditional reweighting mechanisms to adeptly address the class imbalance issue during the data synthesis. The numerical and experimental datasets of a benchmark structure are adopted for validation. The augmented data are confirmed to be capable of improving the prediction accuracy of structural conditions. Ablation experiments are conducted to further substantialize the effectiveness of the integrated improvement tricks. To the best of our current knowledge, this method represents as the first attempt to jointly consider class-conditional DAug and class-imbalance issue for structural condition assessment.

The three methods developed in this thesis can deal in tandem with data scarcity issues in vibration measurement, thus enabling adaptive and reliable structural condition assessment in different data scarcity situations.

8.2 Future work

Real-time SSDA involves numerous fields and complex influencing factors, although this study has made some progress with insight into the critical issues in vibration measurement including data noise, data loss and data scarcity. It delves into corresponding problem-solving methods with superior accuracy and applicability. Future research related to this study can be further investigated and explored in the following aspects:

(1) Multi-task learning for noise-robust structural dynamics identification. The task of vibration signal denoising can be jointly performed with specific tasks in SSDA, such as structural dynamics identification. Unlike pre-task signal denoising, multi-task learning can simultaneously retrieve valuable information of signal noise and structural dynamics, allowing for noise-robust task implementation.

(2) Hybrid physics-informed and GNN-based seismic response modeling. Structural uncertainty parameters or the laws of mechanics can be embedded in a physics-guided way, such as PINNs, whilst the structural topological information can be integrated through GNNs. In this hybrid embedding schema, structural diversities

and uncertainties can be better incorporated, enabling seismic response prediction of various structures using single trained network.

(3) Population-based SHM (PBSHM) for transferring structural condition assessment. As essentially a collaborative approach to SHM, PBSHM extends the concept from a single structural monitoring to facilitating data sharing amongst structural populations, allowing for systematic insights and improved transferring assessment. State-of-the-art domain adaptation/generalization techniques, GNNs, and PINNs can be also exploited in this arising scope.

(4) Digital twins for regional SSDA toward city resilience. Digital twins serve as virtual replicas that enhance regional SSDA, promoting city resilience through accurate, real-time data on structural integrity and risks. Key components include the deployment of sensors and IoT devices for comprehensive data collection, the creation of detailed physical models, and the application of ML for predictive analytics. With multidisciplinary collaboration that ensures community-focused insights generation, digital twins for regional SSDA can enhance proactive vulnerability assessments, real-time damage evaluations during seismic events, and effective post-event recovery strategies, ultimately facilitating informed decision-making and improving city resilience.

REFERENCES

Abdeljaber, O., Avci, O., Kiranyaz, S., Gabbouj, M., & Inman, D. J. (2017). Real-time vibration-based structural damage detection using one-dimensional convolutional neural networks. *Journal of Sound and Vibration*, 388, 154-170.

Abraham, N. B., Albano, A., Das, B., De Guzman, G., Yong, S., Gioggia, R., Puccioni, G., & Tredicce, J. (1986). Calculating the dimension of attractors from small data sets. *Physics Letters A*, 114(5), 217-221.

Ahmadzadeh, M., Zahrai, S. M., & Bitaraf, M. (2024). An integrated deep neural network model combining 1D CNN and LSTM for structural health monitoring utilizing multisensor time-series data. *Structural Health Monitoring*, 24(1), 447-465.

Ambika, G., & Harikrishnan, K. P. (2020). Methods of nonlinear time series analysis and applications: A Review. In *Dynamics and Control of Energy Systems*, 9-27.

American Concrete Institute: Building Code Requirements for Structural Concrete. (2011). In *ACI 318-11*: American Concrete Institute.

Areosa, I., & Torgo, L. (2019). Explaining the performance of black box regression models. In *2019 IEEE international conference on data science and advanced analytics (DSAA)*, 110-118.

Avci, O., Abdeljaber, O., Kiranyaz, S., Hussein, M., Gabbouj, M., & Inman, D. J. (2021). A review of vibration-based damage detection in civil structures: From traditional methods to machine learning and deep learning applications. *Mechanical Systems and Signal Processing*, 147, 107077.

Bayat, A., Jalali, A., & Ahmadi, H. (2021). Nonlinear dynamic analysis and control of FG cylindrical shell fitted with piezoelectric layers. *International Journal of Structural Stability and Dynamics*, 21(06), 2150083.

Bezdek, J. C., Ehrlich, R., & Full, W. (1984). FCM: The fuzzy c-means clustering algorithm. *Computers & Geosciences*, 10(2), 191-203.

Bhatta, S., & Dang, J. (2023). Seismic damage prediction of RC buildings using machine learning. *Earthquake Engineering & Structural Dynamics*, 52(11), 3504-3527.

Bhatta, S., & Dang, J. (2024). Quantum-enhanced machine learning technique for rapid post-earthquake assessment of building safety. *Computer-Aided Civil and Infrastructure Engineering*, 39(21), 3188-3205.

Brophy, E., Wang, Z., She, Q., & Ward, T. (2023). Generative adversarial networks in time series: A systematic literature review. *ACM Computing Surveys*, 55(10), 1-31.

Bull, L., Worden, K., & Dervilis, N. (2020). Towards semi-supervised and probabilistic classification in structural health monitoring. *Mechanical Systems and Signal Processing*, 140, 106653.

Cai, S., Mao, Z., Wang, Z., Yin, M., & Karniadakis, G. E. (2021). Physics-informed neural networks (PINNs) for fluid mechanics: A review. *Acta Mechanica Sinica*, 37(12), 1727-1738.

Cao, X., Feng, D., & Li, Y. (2023). Assessment of various seismic fragility analysis approaches for structures excited by non-stationary stochastic ground motions. *Mechanical Systems and Signal Processing*, 186, 109838.

Cha, Y., & Wang, Z. (2018). Unsupervised novelty detection–based structural damage localization using a density peaks-based fast clustering algorithm. *Structural Health Monitoring*, 17(2), 313-324.

Chegini, S. N., Bagheri, A., & Najafi, F. (2019). Application of a new EWT-based denoising technique in bearing fault diagnosis. *Measurement*, 144, 275-297.

Chen, G. (2007) Dynamic chaos features auto-extraction technique of non-linear time series. *Journal of Aerospace Power* (in Chinese), 1, 1-7.

Chen, H., Yu, J., & Weng, C. (2024). Complexity scaling for speech denoising. In *2024 IEEE International Conference on Acoustics, Speech and Signal Processing (ICASSP)*, 12276-12280.

Chen, H., Yu, Y., & Li, P. (2023a). Transformer-based denoising of mechanical vibration signals. *arXiv preprint*, arXiv:2308.02166.

Chen, S., Dong, X., Xiong, Y., Peng, Z., & Zhang, W. (2017). Nonstationary signal denoising using an envelope-tracking filter. *IEEE/ASME Transactions on Mechatronics*, 23(4), 2004-2015.

Chen, X., Shao, H., Xiao, Y., Yan, S., Cai, B., & Liu, B. (2023b). Collaborative fault diagnosis of rotating machinery via dual adversarial guided unsupervised multi-domain adaptation network. *Mechanical Systems and Signal Processing*, 198, 110427.

Chen, X., Yang, Y., Cui, Z., & Shen, J. (2020). Wavelet denoising for the vibration signals of wind turbines based on variational mode decomposition and multiscale permutation entropy. *IEEE Access*, 8, 40347-40356.

Chen, Y., Sun, Z., Zhang, R., Yao, L., & Wu, G. (2023a). Attention mechanism based neural networks for structural post-earthquake damage state prediction and rapid fragility analysis. *Computers & Structures*, 281, 107038.

Cheng, Q., Zeng, X., Xiong, C., Xu, Z., & Lu, X. (2017). Comparison of seismic damage simulation methods for different regional buildings. *Engineering Mechanics* (in Chinese), 34, 105-110.

Cross, E. J., Gibson, S. J., Jones, M. R., Pitchforth, D. J., Zhang, S., & Rogers, T. J. (2022). Physics-informed machine learning for structural health monitoring. *Structural Health Monitoring Based on Data Science Techniques*, 347-367.

Dang, H. V., Raza, M., Nguyen, T. V., Bui-Tien, T., & Nguyen, H. X. (2021). Deep learning-based detection of structural damage using time-series data. *Structure and Infrastructure Engineering*, 17(11), 1474-1493.

Das, S., & Saha, P. (2018). Structural health monitoring techniques implemented on IASC–ASCE benchmark problem: a review. *Journal of Civil Structural Health Monitoring*, 8(4), 689-718.

Das, S., Saha, P., & Patro, S. K. (2016). Vibration-based damage detection techniques used for health monitoring of structures: a review. *Journal of Civil Structural Health Monitoring*, 6(3), 477-507.

Dell'Acqua, F., & Gamba, P. (2012). Remote sensing and earthquake damage assessment: Experiences, limits, and perspectives. *Proceedings of the IEEE*, 100(10), 2876-2890.

Desjardins, S., & Lau, D. (2022). Advances in intelligent long-term vibration-based structural health-monitoring systems for bridges. *Advances in Structural Engineering, 25*(7), 1413-1430.

Doebling, S. W., Farrar, C. R., Prime, M. B., & Shevitz, D. W. (1996). Damage identification and health monitoring of structural and mechanical systems from changes in their vibration characteristics: a literature review. Report of *Los Alamos National Lab. (LANL)*, Los Alamos, NM, USA.

Du, W., Yang, L., Wang, H., Gong, X., Zhang, L., Li, C., & Ji, L. (2024). LN-MRSCAE: A novel deep learning based denoising method for mechanical vibration signals. *Journal of Vibration and Control*, 30(3-4), 459-471.

Dunphy, K., Fekri, M. N., Grolinger, K., & Sadhu, A. (2022). Data augmentation for deep-learning-based multiclass structural damage detection using limited information. *Sensors*, 22(16).

Dworakowski, Z., Kohut, P., Gallina, A., Holak, K., & Uhl, T. (2016). Vision-based algorithms for damage detection and localization in structural health monitoring. *Structural Control and Health Monitoring*, 23(1), 35-50.

Dyke, S. J., Bernal, D., Beck, J., & Ventura, C. (2003). *Experimental phase II of the structural health monitoring benchmark problem.* In *Proceedings of the 16th ASCE Engineering Mechanics Conference*.

Entezami, A., Sarmadi, H., & Behkamal, B. (2024). Short-term damage alarming with limited vibration data in bridge structures: A fully non-parametric machine learning technique. *Measurement*, 235, 114935.

Entezami, A., Sarmadi, H., Behkamal, B., & De Michele, C. (2023). On continuous health monitoring of bridges under serious environmental variability by an innovative multi-task unsupervised learning method. *Structure and Infrastructure Engineering*, 20(12), 1975-1993.

Entezami, A., & Shariatmadar, H. (2017). An unsupervised learning approach by novel damage indices in structural health monitoring for damage localization and quantification. *Structural Health Monitoring*, 17(2), 325-345.

Erazo, K., Sen, D., Nagarajaiah, S., & Sun, L. (2019). Vibration-based structural health monitoring under changing environmental conditions using Kalman filtering. *Mechanical Systems and Signal Processing*, 117, 1-15.

Fan, G., Li, J., & Hao, H. (2019). Lost data recovery for structural health monitoring based on convolutional neural networks. *Structural Control and Health Monitoring,* 26(10), e2433.

Fan, G., Li, J., & Hao, H. (2020). Vibration signal denoising for structural health monitoring by residual convolutional neural networks. *Measurement*, 157, 107651.

Fang, C., Chen, Y., Deng, X., Lin, X., Han, Y., & Zheng, J. (2023). Denoising method of machine tool vibration signal based on variational mode decomposition and Whale-Tabu optimization algorithm. *Scientific Reports*, 13(1), 1505.

Farahani, A., Voghoei, S., Rasheed, K., & Arabnia, H. R. (2021). A brief review of domain adaptation. *Advances in data science and information engineering: proceedings from ICDATA 2020 and IKE 2020*, 877-894.

Farrar, C. R., & Worden, K. (2012). Structural health monitoring: A machine learning perspective. Wiley.

Federal Emergency Management Agency (2000). Prestandard and Commentary for the Seismic Rehabilitation of Buildings. In *FEMA 356*. Washington, DC.

Fei, Y., Liao, W., Lu, X., & Guan, H. (2023a). Knowledge-enhanced graph neural networks for construction material quantity estimation of reinforced concrete buildings. *Computer-Aided Civil and Infrastructure Engineering*, 39(4), 518-538.

Fei, Y., Liao, W., Lu, X., Taciroglu, E., & Guan, H. (2023b). Semi-supervised learning method incorporating structural optimization for shear-wall structure design using small and long-tailed datasets. *Journal of Building Engineering*, 79, 107873.

Fei, Y., Liao, W., Zhao, P., Lu, X., & Guan, H. (2024). Hybrid surrogate model combining physics and data for seismic drift estimation of shear-wall structures. *Earthquake Engineering & Structural Dynamics*, 53(10), 3093-3112.

Feng, D.-C., Yi, X., Deger, Z. T., Liu, H.-k., Chen, S.-Z., & Wu, G. (2024). Rapid post-earthquake damage assessment of building portfolios through deep learning-based component-level image recognition. *Journal of Building Engineering*, 98, 111380.

Feng, D., Cao, X., Wang, D., & Wu, G. (2023). A PDEM-based non-parametric seismic fragility assessment method for RC structures under non-stationary ground motions. *Journal of Building Engineering*, 63, 105465.

Fichou, D., & Morlock, G. E. (2018). Powerful artificial neural network for planar chromatographic image evaluation, shown for denoising and feature extraction. *Analytical Chemistry*, 90(11), 6984-6991.

Gao, Y., Kong, B., & Mosalam, K. M. (2019). Deep leaf-bootstrapping generative adversarial network for structural image data augmentation. *Computer-Aided Civil and Infrastructure Engineering*, 34(9), 755-773.

Gao, Y., Zhai, P., & Mosalam, K. M. (2021). Balanced semisupervised generative adversarial network for damage assessment from low-data imbalanced-class regime. *Computer-Aided Civil and Infrastructure Engineering*, 36(9), 1094-1113.

Gardner, P., Bull, L. A., Gosliga, J., Dervilis, N., & Worden, K. (2021). Foundations of population-based SHM, Part III: Heterogeneous populations – Mapping and transfer. *Mechanical Systems and Signal Processing*, 149, 107142.

Gardner, P., Liu, X., & Worden, K. (2020). On the application of domain adaptation in structural health monitoring. *Mechanical Systems and Signal Processing*, 138, 106550.

Gawande, A., Bhatlawande, S., Pangavhane, A., & Shilaskar, S. (2024). Image denoising using multi-level wavelet convolutional neural network. In *the Third International Conference on Distributed Computing and Electrical Circuits and Electronics (ICDCECE)*, 1-6.

Ghiasi, R., Khan, M. A., Sorrentino, D., Diaine, C., & Malekjafarian, A. (2024). An unsupervised anomaly detection framework for onboard monitoring of railway track geometrical defects using one-class support vector machine. *Engineering Applications of Artificial Intelligence*, 133, 108167.

Ghose, S., Singh, N., & Singh, P. (2020). Image denoising using deep learning: Convolutional neural network. In *2020 10th International Conference on Cloud Computing, Data Science & Engineering (Confluence)*, 511-517.

Giardina, G., Macchiarulo, V., Foroughnia, F., Jones, J. N., Whitworth, M. R., Voelker, B., Milillo, P., Penney, C., Adams K., & Kijewski-Correa, T. (2024). Combining remote sensing techniques and field surveys for post-earthquake reconnaissance missions. *Bulletin of Earthquake Engineering*, 22(7), 3415-3439.

Giglioni, V., Poole, J., Venanzi, I., Ubertini, F., & Worden, K. (2024). A domain adaptation approach to damage classification with an application to bridge monitoring. *Mechanical Systems and Signal Processing*, 209, 111135.

Goodfellow, I., Pouget-Abadie, J., Mirza, M., Xu, B., Warde-Farley, D., Ozair, S., Courville, A., & Bengio, Y. (2020). Generative adversarial networks. *Communications of the ACM*, 63(11), 139-144.

Goulet, C. A., Kishida, T., Ancheta, T. D., Cramer, C. H., Darragh, R. B., Silva, W. J., Hashash, Y.M., Harmon, J., Parker, G.A., Stewart, J.P., & Youngs, R. R. (2021). PEER NGA-East database. *Earthquake Spectra*, 37(1), 1331-1353.

Goulet, J.-A., Michel, C., & Kiureghian, A. D. (2015). Data-driven post-earthquake rapid structural safety assessment. *Earthquake Engineering & Structural Dynamics*, 44(4), 549-562.

Graves, A., & Schmidhuber, J. (2005). Framewise phoneme classification with bidirectional LSTM and other neural network architectures. *Neural Networks*, 18(5), 602-610.

Haddadi, H., Shakal, A., Stephens, C., Savage, W., Huang, M., Leith, W., ... & Borcherdt, R. (2008). Center for engineering strong-motion data (CESMD). In *Proceedings of the 14th World Conference on Earthquake Engineering*, 12-17.

Han, H., Wang, H., Liu, Z., & Wang, J. (2022). Intelligent vibration signal denoising method based on non-local fully convolutional neural network for rolling bearings. *ISA Transactions*, 122, 13-23.

Hao, H., Bi, K., Chen, W., Pham, T. M., & Li, J. (2023a). Towards next generation design of sustainable, durable, multi-hazard resistant, resilient, and smart civil engineering structures. *Engineering Structures*, 277, 115477.

Hao, F., Ma, Z.-F., Tian, H.-P., Wang, H., & Wu, D. (2023b). Semi-supervised label propagation for multi-source remote sensing image change detection. *Computers & Geosciences*, 170, 105249.

Hao, W., Yin, H., Liu, J., Ma, R., Zhao, D., & Lu, S. (2025). Seismic response prediction of soil tunnel structure based on CNN-LSTM model. *Structures*, 73, 108381.

He, H., & Garcia, E. A. (2009). Learning from imbalanced data. *IEEE Transactions on Knowledge and Data Engineering*, 21(9), 1263-1284.

Shafiq, M., & Gu, Z. (2022). Deep residual learning for image recognition: A survey. *Applied sciences*, 12(18), 8972.

He, K., Zhang, X., Ren, S., & Sun, J. (2016b). *Deep residual learning for image recognition.* In Proceedings of the *IEEE conference on computer vision and pattern recognition*, 770-778.

He, Q., Wang, X., & Zhou, Q. (2013). Vibration sensor data denoising using a time-frequency manifold for machinery fault diagnosis. *Sensors*, 14(1), 382-402.

Grassberger, P., & Procaccia, I. (1983). Measuring the strangeness of strange attractors. *Physica D: nonlinear phenomena*, 9(1-2), 189-208.

Hess, A. S., & Hess, J. R. (2019). Logistic regression. *Transfusion*, 59(7), 2197-2198.

Hinton, G. E., & Roweis, S. (2002). Stochastic neighbor embedding. *Advances in neural information processing systems*, Cambridge: The MIT Press, 833, 840.

Hochreiter, S., & Schmidhuber, J. (1997). Long short-term memory. *Neural Computation*, 9(8), 1735-1780.

Hong, D., & Kim, B. (2023). 1D convolutional neural network-based adaptive algorithm structure with system fault diagnosis and signal feature extraction for noise and vibration enhancement in mechanical systems. *Mechanical Systems and Signal Processing*, 197, 110395.

Houshmand Nanehkaran, F., Lajevardi, S. M., & Mahlouji Bidgholi, M. (2022). Nearest neighbors algorithm and genetic-based collaborative filtering. *Concurrency and Computation: Practice and Experience*, 34(1), e6538.

Hu, H., Ao, Y., Yan, H., Bai, Y., Shi, N., & Diraco, G. (2021). Signal denoising based on wavelet threshold denoising and optimized variational mode decomposition. *Journal of Sensors, 2021*, 1-23.

Hu, Y., Guo, W., Xu, Z. a., & Shi, C. (2024). Physics knowledge-based transfer learning between buildings for seismic response prediction. *Soil Dynamics and Earthquake Engineering*, 177, 108420.

Huang, B., & Wang, J. (2022). Applications of physics-informed neural networks in power systems-a review. *IEEE Transactions on Power Systems*, 38(1), 572-588.

Huang, H., & Burton, H. V. (2022). Dynamic seismic damage assessment of distributed infrastructure systems using graph neural networks and semi-supervised machine learning. *Advances in Engineering Software*, 168, 103113.

Huang, N. E., Shen, Z., Long, S. R., Wu, M. C., Shih, H. H., Zheng, Q., . . . Liu, H. H. (1998). The empirical mode decomposition and the Hilbert spectrum for nonlinear and non-stationary time series analysis. *Proceedings of the Royal Society of London. Series A: Mathematical, Physical and Engineering Sciences*, 454(1971), 903-995.

Huang, P., & Chen, Z. (2021). Deep learning for nonlinear seismic responses prediction of subway station. *Engineering Structures*, 244, 112735.

Iglesias, G., Talavera, E., González-Prieto, Á., Mozo, A., & Gómez-Canaval, S. (2023). Data augmentation techniques in time series domain: a survey and taxonomy. *Neural Computing and Applications*, 35(14), 10123-10145.

Iscen, A., Tolias, G., Avrithis, Y., & Chum, O. (2019). Label propagation for deep semi-supervised learning. In *Proceedings of the IEEE/CVF conference on computer vision and pattern recognition* (pp. 5070-5079).

Ji, X., Zhuang, Y., Miao, Z., & Cheng, Y. (2023). Vision-based seismic damage detection and residual capacity assessment for an RC shaking table test structure. *Earthquake Engineering & Structural Dynamics*, 52(3), 806-827.

Johnson, E. A., Lam, H.-F., Katafygiotis, L. S., & Beck, J. L. (2004). Phase I IASC-ASCE structural health monitoring benchmark problem using simulated data. *Journal of Engineering Mechanics*, 130(1), 3-15.

Juarez, M. G., Botti, V. J., & Giret, A. S. (2021). Digital Twins: Review and Challenges. *Journal of Computing and Information Science in Engineering*, 21(3), 030802.

Jun, Z. (2021). The development and application of support vector machine. *Journal of Physics: Conference Series*, 1748(5), 052006.

Kamariotis, A., Chatzi, E., & Straub, D. (2023). A framework for quantifying the value of vibration-based structural health monitoring. *Mechanical Systems and Signal Processing*, 184, 109708.

Kauss, K., Alves, V., Barbosa, F., & Cury, A. (2024). Semi-supervised structural damage assessment via autoregressive models and evolutionary optimization. *Structures*, 59, 105762.

Kaya, A., Adanur, S., Bello, R. A., Genç, A. F., Okur, F. Y., Sunca, F., . . . Sevim, B. (2023). Post-earthquake damage assessments of unreinforced masonry (URM) buildings by shake table test and numerical visualization. *Engineering Failure Analysis,* 143, 106858.

Kheddar, H., Hemis, M., & Himeur, Y. (2024). Automatic speech recognition using advanced deep learning approaches: A survey. *Information Fusion*, 102422.

Kim, T., Kwon, O.-S., & Song, J. (2019). Response prediction of nonlinear hysteretic systems by deep neural networks. *Neural Networks*, 111, 1-10.

Kingma, D. P., & Ba, J. (2014). Adam: A method for stochastic optimization. *arXiv preprint* arXiv:1412.6980.

Kingma, D. P., & Welling, M. (2019). An introduction to variational autoencoders. *Foundations and Trends® in Machine Learning*, 12(4), 307-392.

Kiranyaz, S., Avci, O., Abdeljaber, O., Ince, T., Gabbouj, M., & Inman, D. J. (2021). 1D convolutional neural networks and applications: A survey. *Mechanical Systems and Signal Processing*, 151, 107398.

Kircher, C. A., & Heintz, J. A. (2008). Overview and key concepts of the ATC-63 methodology. *Structures Congress 2008: Crossing Borders*, 1-10.

Kociuba, D., Sagan, M., & Kociuba, W. (2023). Toward the smart city ecosystem model. *Energies*, 16(6), 2795.

Kong, Q., Gu, J., Xiong, B., & Yuan, C. (2023). Vision-aided three-dimensional damage quantification and finite element model geometric updating for reinforced concrete structures. *Computer-Aided Civil and Infrastructure Engineering*, 38(17), 2378-2390.

Krishna, K., & Murty, M. N. (1999). Genetic K-means algorithm. *IEEE Transactions on Systems, Man, and Cybernetics, Part B (Cybernetics)*, 29(3), 433-439.

Kumar, M., & Varshney, P. (2021). Numerical simulation of van der pol equation using multiple scales modified Lindstedt-Poincaré method. *Proceedings of the National Academy of Sciences India Section a-Physical Sciences, 91*(1), 55-65.

Kuo, P.-C., Chou, Y.-T., Li, K.-Y., Chang, W.-T., Huang, Y.-N., & Chen, C.-S. (2024). GNN-LSTM-based fusion model for structural dynamic responses prediction. *Engineering Structures*, 306, 117733.

Lang, D. H., Singh, Y., & Prasad, J. (2012). Comparing empirical and analytical estimates of earthquake loss assessment studies for the city of Dehradun, India. *Earthquake Spectra*, 28(2), 595-619.

Lewis, J. M., & Burrus, C. S. (1998). Approximate continuous wavelet transform with an application to noise reduction. In *Proceedings of the 1998 IEEE International Conference on Acoustics, Speech and Signal Processing, ICASSP'98*, 3, 1533-1536.

Li, C., Li, H., & Chen, X. (2022a). Fast seismic response estimation of tall pier bridges based on deep learning techniques. *Engineering Structures*, 266, 114566.

Li, L., & Betti, R. (2023). A machine learning-based data augmentation strategy for structural damage classification in civil infrastructure system. *Journal of Civil Structural Health Monitoring*, 13(6), 1265-1285.

Li, L., Morgantini, M., & Betti, R. (2023a). Structural damage assessment through a new generalized autoencoder with features in the quefrency domain. *Mechanical Systems and Signal Processing*, 184, 109713.

Li, M., Wang, Z., Luo, J., Liu, Y., & Cai, S. (2017). Wavelet denoising of vehicle platform vibration signal based on threshold neural network. *Shock and Vibration,* 2017(1), 7962828.

Li, Q., Li, R., Li, S., Wang, T., Cheng, Y., Zhang, S., . . . Wang, L. (2024a). Unpaired low-dose computed tomography image denoising using a progressive cyclical convolutional neural network. *Medical Physics*, 51(2), 1289-1312.

Li, S., Han, J.-C., Li, Y.-R., & Qin, P.-F. (2024b). Intelligent prediction and evaluation models for the seismic risk and vulnerability of reinforced concrete girder bridges in large-scale zones. *Reliability Engineering & System Safety*, 256, 110743.

Li, T., Pan, Y., Tong, K., Ventura, C. E., & Silva, C. W. d. (2022b). Attention-Based Sequence-to-Sequence Learning for Online Structural Response Forecasting Under Seismic Excitation. *IEEE Transactions on Systems, Man, and Cybernetics: Systems,* 52(4), 2184-2200.

Li, Y., Zhang, M., & Yang, W. (2018). Numerical and experimental investigation of modal-energy-based damage localization for offshore wind turbine structures. *Advances in Structural Engineering*, 21(10), 1510-1525.

Li, Z., He, W.-Y., Ren, W.-X., Li, Y.-L., Li, Y.-F., & Cheng, H.-C. (2023b). Damage detection of bridges subjected to moving load based on domain-adversarial neural network considering measurement and model error. *Engineering Structures*, 293, 116601.

Li, Z., Yang, Q., Deng, Q., Gong, Y., Tian, D., Su, P., & Teng, J. (2024c). Time history seismic response prediction of multiple homogeneous building structures using only one deep learning-based Structure Temporal Fusion Network. *Earthquake Engineering & Structural Dynamics*, 53(13), 4076-4098.

Liang, Y., Liang, W., & Jia, J. (2023). Structural Vibration Signal Denoising Using Stacking Ensemble of Hybrid CNN-RNN. *arXiv preprint* arXiv:2303.11413.

Liao, Y., Lin, R., Zhang, R., & Wu, G. (2023). Attention-based LSTM (AttLSTM) neural network for seismic response modeling of bridges. *Computers & Structures*, 275, 106915.

Lim, T. P., & Puthusserypady, S. (2007). Chaotic time series prediction and additive white Gaussian noise. *Physics Letters A*, 365(4), 309-314.

Lin, T. Y., Goyal, P., Girshick, R., He, K., & Dollár, P. (2017b). Focal loss for dense object detection. In *Proceedings of the IEEE international conference on computer vision*, 2980-2988.

Lin, Y.-z., Nie, Z.-h., & Ma, H.-w. (2017a). Structural damage detection with automatic feature-extraction through deep learning. *Computer-Aided Civil and Infrastructure Engineering*, 32(12), 1025-1046.

Lin, Y. z., Nie, Z. h., & Ma, H. w. (2021). Dynamics-based cross-domain structural damage detection through deep transfer learning. *Computer-Aided Civil and Infrastructure Engineering*, 37(1), 24-54.

Liu, J., & Gao, W. (2020). Vibration signal analysis of water seal blasting based on wavelet threshold denoising and HHT transformation. *Advances in Civil Engineering*, 2020(1), 4381480.

Liu, Y., & Fang, S.-E. (2024). Cross-domain structural damage identification using transfer learning strategy. *Engineering Structures*, 311, 118171.

Lu, X., & Guan, H. (2021). Earthquake Disaster Simulation of Civil Infrastructures: From Tall Buildings to Urban Areas. Singapore: Springer.

Lu, X., Han, B., Hori, M., Xiong, C., & Xu, Z. (2014). A coarse-grained parallel approach for seismic damage simulations of urban areas based on refined models and GPU/CPU cooperative computing. *Advances in Engineering Software*, 70, 90-103.

Lu, X., Lu, X., Zhang, W., & Ye, L. (2011). Collapse simulation of a super high-rise building subjected to extremely strong earthquakes. *Science China Technological Sciences*, 54(10), 2549-2560.

Lu, X., Xu, Y., Tian, Y., Cetiner, B., & Taciroglu, E. (2021). A deep learning approach to rapid regional post-event seismic damage assessment using time-frequency distributions of ground motions. *Earthquake Engineering & Structural Dynamics*, 50(6), 1612-1627.

Lu, Y., Tang, L., Chen, C., Zhou, L., Liu, Z., Liu, Y., . . . Yang, B. (2024). Unsupervised structural damage assessment method based on response correlations. *Engineering Structures*, 302, 117413.

Luleci, F., Catbas, F. N., & Avci, O. (2023). Generative adversarial networks for labeled acceleration data augmentation for structural damage detection. *Journal of Civil Structural Health Monitoring*, 13(1), 181-198.

Macchiarulo, V., Giardina, G., Milillo, P., Aktas, Y. D., & Whitworth, M. R. (2024). Integrating post-event very high resolution SAR imagery and machine learning for building-level earthquake damage assessment. *Bulletin of Earthquake Engineering*, 1-27.

Magalhães, F., Cunha, Á., & Caetano, E. (2009). Online automatic identification of the modal parameters of a long span arch bridge. *Mechanical Systems and Signal Processing*, 23(2), 316-329.

Manavski, S. A., & Valle, G. (2008). CUDA compatible GPU cards as efficient hardware accelerators for Smith-Waterman sequence alignment. *BMC Bioinformatics*, 9(2), S10.

Mangalathu, S., Hwang, S.-H., Choi, E., & Jeon, J.-S. (2019). Rapid seismic damage evaluation of bridge portfolios using machine learning techniques. *Engineering Structures*, 201, 109785.

Martakis, P., Reuland, Y., Stavridis, A., & Chatzi, E. (2023). Fusing damage-sensitive features and domain adaptation towards robust damage classification in real buildings. *Soil Dynamics and Earthquake Engineering*, 166, 107739.

Miao, F., Zhao, R., & Wang, X. (2020a). A new method of denoising of vibration signal and its application. *Shock and Vibration*, 2020(1), 7587840.

Miao, M., Liu, C., & Yu, J. (2020b). Adaptive densely connected convolutional auto-encoder-based feature learning of gearbox vibration signals. *IEEE Transactions on Instrumentation and Measurement*, 70, 1-11.

Miele, S., Karve, P., & Mahadevan, S. (2023). Multi-fidelity physics-informed machine learning for probabilistic damage diagnosis. *Reliability Engineering & System Safety*, 235, 109243.

Mohapatra, N., Shreya, K., & Chinmay, A. (2020). Optimization of the random forest algorithm. *Lecture Notes on Data Engineering and Communications Technologies*, 37, 201.

Nanga, S., Bawah, A. T., Acquaye, B. A., Billa, M.-I., Baeta, F. D., Odai, N. A., . . . Nsiah, A. D. (2021). Review of dimension reduction methods. *Journal of Data Analysis and Information Processing*, 9(3), 189-231.

National Standard of the People's Republic of China. Code for design of concrete structures. (2015). In *GB50010-2010*: China Architecture & Building Press.

Nguyen, T. T. S., & Do, P. M. T. (2020). Classification optimization for training a large dataset with Naïve Bayes. *Journal of Combinatorial Optimization*, 40(1), 141-169.

Nielsen, F., & Nielsen, F. (2016). Hierarchical clustering. *Introduction to HPC with MPI for Data Science*, 195-211.

Odena, A., Olah, C., & Shlens, J. (2017). Conditional Image Synthesis with Auxiliary Classifier GANs. In the *34th International Conference on Machine Learning*, 2642-2651.

Oh, B. K., Glisic, B., Park, S. W., & Park, H. S. (2020). Neural network-based seismic response prediction model for building structures using artificial earthquakes. *Journal of Sound and Vibration*, 468, 115109.

Oksuz, K., Cam, B. C., Kalkan, S., & Akbas, E. (2020). Imbalance problems in object detection: A review. *IEEE Transactions on Pattern Analysis and Machine Intelligence*, 43(10), 3388-3415.

Ozcan, I. H., Devecioglu, O. C., Ince, T., Eren, L., & Askar, M. (2021). Enhanced bearing fault detection using multichannel, multilevel 1D CNN classifier. *Electrical Engineering*, 104(2), 435-447.

Pan, S. J., & Yang, Q. (2010). A Survey on Transfer Learning. *IEEE Transactions on Knowledge and Data Engineering*, 22(10), 1345-1359.

Pandey, P., Rai, A., & Mitra, M. (2022). Explainable 1-D convolutional neural network for damage detection using Lamb wave. *Mechanical Systems and Signal Processing*, 164, 108220.

Pantiskas, L., Verstoep, K., & Bal, H. (2020, December). Interpretable multivariate time series forecasting with temporal attention convolutional neural networks. In *2020 IEEE Symposium Series on Computational Intelligence (SSCI)*,1687-1694.

Park, S. R., & Lee, J. (2016). A fully convolutional neural network for speech enhancement. *arXiv preprint* arXiv:1609.07132.

Pasti, L., Walczak, B., Massart, D., & Reschiglian, P. (1999). Optimization of signal denoising in discrete wavelet transform. *Chemometrics and intelligent laboratory systems*, 48(1), 21-34.

Pastor, M., Binda, M., & Harčarik, T. (2012). Modal assurance criterion. *Procedia Engineering*, 48, 543-548.

Pedregosa, F., Varoquaux, G., Gramfort, A., Michel, V., Thirion, B., Grisel, O., . . . Dubourg, V. (2011). Scikit-learn: Machine learning in Python. *Journal of machine Learning research*, 12, 2825-2830.

Pedrycz, W. (2021). Fuzzy clustering. *Intelligent Systems Reference Library*,190, 125-145.

Perez-Ramirez, C. A., Amezquita-Sanchez, J. P., Valtierra-Rodriguez, M., Adeli, H., Dominguez-Gonzalez, A., & Romero-Troncoso, R. J. (2019). Recurrent neural network model with Bayesian training and mutual information for response prediction of large buildings. *Engineering Structures*, 178, 603-615.

Pollastro, A., Testa, G., Bilotta, A., & Prevete, R. (2023). Semi-supervised detection of structural damage using variational autoencoder and a one-class support vector machine. *IEEE Access*, 11, 67098-67112.

Qin, Y., Yao, Q., Wang, Y., & Mao, Y. (2021). Parameter sharing adversarial domain adaptation networks for fault transfer diagnosis of planetary gearboxes. *Mechanical*

Systems and Signal Processing, 160, 107936.

Quinlan, J. R. (1986). Induction of decision trees. *Machine learning*, 1, 81-106.

Raissi, M., Perdikaris, P., & Karniadakis, G. E. (2017). Physics informed deep learning (part i): Data-driven solutions of nonlinear partial differential equations. *arXiv preprint* arXiv:1711.10561.

Raissi, M., Perdikaris, P., & Karniadakis, G. E. (2019). Physics-informed neural networks: A deep learning framework for solving forward and inverse problems involving nonlinear partial differential equations. *Journal of Computational Physics*, 378, 686-707.

Rastin, Z., Ghodrati Amiri, G., & Darvishan, E. (2021). Unsupervised structural damage detection technique based on a deep convolutional autoencoder. *Shock and Vibration*, 2021(1), 6658575.

Ravizza, G., Ferrari, R., Rizzi, E., & Dertimanis, V. (2021). On the denoising of structural vibration response records from low-cost sensors: A critical comparison and assessment. *Journal of Civil Structural Health Monitoring*, 11(5), 1201-1224.

Rogers, T., Worden, K., Fuentes, R., Dervilis, N., Tygesen, U., & Cross, E. (2019). A Bayesian non-parametric clustering approach for semi-supervised structural health monitoring. *Mechanical Systems and Signal Processing*, 119, 100-119.

Rohrbach, M., Stark, M., & Schiele, B. (2011). Evaluating knowledge transfer and zero-shot learning in a large-scale setting. In *CVPR 2011*, 1641-1648.

Rojas, C. R., & Wachel, P. (2022). On state-space representations of general discrete-time dynamical systems. *arXiv preprint* arXiv:2205.03366.

Ronneberger, O., Fischer, P., & Brox, T. (2015). U-net: Convolutional networks for biomedical image segmentation. In Proceedings of *Medical image computing and computer-assisted intervention–MICCAI 2015*, part III 18.

Rössler, O. E. (1976). An equation for continuous chaos. *Physics Letters A*, 57(5), 397-398.

Rytter, A. (1993). Vibrational based inspection of civil engineering structures. PhD Thesis at Deptment of Building Technology and Structural Engineering, Aalborg University.

Sander, J., Ester, M., Kriegel, H.-P., & Xu, X. (1998). Density-based clustering in spatial databases: The algorithm gdbscan and its applications. *Data Mining and Knowledge Discovery*, 2, 169-194.

Santos, I., Castro, L., Rodriguez-Fernandez, N., Torrente-Patiño, Á., & Carballal, A.

(2021). Artificial neural networks and deep learning in the visual arts: a review. *Neural Computing and Applications*, 33(1), 121-157.

Saxena, A., Prasad, M., Gupta, A., Bharill, N., Patel, O. P., Tiwari, A., . . . Lin, C.-T. (2017). A review of clustering techniques and developments. *Neurocomputing*, 267, 664-681.

Scarselli, F., Gori, M., Tsoi, A. C., Hagenbuchner, M., & Monfardini, G. (2008). The graph neural network model. *IEEE Transactions on Neural Networks*, 20(1), 61-80.

Shao, X., & Kim, C. S. (2022). Unsupervised domain adaptive 1D-CNN for fault diagnosis of bearing. *Sensors*, 22(11), 4156.

She, B., & Wang, X. (2022). A hidden feature label propagation method based on deep convolution variational autoencoder for fault diagnosis. *Measurement Science and Technology*, 33(5), 055107.

Shi, H., Chen, J., Si, J., & Zheng, C. (2020). Fault diagnosis of rolling bearings based on a residual dilated pyramid network and full convolutional denoising autoencoder. *Sensors*, 20(20), 5734.

Shi, S., Du, D., Mercan, O., Kalkan, E., & Wang, S. (2022). A novel unsupervised real-time damage detection method for structural health monitoring using machine learning. *Structural Control and Health Monitoring*, 29(10), e3042.

Sigrist, F. (2021). Gradient and Newton boosting for classification and regression. *Expert Systems with Applications*, 167, 114080.

Silva, M., Santos, A., Figueiredo, E., Santos, R., Sales, C., & Costa, J. C. (2016). A novel unsupervised approach based on a genetic algorithm for structural damage detection in bridges. *Engineering Applications of Artificial Intelligence*, 52, 168-180.

Silva, M. F., Santos, A., Santos, R., Figueiredo, E., & Costa, J. C. W. A. (2021). Damage-sensitive feature extraction with stacked autoencoders for unsupervised damage detection. *Structural Control and Health Monitoring*, 28(5), e2714.

Singh, P., & Shankar, A. (2021). A novel optical image denoising technique using convolutional neural network and anisotropic diffusion for real-time surveillance applications. *Journal of Real-Time Image Processing*, 18(5), 1711-1728.

Soleimani-Babakamali, M. H., Soleimani-Babakamali, R., Nasrollahzadeh, K., Avci, O., Kiranyaz, S., & Taciroglu, E. (2023). Zero-shot transfer learning for structural health monitoring using generative adversarial networks and spectral mapping. *Mechanical Systems and Signal Processing*, 198, 110404.

Solorio-Fernández, S., Carrasco-Ochoa, J. A., & Martínez-Trinidad, J. F. (2020). A review of unsupervised feature selection methods. *Artificial Intelligence Review*, 53(2), 907-948.

Song, L. H., Wang, C., Fan, J. S., & Lu, H. M. (2022). Elastic structural analysis based on graph neural network without labeled data. *Computer-Aided Civil and Infrastructure Engineering*, 38(10), 1307-1323.

Stramondo, S., Bignami, C., Chini, M., Pierdicca, N., & Tertulliani, A. (2006). Satellite radar and optical remote sensing for earthquake damage detection: results from different case studies. *International Journal of Remote Sensing*, 27(20), 4433-4447.

Sun, B., & Li, Y. (2021). Evolution and development of earthquake disaster prediction in China. *Engineering Mechanics (in Chinese)*, 38(1), 1-7.

Tavasoli, S., Pan, X., & Yang, T. (2023). Real-time autonomous indoor navigation and vision-based damage assessment of reinforced concrete structures using low-cost nano aerial vehicles. *Journal of Building Engineering*, 68, 106193.

Thabtah, F., Hammoud, S., Kamalov, F., & Gonsalves, A. (2020). Data imbalance in classification: Experimental evaluation. *Information Sciences*, 513, 429-441.

Thai, H., DeBrunner, V., DeBrunner, L. S., Havlicek, J. P., Mish, K., Ford, K., & Medda, A. (2007, August). Deterministic-stochastic subspace identification for bridges. In *2007 IEEE/SP 14th Workshop on Statistical Signal Processing*, 749-753).

Toh, G., & Park, J. (2020). Review of vibration-based structural health monitoring using deep learning. *Applied Sciences*, 10(5), 1680.

Torky, A. A., & Ohno, S. (2021). Deep learning techniques for predicting nonlinear multi-component seismic responses of structural buildings. *Computers & Structures*, 252, 106570.

Tronci, E. M., Beigi, H., Betti, R., & Feng, M. Q. (2023). A damage assessment methodology for structural systems using transfer learning from the audio domain. *Mechanical Systems and Signal Processing*, 195, 110286.

Tsarpalis, D., Vamvatsikos, D., Vayas, I., & Delladonna, F. (2021). Simplified modeling for the seismic performance assessment of automated rack-supported warehouses. *Journal of Structural Engineering*, 147(11), 04021189.

Tsuchimoto, K., Narazaki, Y., & Spencer, B. F. (2024). Rapid post-earthquake safety assessment of low-rise reinforced concrete structures. *Earthquake Engineering and Engineering Vibration*, 24(1), 101-112.

Vadyala, S. R., Betgeri, S. N., Matthews, J. C., & Matthews, E. (2022). A review of physics-based machine learning in civil engineering. *Results in Engineering*, 13, 100316.

Van der Maaten, L., & Hinton, G. (2008). Visualizing data using t-SNE. *Journal of machine learning research*, 9(11).

Vaswani, A., Shazeer, N., Parmar, N., Uszkoreit, J., Jones, L., Gomez, A. N., ... & Polosukhin, I. (2017). Attention is all you need. *Advances in neural information processing systems,* 30.

Vincent, P., Larochelle, H., Lajoie, I., Bengio, Y., & Manzagol, P. A. (2010). Stacked denoising autoencoders: Learning useful representations in a deep network with a local denoising criterion. *Journal of Machine Learning Research*, 11, 3371-3408.

Von Luxburg, U. (2007). A tutorial on spectral clustering. *Statistics and Computing*, 17, 395-416.

Wan, H. P., Zhu, Y. K., Luo, Y., & Todd, M. D. (2025). Unsupervised deep learning approach for structural anomaly detection using probabilistic features. *Structural Health Monitoring, 24*(1), 3-33.

Wan, P., He, H., Guo, L., Yang, J., & Li, J. (2021). InfoGAN-MSF: a data augmentation approach for correlative bridge monitoring factors. *Measurement Science and Technology*, 32(11), 114008.

Wang, H., Barone, G., & Smith, A. (2023a). A novel multi-level data fusion and anomaly detection approach for infrastructure damage identification and localisation. *Engineering Structures*, 292, 116473.

Wang, H., Liu, Z., Peng, D., & Cheng, Z. (2022a). Attention-guided joint learning CNN with noise robustness for bearing fault diagnosis and vibration signal denoising. *ISA Transactions*, 128, 470-484.

Wang, H., Zhang, Y., Liang, J., & Liu, L. (2023c). DAFA-BiLSTM: Deep autoregression feature augmented bidirectional LSTM network for time series prediction. *Neural Networks*, 157, 240-256.

Wang, J., Wu, Y., Wang, S., Narazaki, Y., Liu, H., & Spencer Jr, B. F. (2024). Development and validation of graphics-based digital twin framework for UAV-aided post-earthquake inspection of high-rise buildings. *The Structural Design of Tall and Special Buildings,* 33(13), e2127.

Wang, S., Balarezo, J. F., Kandeepan, S., Al-Hourani, A., Chavez, K. G., & Rubinstein, B. (2021). Machine learning in network anomaly detection: A survey. *IEEE Access*, 9, 152379-152396.

Wang, W., & Sun, D. (2021). The improved AdaBoost algorithms for imbalanced data classification. *Information Sciences*, 563, 358-374.

Wang, X., Du, Y., Zhou, X., & Xia, Y. (2023b). Data anomaly detection through semisupervised learning aided by customised data augmentation techniques. *Structural Control and Health Monitoring*, 2023(1), 2430011.

Wang, X., & Xia, Y. (2022b). Knowledge transfer for structural damage detection through re-weighted adversarial domain adaptation. *Mechanical Systems and Signal Processing*, 172, 108991.

Wang, Y., He, Z., & Zi, Y. (2010). Enhancement of signal denoising and multiple fault signatures detecting in rotating machinery using dual-tree complex wavelet transform. *Mechanical Systems and Signal Processing*, 24(1), 119-137.

Wang, Y., Song, X., Li, R., Yang, F., Xiao, Y., Zheng, S., . . . Li, X. (2025). Channel mode attention network for structural damage identification. *Engineering Structures*, 325, 119389.

Wang, Z., & Cha, Y.-J. (2020). Unsupervised deep learning approach using a deep auto-encoder with a one-class support vector machine to detect damage. *Structural Health Monitoring*, 20(1), 406-425.

Wei, P., Li, Q., Sun, M., & Huang, J. (2023). Modal identification of high-rise buildings by combined scheme of improved empirical wavelet transform and Hilbert transform techniques. *Journal of Building Engineering*, 63, 105443.

Dean, G. C. (1986). An introduction to Kalman filters. *Measurement and Control*, 19(2), 69-73.

Wen, C., & Changzhi, W. (2022). Combine labeled and unlabeled data for immune detector training with label propagation. *Knowledge-Based Systems*, 236, 107661.

Wen, Q., Sun, L., Yang, F., Song, X., Gao, J., Wang, X., & Xu, H. (2020). Time series data augmentation for deep learning: A survey. *arXiv preprint* arXiv:2002.12478.

Wen, W., Zhang, C., & Zhai, C. (2022). Rapid seismic response prediction of RC frames based on deep learning and limited building information. *Engineering Structures*, 267, 114638.

Wernitz, S., Chatzi, E., Hofmeister, B., Wolniak, M., Shen, W., & Rolfes, R. (2022). On noise covariance estimation for Kalman filter-based damage localization. *Mechanical Systems and Signal Processing*, 170, 108808.

Wu, Y., Sicard, B., & Gadsden, S. A. (2024). Physics-informed machine learning: A comprehensive review on applications in anomaly detection and condition monitoring. *Expert Systems with Applications*, 255, 124678.

Wu, Z., Pan, S., Chen, F., Long, G., Zhang, C., & Philip, S. Y. (2020). A comprehensive survey on graph neural networks. *IEEE Transactions on Neural Networks and Learning Systems*, 32(1), 4-24.

Wu, Z., Wang, H., He, C., Zhang, B., Xu, T., & Chen, Q. (2023). The application of physics-informed machine learning in multiphysics modeling in chemical engineering. *Industrial & Engineering Chemistry Research*, 62(44), 18178-18204.

Xie, P., Zhang, L., Li, M., Lau, S. F. S., & Huang, J. (2024). Elevator vibration signal denoising by deep residual U-Net. *Measurement*, 225, 113976.

Xiong, C., Huang, J., & Lu, X. (2020). Framework for city-scale building seismic resilience simulation and repair scheduling with labor constraints driven by time–history analysis. *Computer-Aided Civil and Infrastructure Engineering*, 35(4), 322-341.

Xiong, Q., Xiong, H., Kong, Q., Ni, X., Li, Y., & Yuan, C. (2022). Machine learning-driven seismic failure mode identification of reinforced concrete shear walls based on PCA feature extraction. *Structures*, 44, 1429-1442.

Xu, S., & Noh, H. Y. (2021). PhyMDAN: Physics-informed knowledge transfer between buildings for seismic damage diagnosis through adversarial learning. *Mechanical Systems and Signal Processing*, 151, 107374.

Xu, Y., Kohtz, S., Boakye, J., Gardoni, P., & Wang, P. (2023). Physics-informed machine learning for reliability and systems safety applications: State of the art and challenges. *Reliability Engineering & System Safety*, 230, 108900.

Xu, Y., Lu, X., Cetiner, B., & Taciroglu, E. (2021a). Real-time regional seismic damage assessment framework based on long short-term memory neural network. *Computer-Aided Civil and Infrastructure Engineering*, 36(4), 504-521.

Xu, Y., Lu, X., Tian, Y., & Huang, Y. (2022a). Real-time seismic damage prediction and comparison of various ground motion intensity measures based on machine learning. *Journal of Earthquake Engineering*, 26(8), 4259-4279.

Xu, Z., Chen, J., Shen, J., & Xiang, M. (2022b). Recursive long short-term memory network for predicting nonlinear structural seismic response. *Engineering Structures*, 250, 113406.

Yang, W.-X., & Peter, W. T. (2003). Development of an advanced noise reduction method for vibration analysis based on singular value decomposition. *NDT & E International*, 36(6), 419-432.

Yao, Y., Rosasco, L., & Caponnetto, A. (2007). On Early Stopping in Gradient Descent Learning. *Constructive Approximation*, 26(2), 289-315.

Yazdanpanah, O., Dolatshahi, K. M., & Moammer, O. (2023). Rapid seismic fragility curves assessment of eccentrically braced frames through an output-only nonmodel-based procedure and machine learning techniques. *Engineering Structures*, 278, 115290.

Yu, H., Wang, B., Li, Y., & Gao, Z. (2022). Spectral decomposition-based explicit integration method for fully non-stationary seismic responses of large-scale structures. *Mechanical Systems & Signal Processing*, 168, 108735.

Yu, X., Hu, X., Song, Y., Xu, S., Li, X., Song, X., . . . Wang, F. (2024a). Intelligent assessment of building damage of 2023 Turkey-Syria Earthquake by multiple remote sensing approaches. *npj Natural Hazards*, 1(1), 3.

Yu, R., Li, P., Shan, J., Zhang, Y., & Dong, Y. (2024b). Multi-feature driven rapid inspection of earthquake-induced damage on building facades using UAV-derived point cloud. *Measurement*t, 232, 114679.

Yu, Y., Si, X., Hu, C., & Zhang, J. (2019). A review of recurrent neural networks: LSTM cells and network architectures. *Neural Computation*, 31(7), 1235-1270.

Yu, Y., Yao, H., & Liu, Y. (2020). Structural dynamics simulation using a novel physics-guided machine learning method. *Engineering Applications of Artificial Intelligence*, 96, 103947.

Yuan, C., Zhang, J., Chen, L., Xu, J., & Kong, Q. (2021). Timber moisture detection using wavelet packet decomposition and convolutional neural network. *Smart Materials and Structures*, 30(3), 035022.

Zar, A., Hussain, Z., Akbar, M., Tayeh, B. A., & Lin, Z. (2023). A vibration-based approach for detecting arch dam damage using RBF neural networks and Jaya algorithms. *Smart Structures and Systems*, 32(5), 319-338.

Zeng, Y., Zhao, Z., Qian, G., Todd, M. D., & Hu, Z. (2025). Enhancing Bayesian inference-based damage diagnostics through domain translation with application to miter gates. *Journal of Mechanical Design*, 147(6), 061701.

Zhang, C., Wen, W., Zhai, C., Jia, J., & Zhou, B. (2024a). Structural nonlinear seismic time-history response prediction of urban-scale reinforced concrete frames based on deep learning. *Engineering Structures*, 317, 118702.

Zhang, F., Xiong, H., Shi, W., & Ou, X. (2016). Structural health monitoring of Shanghai Tower during different stages using a Bayesian approach. *Structural Control and Health Monitoring*, 23(11), 1366-1384.

Zhang, G., Zhou, Z., Wan, C., Ding, Z., Wu, Z., Xie, L., & Xue, S. (2025). Substructural damage identification in a digital twin framework using heterogeneous response reconstruction. *Advances in Structural Engineering*, 28(1), 68-88.

Zhang, H., Bittner, M., & Beer, M. (2022a). Seismic response meta-model of high-rise fame structure based on time-delay neural network. *KSCE Journal of Civil Engineering,* 26(5), 2273-2294.

Zhang, R., Chen, Z., Chen, S., Zheng, J., Büyüköztürk, O., & Sun, H. (2019). Deep long short-term memory networks for nonlinear structural seismic response prediction. *Computers & Structures*, 220, 55-68.

Zhang, R., Liu, Y., & Sun, H. (2020). Physics-guided convolutional neural network (PhyCNN) for data-driven seismic response modeling. *Engineering Structure*s, 215, 110704.

Zhang, T., Shi, D., Wang, Z., Zhang, P., Wang, S., & Ding, X. (2022b). Vibration-based structural damage detection via phase-based motion estimation using convolutional neural networks. *Mechanical Systems and Signal Processing*, 178, 109320.

Zhang, X.-P. (2001). Thresholding neural network for adaptive noise reduction. *IEEE Transactions on Neural Networks*, 12(3), 567-584.

Zhang, X., Zhu, X., Yu, Y., & Li, J. (2024b). Transfer learning-based structural damage identification for building structures with limited measurement data. *International Journal of Structural Stability and Dynamics*, 25(9), 2550093.

Zhao, M., & Jia, X. (2017). A novel strategy for signal denoising using reweighted SVD and its applications to weak fault feature enhancement of rotating machinery. *Mechanical Systems and Signal Processing*, 94, 129-147.

Zhao, X., Huang, P., & Shu, X. (2022). Wavelet-Attention CNN for image classification. *Multimedia Systems*, 28(3), 915-924.

Zhou, H., Yan, P., Yuan, Y., Wu, D., & Huang, Q. (2022a). Denoising the hob vibration signal using improved complete ensemble empirical mode decomposition with adaptive noise and noise quantization strategies. *ISA Transactions*, 131, 715-735.

Zhou, X., Wang, X., Wang, H., Xing, Z., Yang, Z., & Cao, L. (2023). Method for denoising the vibration signal of rotating machinery through VMD and MODWPT. *Sensors*, 23(15), 6904.

Zhou, Y., Meng, S., Lou, Y., & Kong, Q. (2024). Physics-Informed Deep Learning-Based Real-Time Structural Response Prediction Method. *Engineering*, 35, 140-157.

Zhou, Y., Zheng, Y., Liu, Y., Pan, T., & Zhou, Y. (2022b). A hybrid methodology for structural damage detection uniting FEM and 1D-CNNs: Demonstration on typical high-pile wharf. *Mechanical Systems and Signal Processing*, 168, 108738.

Zhu, H., Zhou, Y. J., & Hu, Y. M. (2020). Displacement reconstruction from measured accelerations and accuracy control of integration based on a low-frequency attenuation algorithm. *Soil Dynamics and Earthquake Engineering*, 133, 106122.

Zhu, Y. K., Wan, H. P., Ye, Y. J., & Todd, M. D. (2025). A conditional probabilistic deep learning approach for anomaly detection in structures under varying environmental conditions. *Mechanical Systems and Signal Processing*, 236, 113005.

Zhuang, F., Qi, Z., Duan, K., Xi, D., Zhu, Y., Zhu, H., Xiong, H., & He, Q. (2020). A comprehensive survey on transfer learning. *Proceedings of the IEEE*, 109(1), 43-76.